SANDIA REPORT

SAND2005-6988
Unlimited Release
Printed November 2005

Advances in Radiation Modeling in ALEGRA: A Final Report for LDRD-67120, Efficient Implicit Multigroup Radiation Calculations

Thomas A. Brunner, Thomas . Mehlhorn, Ryan McClarren, and Christopher J. Kurecka

Prepared by
Sandia National Laboratories
Albuquerque, New Mexico 87185 and Livermore, California 94550

Sandia is a multiprogram laboratory operated by Sandia Corporation,
a Lockheed Martin Company, for the United States Department of Energy's
National Nuclear Security Administration under Contract DE-AC04-94AL85000.

Approved for public release; further dissemination unlimited.

Sandia National Laboratories

Issued by Sandia National Laboratories, operated for the United States Department of Energy by Sandia Corporation.

NOTICE: This report was prepared as an account of work sponsored by an agency of the United States Government. Neither the United States Government, nor any agency thereof, nor any of their employees, nor any of their contractors, subcontractors, or their employees, make any warranty, express or implied, or assume any legal liability or responsibility for the accuracy, completeness, or usefulness of any information, apparatus, product, or process disclosed, or represent that its use would not infringe privately owned rights. Reference herein to any specific commercial product, process, or service by trade name, trademark, manufacturer, or otherwise, does not necessarily constitute or imply its endorsement, recommendation, or favoring by the United States Government, any agency thereof, or any of their contractors or subcontractors. The views and opinions expressed herein do not necessarily state or reflect those of the United States Government, any agency thereof, or any of their contractors.

Printed in the United States of America. This report has been reproduced directly from the best available copy.

Available to DOE and DOE contractors from
U.S. Department of Energy
Office of Scientific and Technical Information
P.O. Box 62
Oak Ridge, TN 37831

Telephone: (865) 576-8401
Facsimile: (865) 576-5728
E-Mail: reports@adonis.osti.gov
Online ordering: http://www.doe.gov/bridge

Available to the public from
U.S. Department of Commerce
National Technical Information Service
5285 Port Royal Rd
Springfield, VA 22161

Telephone: (800) 553-6847
Facsimile: (703) 605-6900
E-Mail: orders@ntis.fedworld.gov
Online ordering: http://www.ntis.gov/ordering.htm

SAND2005-6988
Unlimited Release
Printed November 2005

Advances in Radiation Modeling in ALEGRA: A Final report for LDRD-67120, Efficient Implicit Multigroup Radiation Calculations

Thomas A. Brunner and Thomas A. Mehlhorn
HEDP Theory & ICF Target Design
Sandia National Laboratories
P.O. Box 5800
Albuquerque, NM 87185-1186
tabrunn@sandia.gov

Ryan McClarren, James Paul Holloway, and Christopher J. Kurecka
Department of Nuclear Engineering and Radiological Sciences
University of Michigan
Ann Arbor, MI 48109-2014

Abstract

The original LDRD proposal was to use a nonlinear diffusion solver to compute estimates for the material temperature that could then be used in a Implicit Monte Carlo (IMC) calculation. At the end of the first year of the project, it was determined that this was not going to be effective, partially due to the concept, and partially due to the fact that the radiation diffusion package was not as efficient as it could be.

The second, and final year, of the project focused on improving the robustness and computational efficiency of the radiation diffusion package in ALEGRA. To this end, several new multigroup diffusion methods have been developed and implemented in ALEGRA. While these methods have been implemented, their effectiveness of reducing overall simulation run time has not been fully tested.

Additionally a comprehensive suite of verification problems has been developed for the diffusion package to ensure that it has been implemented correctly. This process took considerable time, but exposed significant bugs in both the previous and new diffusion packages, the linear solve packages, and even the NEVADA Framework's parser.

In order to manage this large suite of problem, a new tool called Tampa has been developed. It is a general tool for automating the process of running and analyzing many simulations.

Ryan McClarren, at the University of Michigan has been developing a Spherical Harmonics capability for unstructured meshes. While still in the early phases of development, this promises to bridge the gap in accuracy between a full transport solution using IMC and the diffusion approximation.

Acknowledgment

The Trilinos team, especially Mike Heroux, provided a lot of support so that the advanced features of Trilinos could be used effectively in order to get robust, efficient code.

Contents

1 Introduction **17**

2 The Diffusion Method **19**

2.1 The Diffusion Equation 19

2.1.1 The Energy Dependent Equations 19

2.1.2 Boundary Conditions 20

2.1.2.1 Partial Fluxes 21

2.1.2.2 Actual Boundary Conditions 22

2.1.3 Miscellaneous Quantities 23

2.1.4 The Multigroup Approximation 24

2.1.4.1 Group Integrated and Averaged Quantities 25

2.1.4.2 The Multigroup Equations 28

2.1.4.3 The Multigroup Planck Function 28

2.2 Nodal Finite Elements 29

2.2.1 The Generalized Diffusion Equation 29

2.2.2 The Discretization of Energy Density 30

2.2.3 The Integration of the Diffusion Equation 30

2.2.4 Boundary Conditions 31

2.2.5 Lumped Mass Matrix 32

2.2.6 Energy Tallies 32
2.2.6.1 Flux Through Arbitrary Surfaces 33
2.3 Linearized Semi-Implicit Solution 35
2.4 Solution Methods 38
2.4.1 Operator Form 38
2.4.2 Large System Solve 39
2.4.2.1 Diagonal Preconditioner 39
2.4.2.2 Approximate Grey Preconditioner 40
2.5 Conclusions and Future Work 41

3 The Verification Suite **43**
3.1 Tampa 43
3.2 Simplifications 44
3.3 One Dimensional Cartesian Steady State Problems 45
3.3.1 Only Scattering: Linear Solutions 45
3.3.1.1 Dirichlet and Vacuum 46
3.3.1.2 Source and Albedo 46
3.3.2 Absorption and Scattering 47
3.3.2.1 Dirichlet and Vacuum Boundaries 48
3.3.2.2 Source and Albedo Boundaries 48
3.4 Steady Steady Cylindrical and Spherical Problems 49
3.4.1 A Cylinder 49
3.4.2 A Sphere 51
3.5 External Sources 52
3.5.1 Constant Uniform Source: Constant Solution 52

3.5.2 Constant Uniform Source: One Dimensional Quadratic Solution . . . 53

3.5.3 Varying Source . . . 53

3.6 Two Material Steady State Problems . . . 54

3.6.1 Cartesian With Only Scattering . . . 55

3.6.2 Cartesian With Scattering and Absorption . . . 56

3.6.3 One Vacuum Material . . . 57

3.7 Time Dependent Problems . . . 59

3.7.1 A Plane Source . . . 59

3.7.2 A Slab Source . . . 61

3.7.2.1 A Nicer Solution . . . 61

3.8 Polynomial Solutions . . . 62

3.8.1 Constant . . . 62

3.8.2 Linear . . . 63

3.8.3 Quadratic . . . 63

3.9 Manufactured Solutions . . . 65

3.9.1 A Flux Limiter Test . . . 66

3.9.2 Coupling to a Uniform Material . . . 67

3.9.3 Nonuniform Opacities . . . 71

3.9.4 Multigroup . . . 73

3.10 Transport Tests . . . 75

3.11 Meshes . . . 78

3.12 Conclusions and Future Work . . . 78

4 Spherical Harmonics **83**

4.1 The Discretization of the P_n equations . . . 84

4.1.1 The P_n Equations 84
4.1.2 Cell-Averaged Equations and Riemann Solver 85
4.1.3 Slope Reconstruction 86
4.1.4 Time Integration 87
4.2 Implementation 87
4.3 Test Problems 88
4.3.1 Plane Source 88
4.3.2 Reed's Problem 89
4.4 Results 89
4.4.1 Plane Source Problem 89
4.4.2 Reed's Problem 90
4.5 The P_n equations and Riemann discretization 91
4.6 Diffusion properties of the P_n equations 94
4.6.1 Linear solution of the P_n equations 94
4.6.2 Asymptotic Analysis of the P_n equations 95
4.7 Diffusion properties of the Riemann discretization 97
4.8 Modified Riemann Solver in the Diffusive Limit 99
4.9 Computational demonstrations 101
4.9.1 Preserving Linear Solutions 101
4.9.2 Diffusion Correction 101
4.9.2.1 Steady State Problems 102
4.9.2.2 Time Dependent Problems 103
4.10 Conclusions and Future Work 104

References **109**

List of Figures

2.1 A flux tally surface 34

3.1 Steady state solution in a slab with the Dirichlet condition $E(0) = B(T = 5000\,\mathrm{K})$ and the vacuum condition at $x_r = 1\,\mathrm{m}$ with $\sigma_t = \sigma_s = 1\,\mathrm{m}^{-1}$. This second order diffusion method should get this exactly, so there is no expected convergence. 46

3.2 Steady state solution in a slab with the source condition $F_{\text{in}}(0) = B(T = 1000\,\mathrm{K})/4$ and the albedo condition at $x_r = 1\,\mathrm{m}$ with $\alpha = 0.25$ and $\sigma_t = \sigma_s = 100\,\mathrm{m}^{-1}$. This second order diffusion method should get this exactly, so there is no expected convergence. 47

3.3 Steady state solution in a slab with the Dirichlet condition $E(1\,\mathrm{m}) = B(T = 5.0\mathrm{e}6\,\mathrm{K})$ and the vacuum condition at $x_r = 0\,\mathrm{m}$ with $\sigma_s = 1\,\mathrm{m}^{-1}$ and $\sigma_a = 6\,\mathrm{m}^{-1}$. 49

3.4 Steady state solution in a slab with the source condition $F_{\text{in}}(1\,\mathrm{m}) = B(T = 300\,\mathrm{K})/4$ and the albedo condition at $x_r = 0\,\mathrm{m}$ with $\alpha = 0.75$, $\sigma_s = 1\,\mathrm{m}^{-1}$ and $\sigma_a = 6\,\mathrm{m}^{-1}$. 50

3.5 Steady state solution in a cylinder with the source condition at $r_0 = 1\,\mathrm{m}$ of $B(T = 10000\,\mathrm{K})$ with $\sigma_s = 1\,\mathrm{m}^{-1}$ and $\sigma_a = 1\,\mathrm{m}^{-1}$. A convergence study with this problem still needs to be set up and done. 51

3.6 Steady state solution in a sphere with the source condition at $r_0 = 1\,\mathrm{m}$ of $B(T = 6000\,\mathrm{K})$ with $\sigma_s = 2\,\mathrm{m}^{-1}$ and $\sigma_a = 3\,\mathrm{m}^{-1}$. A convergence study with this problem still needs to be set up and done. 52

3.7 Steady state solution in a slab with a uniform source of $S = 1 \times 10^{10}\,\mathrm{W/m^3}$ and $\sigma_t = \sigma_s = 1\,\mathrm{m}^{-1}$. 54

3.8 Convergence rates of the absolute relative error on various meshes for the nonuniform source problem with $\sigma_t = \sigma_s = 1.0$, $S_0 = 1.0e10$, $A = 10$, $E_0 = B(5000)$, and $E_1 = B(10000)$. 55

3.9 Steady state solution in a two material slab with the Dirichlet conditions $E(0) = 0$ and $E(1\,\mathrm{m}) = B(200\,\mathrm{keV})$ with $\sigma_s^l = 0.02\,\mathrm{m}^{-1}$, $\sigma_s^r = 5.0\,\mathrm{m}^{-1}$, and $x_i = 0.5\,\mathrm{m}$. These parameters were chosen to test a thick material followed by a near vacuum. This method should get this solution exactly, so there is no expected convergence on the regular meshes. There is some error in mixed material cells, however, so there is first order convergence on skewed or randomized meshes. 56

3.10 Steady state solution in a two material slab with the Dirichlet conditions $E(0) = 0$ and $E(2\,\mathrm{m}) = B(200\,\mathrm{keV})$ with $\sigma_s^l = 5\,\mathrm{m}^{-1}$, $\sigma_a^l = 20\,\mathrm{m}^{-1}$, $\sigma_s^r = 0.01\,\mathrm{m}^{-1}$, and $\sigma_a^r = 0.01\,\mathrm{m}^{-1}$. These parameters were chosen to test an optically thin material followed by a thick one. The excessive convergence rates of about $O(3)$ are only because there were problems in converging the solution on the coarse meshes. The reason for this is currently unknown. 58

3.11 A problem with a void region. The material region on the right extends from $x = 0$ to $x = 0.5\,\mathrm{m}$ with $\sigma_s = 70\,\mathrm{m}^{-1}$ and $\sigma_a = 0$. The vacuum region extends from $x = 0.5\,\mathrm{m}$ to $x = 1\,\mathrm{m}$. A vacuum boundary condition is applied at $x = 1$ and a Dirichlet boundary condition on the left of $E(0) = B(50000\,\mathrm{K})$ 60

3.12 Pulsed slab source problem. The discontinuity in the initial conditions makes it difficult to converge the problem, and we may not be in the asymptotic regime, making the order of convergence not valid. 62

3.13 Uniform infinite medium problem. This second order diffusion method should get this exactly within the linear solver tolerance, so there is no expected convergence. 63

3.14 Linear problem with Dirichlet boundary conditions. This second order diffusion method should get this exactly within the linear solver tolerance, so there is no expected convergence. 64

3.15 Quadratic problem with Dirichlet boundary conditions. 65

3.16 Regular diffusion MMS test. 68

3.17 Larsen-2 flux limiter MMS test. 69

3.18 Radiation energy density results in a MMS test with coupling to a uniform material using regular diffusion. This problem does not converge as expected and is still be investigated. 71

3.19 Material temperature results in a MMS test with coupling to a uniform material using regular diffusion. This problem does not converge as expected and is still be investigated. 72

3.20 MMS test with spatially varying opacities and regular diffusion. 73

3.21 MMS test of the multigroup equations integrating all groups. Because of the opacities, the higher groups are optically thin, and an automatic diffusion coefficient limiter kicks in to keep the matrix well-conditions. This causes it to diverge from the correct answer, however. 75

3.22 MMS of Multigroup, looking at only the second group's results. Without the influence of the thin groups, this converges as expected. 76

3.23 A hot, uniform box calculated using Implicit Monte Carlo. As the number of particles (N) increases, the error should be proportional to $1/\sqrt{N}$. 77

3.24 Two Dimensional Meshes 79

3.25 Three Dimensional Meshes, part 1. 80

4.1 The scalar flux for the first test problem at $T = 10$ after the initial pulse 88

4.2 Results of P_1 calculations $T = 5$ after the initial pulse of particles is introduced 90

4.3 Results from P_5 solution at $T = 10$ after pulse 91

4.4 Steady state results from Reed's problem 92

4.5 Time dependent results from Reed's problem at $T = 1$ 93

4.6 The scalar flux and first moments for the standard Riemann solver for the linear source problem (cf. Sec. 4.6) 101

4.7 The scalar flux and first moments for the diffusion-corrected Riemann solver for the linear source problem 102

4.8 The P_5, steady state solution with incident beam on the left, and two regions: a strong absorber and a strong scatterer 103

4.9 The P_1, steady-state solution to a uniform source problem with $Q = \frac{1}{2\pi}$ and $\Sigma_a = 0.01, \Sigma_t = 10$ 104

4.10 The solution to the modified Reed's problem. 105

4.11 The P7 solution at $t = 35$ after the initial pulse of particles 105

4.12 The P1 solution at t=35 after the initial pulse of particles 106

List of Tables

2.1 Coefficients for the diffusion boundary conditions. 24

4.1 Material Layout in Reed's Problem 89

Chapter 1

Introduction

The original LDRD proposal was to use a nonlinear diffusion solver to compute estimates for the material temperature that could then be used in a Implicit Monte Carlo (IMC) calculation. At the end of the first year of the project, it was determined that this was not going to be effective, partially due to the concept, and partially due to the fact that the radiation diffusion package was not as efficient as it could be.

The second, and final year, of the project focused on improving the robustness and computational efficiency of the radiation diffusion package in ALEGRA. To this end, several new multigroup diffusion methods have been developed and implemented in ALEGRA. While these methods have been implemented, their effectiveness of reducing overall simulation run time has not been fully tested.

Additionally a comprehensive suite of verification problems has been developed for the diffusion package to ensure that it has been implemented correctly. This process took considerable time, but exposed significant bugs in both the previous and new diffusion packages, the linear solve packages, and even the NEVADA Framework's parser.

In order to manage this large suite of problem, a new tool called Tampa has been developed. It is a general tool for automating the process of running and analyzing many simulations.

Ryan McClarren, at the University of Michigan has been developing a Spherical Harmonics capability for unstructured meshes. While still in the early phases of development, this promises to bridge the gap in accuracy between a full transport solution using IMC and the diffusion approximation.

Chapter 2

The Diffusion Method

The radiation diffusion package in ALEGRA uses a Galerkin finite element method with linear continuous shape functions on isoparametric elements. The details of the method, including the discretization, linearization, and details of the algorithm are outlined here.

Some details are omitted here; specifically how the radiation couples to other physics, such as hydrodynamics and magnetohydrodynamics.

2.1 The Diffusion Equation

The diffusion equation is an approximation to the Boltzmann transport equation for radiation transport [3]. The photons couple to the materials through absorption and emission processes. The materials emit and absorb photons at different rates for different photon energies, which leads to an energy dependent diffusion equation.

2.1.1 The Energy Dependent Equations

The photon energy dependent diffusion equation and the equations describing each material are

$$\frac{1}{c}\frac{\partial E_r(\epsilon)}{\partial t} - \nabla \cdot D(\epsilon)\nabla E_r(\epsilon) = \sum_{m=1}^{M} \alpha_m \sigma_{a,m}(\epsilon)(B(T_m,\epsilon) - E_r(\epsilon)) + \frac{1}{c}S_r(\epsilon) \tag{2.1.1}$$

$$\frac{\partial u_m}{\partial t} = \int_0^\infty \alpha_m c \sigma_{a,m}(\epsilon)\left(E_r(\epsilon) - B(T_m,\epsilon)\right) \mathrm{d}\epsilon + Q_m, \tag{2.1.2}$$

where E_r and u_m are the radiation and material energy densities, ϵ is the photon energy, M is the number of materials, S_r and Q_m are external power density sources, c is the speed of light, σ_a is the absorption opacity with units of inverse length, D_m is the diffusion coefficient with units of length, $B(T_m, \epsilon)$ is the Planck (or black body) function, T_m is the material temperature which is a function of u_m, α_m is the material volume fraction, and $D(\epsilon)$ is the diffusion coefficient. It is assumed there is a mixture of materials at each point, and that volume fraction averaging the opacities is reasonable. The angle integrated Planck function is defined as

$$B(T_m, \epsilon) = \frac{8\pi}{h^3 c^3} \frac{\epsilon^3}{\mathrm{e}^{\epsilon/kT_m} - 1} \tag{2.1.3}$$

For regular diffusion, the diffusion coefficient is defined as

$$D(\epsilon) = \frac{1}{3\sum_{m=1}^{M} \alpha_m \sigma_{t,m}(\epsilon)} \tag{2.1.4}$$

where $\sigma_{t,m}$ is the total opacity (scattering plus absorption). This choice for the diffusion coefficient can allow the radiation flux

$$\mathbf{F} = -cD\nabla E_r \tag{2.1.5}$$

to be greater in magnitude than E_r, which implies that more energy is flowing through a surface than exists at the surface. This problem typically arises when the gradients are very sharp. The diffusion coefficient can be modified in many ways to limit the radiation flux. The Larsen flux limiter[23, 29] is available in ALEGRA, and it defines the the diffusion coefficient to be

$$D = \frac{1}{\left[(3\sigma_t)^n + \left(\frac{|\nabla E|}{E}\right)^n\right]^{\frac{1}{n}}}, \tag{2.1.6}$$

where n is an arbitrary parameter. The value of $n = 2$ works well for most cases, but the behavior of most other flux limiters can be captured with other values of n. Many more flux limiters have been developed and are included in the code, but only for comparison purposes.

2.1.2 Boundary Conditions

In radiation transport and in real-world experiments systems are driven by internal energy sources and the energy that enters the system through the boundary. The term S_r in Eq. 2.1.1 is the arbitrary internal energy sources that are not modeled elsewhere in ALEGRA; these are primarily used for testing purposes. At the boundaries, physically we can only specify the angular distribution entering the system. Unfortunately, the diffusion equation only works with angle-integrated quantities namely the energy density E_r and the flux $\mathbf{F}$, so that the best that we can do is make sure certain integral quantities are conserved at the boundaries.

2.1.2.1 Partial Fluxes

The radiation intensity $I(\mathbf{x}, \mathbf{\Omega}, \varepsilon, t)$ can be written in terms of the quantities in the diffusion approximation as [21, 19, 24, 3]

$$I(\mathbf{\Omega}) = \frac{c}{4\pi} E_r + \frac{3}{4\pi} \mathbf{\Omega} \cdot \mathbf{F} \tag{2.1.7}$$

where $\mathbf{\Omega}$ is the unit cosine vector the defines the direction of travel of the photons.

The flux $\mathbf{F}$ can also be computed from I using

$$\mathbf{F} = \int_{4\pi} \mathbf{\Omega} I \ \mathrm{d}\mathbf{\Omega} \,. \tag{2.1.8}$$

Since we only know the information for the incoming $I(\mathbf{\Omega}')$, we can integrate $I(\mathbf{\Omega}')$ over the incoming angles to get constraints on E_r and $\mathbf{F}$. If we have some surface with an outward unit normal $\hat{\mathbf{n}}$, then for the incoming angles the following is true

$$\mathbf{\Omega}_{\text{in}} \cdot \hat{\mathbf{n}} < 0. \tag{2.1.9}$$

The outgoing angles are then

$$\mathbf{\Omega}_{\text{out}} \cdot \hat{\mathbf{n}} > 0. \tag{2.1.10}$$

With the angles defined, we can now define an incoming and outgoing flux to be

$$\mathbf{F}_{\text{in}} = \int_{\mathbf{\Omega} \cdot \hat{\mathbf{n}} < 0} \mathbf{\Omega} I \ \mathrm{d}\mathbf{\Omega} \text{ and} \tag{2.1.11}$$

$$\mathbf{F}_{\text{out}} = \int_{\mathbf{\Omega} \cdot \hat{\mathbf{n}} > 0} \mathbf{\Omega} I \ \mathrm{d}\mathbf{\Omega} \,, \tag{2.1.12}$$

and $\mathbf{F} = \mathbf{F}_{\text{in}} + \mathbf{F}_{\text{out}}$. Since we don't need (or want) to deal in vector quantities, we can write

$$F_{\text{in}} = -\hat{\mathbf{n}} \cdot \mathbf{F}_{\text{in}} = -\int_{\mathbf{\Omega} \cdot \hat{\mathbf{n}} < 0} \hat{\mathbf{n}} \cdot \mathbf{\Omega} I \ \mathrm{d}\mathbf{\Omega} \tag{2.1.13}$$

$$F_{\text{out}} = \hat{\mathbf{n}} \cdot \mathbf{F}_{\text{out}} = \int_{\mathbf{\Omega} \cdot \hat{\mathbf{n}} > 0} \hat{\mathbf{n}} \cdot \mathbf{\Omega} I \ \mathrm{d}\mathbf{\Omega} \tag{2.1.14}$$

Inserting Eq. 2.1.7 we get

$$F_{\text{in}} = -\frac{1}{4\pi} \int_{\mathbf{\Omega} \cdot \hat{\mathbf{n}} < 0} \hat{\mathbf{n}} \cdot \mathbf{\Omega} \left(c E_r + 3 \mathbf{\Omega} \cdot \mathbf{F} \right) \ \mathrm{d}\mathbf{\Omega} \tag{2.1.15}$$

$$F_{\text{out}} = \frac{1}{4\pi} \int_{\mathbf{\Omega} \cdot \hat{\mathbf{n}} > 0} \hat{\mathbf{n}} \cdot \mathbf{\Omega} \left(c E_r + 3 \mathbf{\Omega} \cdot \mathbf{F} \right) \ \mathrm{d}\mathbf{\Omega} \tag{2.1.16}$$

Without loss of generality, we can assume that $\hat{\mathbf{n}}$ is the pole of $\mathbf{\Omega}$, yielding

$$F_{\text{in}} = -\frac{1}{4\pi}\int_{-1}^{0}\int_{0}^{2\pi} \mu\left(cE_r + 3\mu F_{\hat{\mathbf{n}}}\right)\,\mathrm{d}\vartheta\,\mathrm{d}\mu \tag{2.1.17}$$

$$F_{\text{out}} = \frac{1}{4\pi}\int_{0}^{1}\int_{0}^{2\pi} \mu\left(cE_r + 3\mu F_{\hat{\mathbf{n}}}\right)\,\mathrm{d}\vartheta\,\mathrm{d}\mu \tag{2.1.18}$$

Doing the integration gives us

$$F_{\text{in}} = \frac{c}{4}E_r - \frac{1}{2}\hat{\mathbf{n}}\cdot\mathbf{F} \tag{2.1.19}$$

$$F_{\text{out}} = \frac{c}{4}E_r + \frac{1}{2}\hat{\mathbf{n}}\cdot\mathbf{F} \tag{2.1.20}$$

Note that F_{in} and F_{out} are usually positive. They are strictly nonnegative for in the transport equation, but the diffusion approximation doesn't ensure that $I(\mathbf{\Omega})$ is positive. We can see that here because if $\mathbf{F}$ is large, it can change the sign of either F_{in} or F_{out}.)

2.1.2.2 Actual Boundary Conditions

With this machinery, we can specify any type of boundary condition that we want. It turns out that all boundary conditions for diffusion can be written in the form

$$\mathcal{A}cE_r + \mathcal{B}\hat{\mathbf{n}}\cdot\mathbf{F} = \mathcal{C}c \tag{2.1.21}$$

Dirichlet boundary conditions specify the energy density on the boundary, namely

$$E_r(x_{\text{boundary}}) = E_0. \tag{2.1.22}$$

These are not useful physically, but are useful for testing purposes.

For vacuum boundaries we know that there is no radiation entering the system, but we do not know how much radiation is leaving. This means we can specify F_{in} but not F_{out}. So

$$F_{\text{in}} = 0 = \frac{c}{4}E_r - \frac{1}{2}\hat{\mathbf{n}}\cdot\mathbf{F}. \tag{2.1.23}$$

Writing this in terms of Eq. 2.1.21 and setting $\mathcal{B} = 1$, we get

$$-\frac{c}{2}E_r + \hat{\mathbf{n}}\cdot\mathbf{F} = 0 \tag{2.1.24}$$

A source boundary again specifies the incoming flux F_{in}, but sets it to something nonzero. If we know that the radiation entering the system is being emitted from a large hot body of temperature T, the incoming distribution essentially looks

like a black body function. We can insert this into Eq. 2.1.11 to get what we should specify

$$F_{\text{in}} = -\int_{\mathbf{\Omega}\cdot\hat{\mathbf{n}}<0} \hat{\mathbf{n}}\cdot\mathbf{\Omega}\frac{cB(T)}{4\pi}\ \mathrm{d}\mathbf{\Omega}\ = \frac{c}{4}B(T) \tag{2.1.25}$$

With this, our boundary condition is

$$\frac{c}{4}E_r - \frac{1}{2}\hat{\mathbf{n}}\cdot\mathbf{F} = \frac{c}{4}B(T) \tag{2.1.26}$$

or

$$-\frac{c}{2}E_r + \hat{\mathbf{n}}\cdot\mathbf{F} = -\frac{c}{2}B(T) \tag{2.1.27}$$

In some problems, you don't really want to model the entire physical system, but you do know that a certain fraction of the radiation crossing the boundary will be reflected back into the system. If we define the albedo α as the reflected fraction of energy back into the system, we know that

$$F_{\text{in}} = \alpha F_{\text{out}} \tag{2.1.28}$$

Using the expressions for these, we get

$$\frac{c}{4}E_r - \frac{1}{2}\hat{\mathbf{n}}\cdot\mathbf{F} = \frac{c\alpha}{4}E_r + \frac{\alpha}{2}\hat{\mathbf{n}}\cdot\mathbf{F} \tag{2.1.29}$$

Simplifying some we get

$$-\frac{1}{2}\frac{1-\alpha}{1+\alpha}cE_r + \hat{\mathbf{n}}\cdot\mathbf{F} = 0 \tag{2.1.30}$$

Here we know that $F_{\text{in}} = F_{\text{out}}$, which should look a lot like the $\alpha = 1$ case for the albedo boundary condition. The reflection boundary condition is

$$\hat{\mathbf{n}}\cdot\mathbf{F} = 0 \tag{2.1.31}$$

Table 2.1 lists the factors $\mathcal{A}$, $\mathcal{B}$, and $\mathcal{C}$ for all the different boundary conditions in the form of Eq. 2.1.21 listed here.

2.1.3 Miscellaneous Quantities

The Planck function [21, 26] is defined as

$$B(T_m, \epsilon) = \frac{8\pi\epsilon^3}{h^3c^3\left(e^{\epsilon/kT} - 1\right)}. \tag{2.1.32}$$

where k is Boltzmann's constant, and h is Planck's constant. This normalization for the angle integrated Planck function in Eq. 2.1.32 makes $B(T_m, \epsilon)$ have the same

Boundary Condition	$\mathcal{A}$	$\mathcal{B}$	$\mathcal{C}$
Dirichlet	1	0	E_0
Vacuum	$-1/2$	1	0
Source	$-1/2$	1	$-2F_{\text{in}} = -B(T_{\text{source}})/2$
Reflection	0	1	0
Albedo	$-\frac{1}{2}(1-\alpha)/(1+\alpha)$	1	0

Table 2.1. Coefficients for the diffusion boundary conditions.

units as the radiation energy density E_r. Integrating Eq. 2.1.32 over all photon energies yields

$$B(T_m) = \frac{8\pi^5 k^4}{15h^3c^3} T_m^4 = aT_m^4 \tag{2.1.33}$$

where a is called the black body constant. When the material is in equilibrium with the radiation field, the energy density is equal to the Planck function, or $E_r(\epsilon) = B(T_m, \epsilon)$.

The radiation flux $\mathbf{F}$ (Eq. 2.1.5) is used to calculate the net power though a surface, namely

$$P_{\text{surface}} = \int_S \int_0^\infty c\mathbf{F}(\epsilon) \cdot \, \mathrm{d}\epsilon \, \mathrm{d}\mathbf{A} \tag{2.1.34}$$

where S is the surface and $\mathrm{d}\mathbf{A}$ is a surface area element which points outward.

Another quantity, the radiation temperature, is defined as

$$T_r = \left(\frac{1}{a} \int_0^\infty E_r(\epsilon) \, \mathrm{d}\epsilon \right)^{\frac{1}{4}}. \tag{2.1.35}$$

2.1.4 The Multigroup Approximation

In order to deal with the energy dependence of the diffusion equation, Eq. 2.1.1 is typically integrated over an photon energy ranges to define new diffusion equations for groups of photon energies. Each term in the integrated equation is defines integrated quantities that will be used. Integrating Eq. 2.1.1 yields

$$\int_{\epsilon_g}^{\epsilon_{g+1}} \left[\frac{1}{c} \frac{\partial E_r(\epsilon)}{\partial t} - \nabla \cdot D(\epsilon) \nabla E_r(\epsilon) = \sum_{m=1}^{M} \alpha_m \sigma_{a,m}(\epsilon)(B(T_m, \epsilon) - E_r(\epsilon)) + \frac{1}{c} S_r(\epsilon) \right] \mathrm{d}\epsilon. \tag{2.1.36}$$

2.1.4.1 Group Integrated and Averaged Quantities

We can use Eq. 2.1.36 to come up group integrated and averaged quantities that make the group equations as close the to integrated equation as possible.

The energy integral can be pushed through the time derivative as follows:

$$\int_{\epsilon_g}^{\epsilon_{g+1}} \frac{1}{c}\frac{\partial E_r(\epsilon)}{\partial t}\,\mathrm{d}\epsilon = \frac{1}{c}\frac{\partial}{\partial t}\int_{\epsilon_g}^{\epsilon_{g+1}} E_r(\epsilon)\,\mathrm{d}\epsilon. \tag{2.1.37}$$

This defines a new quantity

$$E_g = \int_{\epsilon_g}^{\epsilon_{g+1}} E_r(\epsilon)\,\mathrm{d}\epsilon \tag{2.1.38}$$

where E_g is the radiation energy density in group g. Similarly the group inhomogeneous source, S_g, can be defined as

$$S_g = \int_{\epsilon_g}^{\epsilon_{g+1}} S_r(\epsilon)\,\mathrm{d}\epsilon. \tag{2.1.39}$$

Because $E_r(\epsilon) = B(T_m, \epsilon)$, it is convenient to define a group black body value as

$$B_g(T_m) = \int_{\epsilon_g}^{\epsilon_{g+1}} B(T_m, \epsilon)\,\mathrm{d}\epsilon. \tag{2.1.40}$$

We can define a group averaged opacity by ensuring that the group averaged terms is consistent with the integral terms in Eq. 2.1.36. This leads to

$$\int_{\epsilon_g}^{\epsilon_{g+1}} \sigma_{a,m}(\epsilon)B(T_m, \epsilon)\,\mathrm{d}\epsilon = \sigma_{a,g,m}B_g(T_m) \tag{2.1.41}$$

or

$$\sigma_{a,g,m} = \frac{\int_{\epsilon_g}^{\epsilon_{g+1}} \sigma_{a,m}(\epsilon)B(T_m, \epsilon)\,\mathrm{d}\epsilon}{\int_{\epsilon_g}^{\epsilon_{g+1}} B(T_m, \epsilon)\,\mathrm{d}\epsilon} \tag{2.1.42}$$

This is also known as the Planck-averaged opacity. If the material is in equilibrium with the radiation field, this average would also make the the removal term $\sigma_{a,m}E_r$ exact. However, this is not normally the case, and we should define another opacity average using

$$\sigma'_{a,g,m} = \frac{\int_{\epsilon_g}^{\epsilon_{g+1}} \sigma_{a,m}(\epsilon)E_r(\epsilon)\,\mathrm{d}\epsilon}{\int_{\epsilon_g}^{\epsilon_{g+1}} E_r(\epsilon)\,\mathrm{d}\epsilon} \tag{2.1.43}$$

However, we don't know the details of the energy density since that's what we're solving. Typically, Eq. 2.1.42 is used as an approximation.

We would also like to define a group-averaged diffusion coefficient so that

$$D_g \nabla E_g = \int_{\epsilon_g}^{\epsilon_{g+1}} D \nabla E_r(\epsilon)\, \mathrm{d}\epsilon, \tag{2.1.44}$$

but this is impossible to do because we cannot know E_r. Assuming again that the equilibrium condition $E_r = B(T, \epsilon)$ holds, we get

$$D_g \nabla B_g = \int_{\epsilon_g}^{\epsilon_{g+1}} D \nabla B(T, \epsilon)\, \mathrm{d}\epsilon, \tag{2.1.45}$$

and T is some average material temperature. (Exactly how to get this average isn't important, because we're not going to use it anyway.) Using the chain rule on the gradient of B, we get

$$D_g \frac{\partial B_g}{\partial T} \nabla T = \int_{\epsilon_g}^{\epsilon_{g+1}} D \frac{\partial B(T, \epsilon)}{\partial T}\, \mathrm{d}\epsilon \nabla T. \tag{2.1.46}$$

And finally we get

$$D_g = \int_{\epsilon_g}^{\epsilon_{g+1}} D f_B\, \mathrm{d}\epsilon \tag{2.1.47}$$

where

$$f_B = \frac{\frac{\partial B(T,\epsilon)}{\partial T}}{\frac{\partial B_g}{\partial T}} \tag{2.1.48}$$

is the normalized derivative. Eq. 2.1.47 is the best approximation possible, and we can compute this approximation exactly for one material problems without a flux limiter. Further approximations must be done when using flux limiters and multiple materials. Generally, the flux limiter argument is assumed to be constant over the group, namely

$$\chi(E_r, \nabla E_r, \sigma_t) \approx \chi(E_g, \nabla E_g, \sigma_t^g) \tag{2.1.49}$$

where σ_t^g is some group averaged total opacity, which is about to be defined. Once we make the approximation in Eq. 2.1.49, Eq. 2.1.47 reduces to

$$\frac{1}{\sigma_t^g} = \left\langle \frac{1}{\sum_{m=1}^{M} \alpha_m \sigma_{t,m}} \right\rangle_g = \int_{\epsilon_g}^{\epsilon_{g+1}} \frac{f_B}{\sum_{m=1}^{M} \alpha_m \sigma_{t,m}}\, \mathrm{d}\epsilon \tag{2.1.50}$$

where σ_t^g is a Rosseland weighted total opacity. Typically the code only has access to the Rosseland opacities for the individual materials, namely

$$\frac{1}{\sigma_{t,m}^g} = \left\langle \frac{1}{\sigma_{t,m}} \right\rangle_g = \int_{\epsilon_g}^{\epsilon_{g+1}} \frac{f_B}{\sigma_{t,m}}\, \mathrm{d}\epsilon \tag{2.1.51}$$

where $\sigma_{t,m}^g$ is a Rosseland weighted total opacity for the single material. These need to be combined multi-material cells in such a way to preserve certain properties. If the materials have identical detailed opacities, the average of the individual

opacities should be the same as the average of the combination. For example, for two materials and for $\sigma_{t,1} = \sigma_{t,2} = \sigma$, then Eq. 2.1.50 becomes

$$\int_{\epsilon_g}^{\epsilon_{g+1}} \frac{f_B}{\alpha_1\sigma + \alpha_2\sigma}\,\mathrm{d}\epsilon = \int_{\epsilon_g}^{\epsilon_{g+1}} \frac{f_B}{\sigma}\,\mathrm{d}\epsilon = \left\langle \frac{1}{\sigma} \right\rangle_g = \frac{1}{\sigma^g} \tag{2.1.52}$$

Also, if any of the volume fractions are zero, we would like the multi-material average to be the average of the remaining opacities. For example, for two materials and $\alpha_1 = 1$ and $\alpha_2 = 0$, then Eq. 2.1.50 becomes

$$\int_{\epsilon_g}^{\epsilon_{g+1}} \frac{f_B}{\sigma_{t,1}}\,\mathrm{d}\epsilon = \left\langle \frac{1}{\sigma_{t,1}} \right\rangle_g = \frac{1}{\sigma_{t,1}^g} \tag{2.1.53}$$

Finally, if any of the opacities are zero, the correct thing should happen. Again, using our two material example, but now $\sigma_{t,2} = 0$, Eq. 2.1.50 becomes

$$\int_{\epsilon_g}^{\epsilon_{g+1}} \frac{f_B}{\alpha_1\sigma_{t,1}}\,\mathrm{d}\epsilon = \left\langle \frac{1}{\alpha_1\sigma_{t,1}} \right\rangle_g = \frac{1}{\alpha_1\sigma_{t,1}^g} \tag{2.1.54}$$

An approximation that meets these three conditions is

$$\sigma_t^g \approx \sum_{m=1}^{M} \alpha_m \sigma_{t,m}^g \tag{2.1.55}$$

While it looks like we went through a lot of work to define something simple, there are several other simple averages that would not have been appropriate.

The simple volume fraction averaging of the individual Rosseland averages is an approximation. Depending on the detailed energy dependence of the opacities, it is possible to get an extremely inaccurate total opacity, especially for one group calculations.

With these approximations, the estimate for the group diffusion coefficient (Eq. 2.1.47) is

$$D_g = \frac{\chi(E_g, \nabla E_g, \sigma_t^g)}{\sigma_t^g}. \tag{2.1.56}$$

For problems with void, the diffusion coefficient can be infinite. In practice, this value is limited to some large value that allows the problem to be solved numerically without changing the answer too much. (Typically the large value is about one hundred times the physical problem domain.)

Many approximations were made to get the group averaged material values. This is why multigroup simulations are very important. It is impossible to define an exact integrated equation. Using many groups reduces the error of all of the approximations made to an acceptable level.

2.1.4.2 The Multigroup Equations

Using all the group averaged quantities from the last section, we can approximate Eq. 2.1.36 as

$$\frac{1}{c}\frac{\partial E_g}{\partial t} - \nabla \cdot D_g \nabla E_g = \sum_{m=1}^{M} \alpha_m \sigma_{a,g,m}(B_g(T_m) - E_g) + \frac{1}{c} S_g. \tag{2.1.57}$$

The material equation becomes

$$\frac{\partial u_m}{\partial t} = Q_m + \sum_g \alpha_m c \sigma_{a,g,m} \left(E_g - B_g(T_m)\right). \tag{2.1.58}$$

Note that the energy groups are only coupled to each other through the material equation. This is a nonlinear system of equations.

2.1.4.3 The Multigroup Planck Function

The work in this section is a summary of the work presented in [12, 7], and is included for completeness. In the multigroup equations, the Planck function, Eq. 2.1.3, integrated over the energy group appears as

$$B_g(T) = \int_{\epsilon_g}^{\epsilon_{g+1}} \frac{8\pi}{h^3 c^3} \frac{\epsilon^3}{\mathrm{e}^{\epsilon/kT} - 1} \, \mathrm{d}\epsilon. \tag{2.1.59}$$

Introducing a change of variables, $\varepsilon = \epsilon/kT$, yields

$$B_g(T) = \frac{8\pi k^4 T^4}{h^3 c^3} \int_{\varepsilon_g}^{\varepsilon_{g+1}} \frac{\varepsilon^3}{\mathrm{e}^{\varepsilon} - 1} \, \mathrm{d}\varepsilon. \tag{2.1.60}$$

To compute the integral, we will introduce another change of variables, namely

$$z = \mathrm{e}^{-\varepsilon}, \tag{2.1.61}$$

to give us

$$\int_{\varepsilon_g}^{\varepsilon_{g+1}} \frac{\varepsilon^3}{\mathrm{e}^{\varepsilon} - 1} \, \mathrm{d}\varepsilon = \int_{z_g}^{z_{g+1}} \frac{(\ln z)^3}{1 - z} dz \tag{2.1.62}$$

Computing the integral gives us

$$\int_{z_g}^{z_{g+1}} \frac{(\ln z)^3}{1 - z} dz = \frac{\pi^4}{15} + (\ln z)^3 \operatorname{Li}_1 z - 3(\ln z)^2 \operatorname{Li}_2 z + 6(\ln z) \operatorname{Li}_3 z - 6 \operatorname{Li}_4 z \Big|_{z_g}^{z_{g+1}} \tag{2.1.63}$$

where $\operatorname{Li}_n z$ is the polylog function defined by

$$\operatorname{Li}_n z = \sum_{k=1}^{\infty} \frac{z^k}{k^n}. \tag{2.1.64}$$

In practice, Eq. 2.1.63 is evaluated only for large $\varepsilon > 2.061981$, which implies small z. In this limit, we can evaluate the first several terms of the series that defines the polylog functions, Eq. 2.1.64. For small ε, where it is difficult to evaluate the polylog, we expand the exact integral as

$$\begin{aligned}\int_{\varepsilon_g}^{\varepsilon_{g+1}} \frac{\varepsilon^3}{\mathrm{e}^{\varepsilon}-1}\,\mathrm{d}\varepsilon \approx & \frac{\varepsilon^3}{3} - \frac{\varepsilon^4}{8} + \frac{\varepsilon^5}{60} - \frac{\varepsilon^7}{5040} + \frac{\varepsilon^9}{272160} \\ & - \frac{\varepsilon^{11}}{13305600} + \frac{\varepsilon^{13}}{622702080} - \frac{691\varepsilon^{15}}{19615115520000} \\ & + \frac{\varepsilon^{17}}{1270312243200} - \frac{3617\varepsilon^{19}}{202741834014720000} \\ & + \frac{43867\varepsilon^{21}}{10729097856058982400 0} + O\left(\varepsilon^{23}\right)\Big|_{\varepsilon_g}^{\varepsilon_{g+1}}.\end{aligned} \tag{2.1.65}$$

Additionally, the derivative with respect to temperature of the group integrated Planck function is also needed,

$$\frac{\partial B_g(T)}{\partial T} = \frac{8\pi k^4 T^3}{h^3 c^3}\left[4\int_{\varepsilon_g}^{\varepsilon_{g+1}} \frac{\varepsilon^3}{\mathrm{e}^{\varepsilon}-1}\,\mathrm{d}\varepsilon + \frac{\varepsilon_g^4}{\mathrm{e}^{\varepsilon_g}-1} - \frac{\varepsilon_{g+1}^4}{\mathrm{e}^{\varepsilon_{g+1}}-1}\right] \tag{2.1.66}$$

where the Leibniz Integration Rule has been applied since the integration limits, ε, also depend on temperature.

2.2 Nodal Finite Elements

The NEVADA framework centers material properties on element centers. The discretization used for the diffusion is based on node centered variables using a Galerkin finite element method with linear continuous shape functions on isoparametric elements.

The code is meant to support different diffusion approximations and even different physics. Instead of working with the specific instance of Eq. 2.1.57, a general diffusion equation will be used.

2.2.1 The Generalized Diffusion Equation

We will assume that there are G diffusion equations that can be coupled together through some sort of inelastic scattering process (or something that acts like it. The general diffusion equation we will use is

$$\frac{\partial \mathsf{E}_g}{\partial t} = \nabla\cdot \mathsf{D}_g \nabla \mathsf{E}_g - \sigma_g \mathsf{E}_g + \sum_{g'} \sigma_s^{g'\to g}\mathsf{E}_{g'} + \mathsf{S}_g \tag{2.2.1}$$

The notation here is very similar to that of Eq. 2.1.57, but the terms are slightly different. In this form, the σ's have units of inverse time and represent reaction rates. Note that the group to group source includes within-group scattering, the σ_g removal term should contain a removal term equivalent to this source.

2.2.2 The Discretization of Energy Density

The radiation energy density, E_g, is assumed to have the form

$$\mathsf{E}_g(\mathbf{x}, t) = \sum_{j=1}^{n_{\text{nodes}}} \mathsf{E}_j(t)\phi_j(\mathbf{x}). \tag{2.2.2}$$

where the shape functions ϕ_j are linear basis functions that cover the domain, and have a value of one at node j linearly decreasing to zero at each of the neighboring nodes.

2.2.3 The Integration of the Diffusion Equation

First we multiply the diffusion equation, Eq. 2.2.1, by an arbitrary weight function and integrate over the entire problem domain D, yielding

$$\int_D w\frac{\partial \mathsf{E}_g}{\partial t}\,\mathrm{d}V = \int_D w\left[\nabla\cdot\mathsf{D}_g\nabla\mathsf{E}_g - \sigma_g\mathsf{E}_g + \sum_{g'}\sigma_s^{g'\to g}\mathsf{E}_{g'} + \mathsf{S}_g\right]\mathrm{d}V. \tag{2.2.3}$$

Integrating by parts and using the divergence theorem on the diffusion term yields

$$\int_D w\frac{\partial \mathsf{E}_g}{\partial t}\,\mathrm{d}V = \int_S w\mathsf{D}_g\nabla\mathsf{E}_g\cdot\mathrm{d}\mathbf{A} + \int_D\left[w\sum_{g'}\sigma_s^{g'\to g}\mathsf{E}_{g'} - (\nabla w)\cdot(\mathsf{D}_g\nabla\mathsf{E}_g) - w\sigma_g\mathsf{E}_g + w\mathsf{S}_g\right]\mathrm{d}V \tag{2.2.4}$$

where $\mathrm{d}\mathbf{A}$ is a differential surface area and points outward from the element and S is the surface of the domain D. The next step is to insert the approximate form of E_g expressed in Eq. 2.2.2 into Eq. 2.2.4 and divide the integral the entire domain into a sum of volume integrals over each element in the problem; this yields

$$\sum_e\sum_j\int_{D_e} w\frac{\partial}{\partial t}\mathsf{E}_j^g\phi_j\,\mathrm{d}V = \sum_e\sum_j\int_{S_e} w\mathsf{D}_g\nabla\mathsf{E}_j^g\phi_j\cdot\mathrm{d}\mathbf{A} + \sum_e\int_{D_e} w\mathsf{S}_g\,\mathrm{d}V$$
$$+\sum_e\sum_j\int_{D_e}\left[w\sum_{g'}\sigma_s^{g'\to g}\mathsf{E}_j^{g'}\phi_j - (\nabla w)\cdot(\mathsf{D}_g\nabla\mathsf{E}_j^g\phi_j) - w\sigma_g\mathsf{E}_j^g\phi_j\right]\mathrm{d}V. \tag{2.2.5}$$

All the weight functions ϕ_i are linearly independent, so using them as the weight functions w will give us n_{nodes} linearly independent equations that we can solve for the nodal values of the radiation energy density E_j^g. Inserting ϕ_i for w yields

$$\sum_e \sum_j \frac{\partial}{\partial t} \mathsf{E}_j^g \int_{D_e} \phi_i \phi_j \, \mathrm{d}V = \sum_e \sum_j \mathsf{E}_j^g \int_{S_e} \phi_i \mathsf{D}_g \nabla \phi_j \cdot \mathrm{d}\mathbf{A} + \sum_e \int_{D_e} \mathsf{S}_g \phi_i \, \mathrm{d}V$$
$$+ \sum_e \sum_j \int_{D_e} \left[\sum_{g'} \sigma_s^{g' \to g} \mathsf{E}_j^{g'} \phi_i \phi_j - (\nabla \phi_i) \cdot (\mathsf{D}_g \nabla \mathsf{E}_j^g \phi_j) - \sigma_g \mathsf{E}_j^g \phi_i \phi_j \right] \mathrm{d}V. \quad (2.2.6)$$

Because the weight functions are zero everywhere except in the elements surrounding the node to which they belong, the sum over all elements and all nodes can be reduced to a sum over all elements adjacent to node i and to a sum over nodes j in this restricted set of elements. Additionally, all the integrals on the internal surfaces of the elements cancel except on the boundary of the domain. We will compute these integrals over the weight functions in normalized coordinates, so $\mathrm{d}V$ is replaced by $|J(\xi)| \, \mathrm{d}\xi$ and similarly for the surface integral; $|J(\xi)|$ is the Jacobian of transformation between the real coordinates and the normalized coordinates. The NEVADA framework provides these Jacobians, along with convenient quadrature integration mechanisms. (This needs to be better documented.)

2.2.4 Boundary Conditions

The boundary term in Eq. 2.2.6 does not have to be evaluated directly. We can break the boundary conditions listed in Section 2.1.2 into two classes: Dirichlet and all the others. We implement Dirichlet boundary conditions by modifying the matrix rows associated with the nodal value E_i^g on the boundary so that $\mathsf{E}_i^g = \mathsf{E}_0^g$, where E_0^g is the prescribed boundary value.

All the other boundary conditions can then be written in the form of Eq. 2.1.21 with $\mathcal{B}$ set to one. Just as we did for the diffusion equation, we multiply Eq. 2.1.21 by a weight function and integrate over a surface. Integrating Eq. 2.1.21 over the boundary face of the element yields

$$-\sum_j \mathsf{D}_g \mathsf{E}_j^g \int_{\Gamma_s} \phi_i \nabla \phi_j \cdot \mathrm{d}\mathbf{A} = \mathcal{C}_g \int_{\Gamma_s} \phi_i \hat{\mathbf{n}} \cdot \mathrm{d}\mathbf{A} - \sum_j \mathcal{A}_g \mathsf{E}_j \int_{\Gamma_s} \phi_i \phi_j \hat{\mathbf{n}} \cdot \mathrm{d}\mathbf{A}. \quad (2.2.7)$$

where the values of $\mathcal{A}_g$ and $\mathcal{C}_g$ are set according to Table 2.1. We can use the right hand side of Eq. 2.2.7 to compute the surface integration term in Eq. 2.2.6.

2.2.5 Lumped Mass Matrix

All of the terms in Eq. 2.2.6 and Eq. 2.2.7 that have a $\phi_i\phi_j$ factor contribute to part of the linear system called the mass matrix. The mass matrix for an element couples all the nodes of that element together, but typically these terms describe local processes such as absorption, for instance. This can lead to unphysical instabilities in the solution. The mass matrix can be lumped by summing each row and placing the sum on the diagonal of the matrix. The off diagonals are then zeroed. This procedure is called lumping. With the mass matrix terms lumped, Eq. 2.2.6 becomes

$$\sum_e \frac{\partial}{\partial t}\mathsf{E}_i^g \int_{D_e} \phi_i \,\mathrm{d}V = \sum_e \sum_j \mathsf{E}_j^g \int_{S_e} \phi_i \mathsf{D}_g \nabla\phi_j \cdot \mathrm{d}\mathbf{A} + \sum_e \int_{D_e} \mathsf{S}_g \phi_i \,\mathrm{d}V$$
$$+\sum_e \sum_{g'} \mathsf{E}_i^{g'} \int_{D_e} \sigma_s^{g'\to g}\phi_i \,\mathrm{d}V - \sum_e \sum_j \mathsf{E}_j^g \int_{D_e} (\nabla\phi_i)\cdot(\mathsf{D}_g\nabla\phi_j)\,\mathrm{d}V - \sum_e \mathsf{E}_i^g \int_{D_e} \sigma_g \phi_i \,\mathrm{d}V. \tag{2.2.8}$$

The boundary conditions, Eq. 2.2.7 should also be lumped to yield

$$-\sum_j \mathsf{E}_j^g \int_{\Gamma_s} \phi_i \mathsf{D}_g \nabla\phi_j \cdot \mathrm{d}\mathbf{A} = \mathcal{C}_g \int_{\Gamma_s} \phi_i \hat{\mathbf{n}} \cdot \mathrm{d}\mathbf{A} - \mathcal{A}_g \mathsf{E}_i \int_{\Gamma_s} \phi_i \hat{\mathbf{n}} \cdot \mathrm{d}\mathbf{A}. \tag{2.2.9}$$

The left hand side of Eq. 2.2.9 is also in Eq. 2.2.8; the right hand side of Eq. 2.2.9 is substitute for this term at the boundaries of the system.

Lumping the equations is also critical to conserving energy. Integrating the material equation (done below) using the approximation in Eq. 2.2.2 results in emission and absorption terms that are exactly the ones found in Eq. 2.2.8, but not Eq. 2.2.6. *This needs to be proved more rigorously.*

2.2.6 Energy Tallies

If we set $w = 1$ in Eq. 2.2.5, we get an equation that defines energy conservation for our problem. This defines several processes that we can tally for the user. The power emitted by the source is

$$P_{\text{source}} = \sum_e \int_{D_e} \mathsf{S}_g \,\mathrm{d}V. \tag{2.2.10}$$

The source power P_{source} can be further broken down into various sources, such as the power from black body emission or arbitrary external sources. Radiation is absorbed by the material with the power

$$P_{\text{absorb}} = \sum_e \sum_j \sum_g \int_{D_e} \sigma_g \mathsf{E}_j^g \phi_j \,\mathrm{d}V. \tag{2.2.11}$$

The total energy in the radiation field is a sum over all elements e

$$\hat{E}_{\text{rad}} = \sum_e \int_{D_e} \sum_i \sum_g \mathsf{E}_i^g \phi_i \, \mathrm{d}V \tag{2.2.12}$$

This leaves the net leak rate from the entire surface of the problem. The most accurate (and convenient) way to calculate this is to use the other terms, namely

$$P_{\text{net leak}} = P_{\text{source}} - P_{\text{absorb}} - \frac{\hat{E}_{\text{rad}}^{n+1} - \hat{E}_{\text{rad}}^{n}}{\Delta t} \tag{2.2.13}$$

2.2.6.1 Flux Through Arbitrary Surfaces

The net radiation power through a surface is defined by Eq. 2.1.34; in multigroup form this equation is

$$P_{\text{surface}} = -\int_S \sum_g \mathsf{D}_g (\nabla \mathsf{E}_g) \cdot \hat{\mathbf{n}} \, \mathrm{d}A \tag{2.2.14}$$

where $\hat{\mathbf{n}}$ is the orientation of the surface. In our discretized system, D_g is an element centered variable and can be discontinuous at the surface of interest. Additionally, the gradient, $\nabla \mathsf{E}_g$, is discontinuous at the surface because of the shape of our basis functions ϕ_i. These two problems make it difficult to do the surface integral accurately, so something more complicated than the simple integral in Eq. 2.2.14 is needed to calculate the power accurately.

We can change the open surface integral into a closed surface integral with the same result by multiplying by some function w that is equal to one on the original open surface and zero on the rest of the surface.

$$P_{\text{surface}} = -\int_{S'} \sum_g w \mathsf{D}_g (\nabla \mathsf{E}_g) \cdot \hat{\mathbf{n}} \, \mathrm{d}A \tag{2.2.15}$$

where S' is the closed surface that contains S. Figure 2.1 shows the original surface one which the flux tally is requested, and the augmented surfaces added to make it a closed surface.

The function w is still unspecified on the interior of the closed surface, but it should have reasonably nice properties in order to proceed. Inspecting Eq. 2.2.4, we notice that the right hand side of Eq. 2.2.15 is the sum over all groups of one of the terms. Solving for this term in Eq. 2.2.4 gives us the surface power in terms of volume integrals, namely

$$\begin{aligned} P_{\text{surface}} = &-\sum_g \int_{D'} w \frac{\partial \mathsf{E}_g}{\partial t} \, \mathrm{d}V \\ &+ \sum_g \int_{D'} \left[w \sum_{g'} \sigma_s^{g' \to g} \mathsf{E}_{g'} - (\nabla w) \cdot (\mathsf{D}_g \nabla \mathsf{E}_g) - w \sigma_g \mathsf{E}_g + w \mathsf{S}_g \right] \mathrm{d}V \end{aligned} \tag{2.2.16}$$

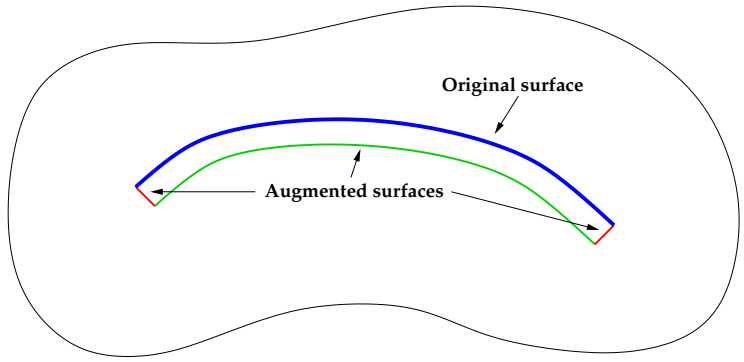

Figure 2.1. The blue curve is the surface on which the flux tally is requested. The original surface is augmented with extra surfaces in order to create a closed surface. The function w is set to one on the blue surface and zero on the green surface. Ideally w would be zero on the two red surfaces at the end, but this is not possible because w must be representable by a finite element expansion (Eq. 2.2.2). There will be some contribution to the tally by flux crossing the red surfaces. In some cases this can lead to a considerable error.

where D' is the volume enclosed by the surface S'.

In order to actually perform the integration, w must be defined. Because this is a finite element method, we must restrict our choice of w to something that can be represented in a finite element expansion, Eq. 2.2.2. This however, means that we cannot exactly represent the w that makes the Eq. 2.2.15 true; we can only use a w that makes this expression approximate. We will use

$$w = \sum_{\{k:\text{nodes on } S\}} \phi_k, \tag{2.2.17}$$

where k is the set of nodes on the original surface S'. There will some contribution of particles leaving the volume out the "ends", where w is decreasing from one to zero in an element.

In addition to the net flux across the surface, we also want to calculate the positive and negative going components of the flux. There are two terms in the

partial flux expressions, Eq. 2.1.19 and Eq. 2.1.20.

$$F_{\text{in}} = \frac{1}{4}\sum_g \mathsf{E}_g + \frac{1}{2}\hat{\mathbf{n}} \cdot \sum_g \mathsf{D}_g \nabla \mathsf{E}_g \tag{2.2.18}$$

$$F_{\text{out}} = \frac{1}{4}\sum_g \mathsf{E}_g - \frac{1}{2}\hat{\mathbf{n}} \cdot \sum_g \mathsf{D}_g \nabla \mathsf{E}_g, \tag{2.2.19}$$

The first term is simply the energy density; we can perform a simple surface integral for this. The other term is the net flux we've already calculated.

2.3 Linearized Semi-Implicit Solution

The coupled radiation diffusion equations, Eq. 2.1.57 and Eq. 2.1.58, are nonlinear. In many cases linearizing these equations is sufficient. The first step is to assume that all material properties are evaluated at the beginning of the time step. Even so, we are still left with the nonlinear function $B_g(T_m)$ in the equations. What follows linearizes this term as well. The radiation energy density is still solved for implicitly; only the material quantities are explicit.

Rewriting Eq. 2.1.57 and Eq. 2.1.58 again as

$$\frac{1}{c}\frac{\partial E_g}{\partial t} - \nabla \cdot D_g \nabla E_g = \frac{1}{c} S_g + \sum_m \alpha_m \sigma_{a,g,m}(B_g(T_m) - E_g) \tag{2.3.1}$$

$$\frac{\partial u_m}{\partial t} = Q_m + \sum_g \alpha_m c \sigma_{a,g,m}(E_g - B_g(T_m)), \tag{2.3.2}$$

We can now discretize in time using first order implicit differencing to yield

$$\frac{1}{\Delta t}(E_g^{n+1} - E_g^n) - \nabla \cdot c D_g \nabla E_g^{n+1} = S_g + \sum_m \alpha_m c \sigma_{a,g,m}(B_g(T_m^{n+1}) - E_g^{n+1}) \tag{2.3.3}$$

$$\frac{\rho_m C_{v,m}}{\Delta t}(T_m^{n+1} - T_m^n) = Q'_m + \sum_g c \sigma_{a,g,m}(E_g^{n+1} - B_g(T_m^{n+1})), \tag{2.3.4}$$

where $u_m = \rho_m C_{v,m} T_m$, ρ_m is the material density, $Q'_m = Q_m/\alpha_m$, and $C_{v,m}$ is the heat capacity. All quantities, unless otherwise notated by a superscript, are evaluated at the beginning of the time step.

Because $B_g(T)$ is the only term which is always nonlinear (the opacities could be constant), we will linearly expand it around the old temperature in order to evaluate it at the new temperature to get

$$B_g(T_m^{n+1}) \approx B_g(T_m^n) + \frac{\partial B_g(T_m^n)}{\partial T}(T_m^{n+1} - T_m^n) = B_g^\star(T_m). \tag{2.3.5}$$

We will solve for $B_g^\star(T_m^n)$ using Eq. 2.3.5 and Eq. 2.3.4. We will then be able to insert this expression for $B_g^\star(T_m^n)$ into Eq. 2.3.3. The resulting equation will be linear.

To do this, we will first solve for the new material temperature and insert into Eq. 2.3.4 yielding

$$\frac{\rho_m C_{v,m}}{\Delta t}\frac{B_g^\star(T_m) - B_g(T_m^n)}{B_g'(T_m^n)} = Q_m' + \sum_{g'} c\sigma_{a,g',m}E_{g'}^{n+1} - \sum_{g'} c\sigma_{a,g',m}B_{g'}^\star(T_m), \quad (2.3.6)$$

where $B_g'(T_m^n)$ is the temperature derivative of $B_g(T_m^n)$. Expanding $B_{g'}^\star(T_m^n)$ and inserting the temperature difference solved from Eq. 2.3.5 yields

$$\begin{aligned}&\frac{\rho_m C_{v,m}}{\Delta t}\frac{B_g^\star(T_m^n) - B_g(T_m^n)}{B_g'(T_m^n)}\\ &= Q_m' + \sum_{g'} c\sigma_{a,g',m}E_{g'}^{n+1} - \sum_{g'} c\sigma_{a,g',m}B_{g'}(T_m^n) - \frac{B_g^\star(T_m) - B_g(T_m^n)}{B_g'(T_m^n)}\sum_{g'} c\sigma_{a,g',m}B_{g'}'(T_m^n)\end{aligned} \quad (2.3.7)$$

This last step eliminated the sum over groups on $B_{g'}^\star(T_m^n)$, allowing us to solve for $B_g^\star(T_m^n)$. Before doing this, however, we will define some new variables to make life easier:

$$\tau = \frac{1}{\Delta t} \qquad \kappa_m = \left[\sum_{g'} c\sigma_{a,g',m}B_{g'}'(T_m^n) + \frac{\rho_m C_{v,m}}{\Delta t}\right]^{-1} \quad (2.3.8)$$

Finally solving for $B_g^\star(T_m^n)$ yields

$$B_g^\star(T_m) = B_g(T_m^n) + B_g'(T_m^n)\kappa_m\left(Q_m' + \sum_{g'} c\sigma_{a,g',m}E_{g'}^{n+1} - \sum_{g'} c\sigma_{a,g',m}B_{g'}(T_m^n)\right). \quad (2.3.9)$$

Finally inserting all of this into the diffusion equation (Eq. 2.3.3) give us

$$\begin{aligned}&\left(\tau + \sum_m \alpha_m c\sigma_{a,g,m}\right)E_g^{n+1} - \nabla\cdot cD_g\nabla E_g^{n+1} = S_g + \tau E_g^n\\ &+\sum_m \alpha_m c\sigma_{a,g}\left(B_g(T_m^n) + B_g'(T_m^n)\kappa_m\left[Q_m' + \sum_{g'} c\sigma_{a,g',m}E_{g'}^{n+1} - \sum_{g'} c\sigma_{a,g',m}B_{g'}(T_m^n)\right]\right)\end{aligned} \quad (2.3.10)$$

Eq. 2.3.10 is an equation for energy group g, and it is coupled to the other group

equations. We can now define the terms of Eq. 2.2.8 as

$$\mathsf{E}_g = E_g^{n+1} \tag{2.3.11}$$

$$\mathsf{D}_g = cD_g \tag{2.3.12}$$

$$\mathsf{S}_g = S_g + \sum_m \alpha_m c\sigma_{a,g} \left(B_g(T_m^n) + B_g'(T_m^n)\kappa_m \left[Q_m' - \sum_{g'} c\sigma_{a,g',m} B_{g'}(T_m^n) \right] \right) \tag{2.3.13}$$

$$\sigma_g = \sum_m \alpha_m c\sigma_{a,g,m} \tag{2.3.14}$$

$$\sigma_s^{g'\to g} = \sum_m \alpha_m c\sigma_{a,g} B_g'(T_m^n)\kappa_m c\sigma_{a,g',m} \tag{2.3.15}$$

The $\sigma_s^{g'\to g}$ terms couple each group equation to all other groups. Additionally, the full linear system is non-symmetric.

It is also possible to decouple the group equations by evaluating some of the energy density terms at the beginning of the time step. We define an estimated temperature change as

$$\Delta T_{\text{est}} = \kappa_m \left(Q_m' + \sum_{g'} c\sigma_{a,g',m} E_{g'}^n - \sum_{g'} c\sigma_{a,g',m} B_{g'}(T_m^n) \right). \tag{2.3.16}$$

We can then use Eq. 2.3.16 in Eq. 2.3.10 to define another set of coefficients for Eq. 2.2.8 as

$$\mathsf{E}_g = E_g^{n+1} \tag{2.3.17}$$

$$\mathsf{D}_g = cD_g \tag{2.3.18}$$

$$\mathsf{S}_g = S_g + \sum_m \alpha_m c\sigma_{a,g} \left[B_g(T_m^n) + B_g'(T_m^n)\Delta T_{\text{est}} \right] \tag{2.3.19}$$

$$\sigma_g = \sum_m \alpha_m c\sigma_{a,g,m} \tag{2.3.20}$$

$$\sigma_s^{g'\to g} = 0 \tag{2.3.21}$$

This approximation makes the equations much simpler to solve. Each group be solved separately, and the linear system is symmetric.

Once the radiation energy densities have been solved for using one of these two approximations, the estimated temperature difference can be computed using Eq. 2.3.16 by using the appropriate energy density, either E_g^{n+1} or E_g^n for the fully coupled problem or the decoupled problem, respectively. Once ΔT_{est} is calculated,

the energy increments can be calculated using

$$\delta u_m = \Delta t Q_m + \Delta t \sum_g \alpha_m c \sigma_{a,m,g} E_g^{n+1} - \Delta t \sum_g \alpha_m c \sigma_{a,m,g} B_g(T_m^n) - \Delta t \sum_g \alpha_m c \sigma_{a,m,g} B_g'(T_m^n) \Delta T_{\text{est}}. \quad (2.3.22)$$

2.4 Solution Methods

In this section, the heart of the new ideas developed with LDRD are presented. Several different solution techniques for solving the system of equations defined by Eq. 2.2.1 are presented. Most methods in the past have used simple, Richardson-like iteration methods to converge the between group coupling. Morel [22] presents this history as well as proposes another advanced method. Morel's method should be compared against the ones presented here as well as with a full nonlinear solve.

The methods below have been implemented and correctly solve the equations, but significant testing to determine their effectiveness still needs to be done.

2.4.1 Operator Form

Eq. 2.2.1 is a system of equations for the energy densities in each group. We can rewrite Eq. 2.2.1 in term of operators as

$$\mathbf{D}_g x_g + \sum_{g'=1}^{G} \mathbf{C}_{g,g'} x_{g'} = b_g, \quad (2.4.1)$$

where

$$\mathbf{D}_g = -\nabla \cdot \mathsf{D}_g \nabla + \frac{1}{\Delta t} + \sigma_g, \quad (2.4.2)$$

$$\mathbf{C}_{g,g'} = -\sigma_s^{g' \to g}, \quad (2.4.3)$$

$$x_g = \mathsf{E}_g, \quad (2.4.4)$$

and

$$b_g = \mathsf{S}_g + \frac{\mathsf{E}_g^{n-1}}{\Delta t}. \quad (2.4.5)$$

The time derivative has also been discretized implicitly using backward Euler. The discrete forms of these operators, defined by Eq. 2.2.8, can also be used. While, when coupled with the material equation, this system is nonlinear, typically some linearizion is used so that a linear system can be solved instead. In the following discussion, we will assume some linearizion.

We can define a large block structured linear system as

$$\mathbf{A}x = b, \tag{2.4.6}$$

where

$$x = \begin{pmatrix} x_1 \\ x_2 \\ \vdots \\ x_G \end{pmatrix} \tag{2.4.7}$$

is the vector of unknown energy densities,

$$b = \begin{pmatrix} b_1 \\ b_2 \\ \vdots \\ b_G \end{pmatrix} \tag{2.4.8}$$

is the right hand side, and

$$\mathbf{A} = \begin{pmatrix} \mathbf{D}_1 + \mathbf{C}_{1,1} & \mathbf{C}_{1,2} & \dots & \mathbf{C}_{1,G} \\ \mathbf{C}_{1,2} & \mathbf{D}_2 + \mathbf{C}_{2,2} & \dots & \mathbf{C}_{2,G} \\ \vdots & \vdots & \ddots & \vdots \\ \mathbf{C}_{1,G} & \mathbf{C}_{2,G} & \dots & \mathbf{D}_G + \mathbf{C}_{G,G} \end{pmatrix} \tag{2.4.9}$$

This large linear system can be solved several ways, two of which are outlined below.

2.4.2 Large System Solve

The obvious method would build the linear system in Eq. 2.4.6 and solve it directly. The $\mathbf{C}_{g,g'}$ terms make $\mathbf{A}$ asymmetric, so some method such as GMRES must be used. With a Krylov method such as GMRES, using a preconditioner is critical to getting good performance. Two preconditioners are suggested here, and are implemented in ALEGRA using the Trilinos solver suite [14].

2.4.2.1 Diagonal Preconditioner

The $\mathbf{C}_{g,g'}$ terms can be small since they come from a linearizion. This suggests one preconditioner, namely a block diagonal approximation to $\mathbf{A}$ that ignores the coupling terms, or

$$\mathbf{A} \approx \mathbf{M}_{\text{diag}} = \begin{pmatrix} \mathbf{D}_1 & & & \\ & \mathbf{D}_2 & & \\ & & \ddots & \\ & & & \mathbf{D}_G \end{pmatrix}. \tag{2.4.10}$$

2.4.2.2 Approximate Grey Preconditioner

If the group to group coupling are non-negligible, another preconditioner can be developed that estimates this coupling. Summing Eq. 2.4.1 over groups yields

$$\sum_{g=1}^{G} \mathbf{D}_g x_g + \sum_{g=1}^{G} \sum_{g'=1}^{G} \mathbf{C}_{g,g'} x_{g'} = \sum_{g=1}^{G} b_g. \tag{2.4.11}$$

We can define a new solution variable,

$$\tilde{x} = \sum_{g} x_g \tag{2.4.12}$$

where $\tilde{x}$ is gray, or one group, energy density. We can also define

$$\eta_g = \frac{x_g}{\tilde{x}} \tag{2.4.13}$$

so that $x_g = \eta_g \tilde{x}$. Inserting this into Eq. 2.4.11 yields

$$\left[\tilde{\mathbf{D}} + \tilde{\mathbf{C}}\right] \tilde{x} = \tilde{b} \tag{2.4.14}$$

where the average diffusion operator $\tilde{\mathbf{D}}$ is

$$\tilde{\mathbf{D}} = \sum_{g=1}^{G} \mathbf{D}_g \eta_g, \tag{2.4.15}$$

the summed right hand side $\tilde{b}$ is

$$\tilde{b} = \sum_{g=1}^{G} b_g, \tag{2.4.16}$$

and the group coupling $\tilde{\mathbf{C}}$ is

$$\tilde{\mathbf{C}} = \sum_{g=1}^{G} \sum_{g'=1}^{G} \mathbf{C}_{g,g'} \eta_{g'}. \tag{2.4.17}$$

Eq. 2.4.14 is again a nonlinear system because η_g depends on the solution at the end of the time step. However, if the spectrum does not change much from time step to time step, we can use old time step information to approximate it, namely

$$\eta_g \approx \eta_g^{n-1} = \frac{x_g^{n-1}}{\tilde{x}^{n-1}} \tag{2.4.18}$$

to linearize the system. Another possibility would be to linearize the system by using a normalized Planck spectrum instead of η_g. This might be easier to assume

when there is no good initial guess, but the nonlocal information in η_g will be a better approximation than a normalized black body spectrum.

Once we solve for $\tilde{x}$, the group equations, Eq. 2.4.1, are decoupled and each group can be solved for separately using

$$x_g = \mathbf{D}_g^{-1} \left[b_g - \sum_{g'=1}^{G} \mathbf{C}_{g,g'} \eta_{g'} \tilde{x} \right] . \tag{2.4.19}$$

2.5 Conclusions and Future Work

While new method has been developed and implemented, extensive testing of the method has not been completed. Construction of the matrix is considerably faster than in previous versions of the code. The solution for a given time step may be more expensive than the previous version, much larger time steps should be possible, reducing run time. This will be tested on several benchmarks and user problems.

Chapter 3

The Verification Suite

A suite of problems has been developed to test the radiation diffusion package in ALEGRA. All problems and data analysis are run automatically, so that much of this document can be generated for any version of the code. An error history is also kept so that improvements (or regressions) in the algorithms can be identified.

The test suite includes twenty one different problems. Ten of these are simple analytic solutions to the one dimensional Cartesian geometry diffusion equation, and test different terms in the equation, including material discontinuities. Two more problems are one dimensional solutions to the diffusion equation in cylindrical and spherical geometry and can be used to test the multi-dimensional code. Eight problems are based on the method of manufactures solutions. These test the code in situations where it is difficult to get an analytic solution, specifically in the cases of varying material properties, nonlinear flux limiters, the multigroup equations, and coupling with the material energy equation. One test does not test the diffusion code, but rather the Implicit Monte Carlo package.

A six convergence studies are run on each of these problems with a rectilinear Cartesian mesh, a randomized mesh, and the highly skewed Kershaw Z-Mesh in both two and three dimensions. In total, 685 simulations are run as part of this test suite.

3.1 Tampa

A new tool, named Tampa, has been developed to manage the verification suite. Tampa is designed to automate the processes of running a large number of simulations, do the analysis of the results, and finally make a document with the results. It is not specific to the radiation package, and only loosely coupled to ALEGRA. A full users manual will be written to explain the usage of Tampa. Already, several

others are beginning to use Tampa for their own verification suites within ALEGRA.

Tampa is a collection of tools, written in Python, that build input decks for ALEGRA given a problem specification and several different parameters to run that problem with. Typically, this is a given problem on different mesh refinements, but one could also vary material properties, time step sizes, convergence norms, etc. Once the specific combinations of problems and parameters have been made, Tampa will run ALEGRA on each combination. Tampa can use the `testAlegra` script to run these problems on workstations or clusters.

After all the simulations are completed, Tampa will run a post processing script of the user's choice, allowing great flexibility in how the analysis is accomplished. Several sets of tools are provided to do the analysis used in the radiation verification suite. These compute various error norms for the computed solution on different meshes. The convergence rate is then computed. All of this data is plotted to be included in a document later on. Additionally, the errors for each problem-parameter combination and the convergence rates are stored in a history file. The histories can also be plotted so that improvements or regressions to the algorithm can be detected.

Once all the analysis is finished, Tampa will build a document incorporating the results. The results and document can then be archived; the radiation suite stores the latest plots, histories, and document in a CVS repository.

3.2 Simplifications

The energy dependence of Eq. 2.1.1 is usually handled by integrating the equation over an energy range, or group, and solving a coupled set of diffusion equations. In the extreme case, the equation is integrated over all energies, and a single diffusion equation needs to be solved. Most of the following tests are one-group, designed to check the core functionality of the diffusion solver. Several multi-group tests are then performed to check the group to group coupling.

If we ignore both the energy dependence and the coupling with the material equation, we get the one-group, or gray, diffusion equation, namely

$$\frac{1}{c}\frac{\partial E}{\partial t} - \frac{1}{3\sigma_t}\nabla^2 E = -\sigma_a E + \frac{1}{c}S \tag{3.2.1}$$

where E is the energy integrated radiation energy density, S is external power density source, c is the speed of light, σ_a is the absorption opacity, and σ_t is the total opacity. Since many of the problems are one dimensional, we can also simplify the

boundary conditions, Eq. 2.1.21, to

$$\mathcal{A}_r E - \mathcal{B}_r D \frac{\partial}{\partial x} E = \mathcal{C}_r \tag{3.2.2}$$

$$\mathcal{A}_l E + \mathcal{B}_l D \frac{\partial}{\partial x} E = \mathcal{C}_l \tag{3.2.3}$$

where Eq. 3.2.2 is applied at the right boundary and Eq. 3.2.3 is applied at the left boundary.

3.3 One Dimensional Cartesian Steady State Problems

These tests are designed to test the diffusion solver with various boundary conditions on various meshes. While reflective and periodic boundary conditions are never explicitly tested in any of the problems listed here, to run all of these problems in two or three dimensions will require the use of reflective or periodic boundary conditions.

3.3.1 Only Scattering: Linear Solutions

The simplest diffusion equation eliminates nearly all the terms in Eq. 3.2.1 so that just the diffusion operator is tested, namely

$$\frac{\partial^2 E}{\partial x^2} = 0, \tag{3.3.1}$$

where it has been assumed that $\sigma_a = 0$, $\sigma_t = \sigma_s$, and $S = 0$. In this case, we have a linear solution for E, namely

$$E(x) = ax + b, \tag{3.3.2}$$

where a and b are to be determined by the boundary conditions. Inserting Eq. 3.3.2 into Eq. 3.2.2 and Eq. 3.2.3 yields

$$\mathcal{A}_r(ax_r + b) - \mathcal{B}_r D a = \mathcal{C}_r \tag{3.3.3}$$

$$\mathcal{A}_l(ax_l + b) + \mathcal{B}_l D a = \mathcal{C}_l \tag{3.3.4}$$

Solving for a and b yields

$$a = \frac{\mathcal{A}_r \mathcal{C}_l - \mathcal{A}_l \mathcal{C}_r}{D(\mathcal{A}_r \mathcal{B}_l + \mathcal{A}_l \mathcal{B}_r) - \mathcal{A}_l \mathcal{A}_r (x_r - x_l)} \tag{3.3.5}$$

$$b = \frac{D(\mathcal{B}_r \mathcal{C}_l + \mathcal{B}_l \mathcal{C}_r) + \mathcal{A}_l \mathcal{C}_r x_l - \mathcal{A}_r \mathcal{C}_l x_r}{D(\mathcal{A}_r \mathcal{B}_l + \mathcal{A}_l \mathcal{B}_r) - \mathcal{A}_l \mathcal{A}_r (x_r - x_l)} \tag{3.3.6}$$

Since we have a second order method in space, we expect to recover the exact solution regardless of the mesh spacing. This is a general expression for arbitrary boundary conditions. Two specific combinations of the boundary conditions will be shown next.

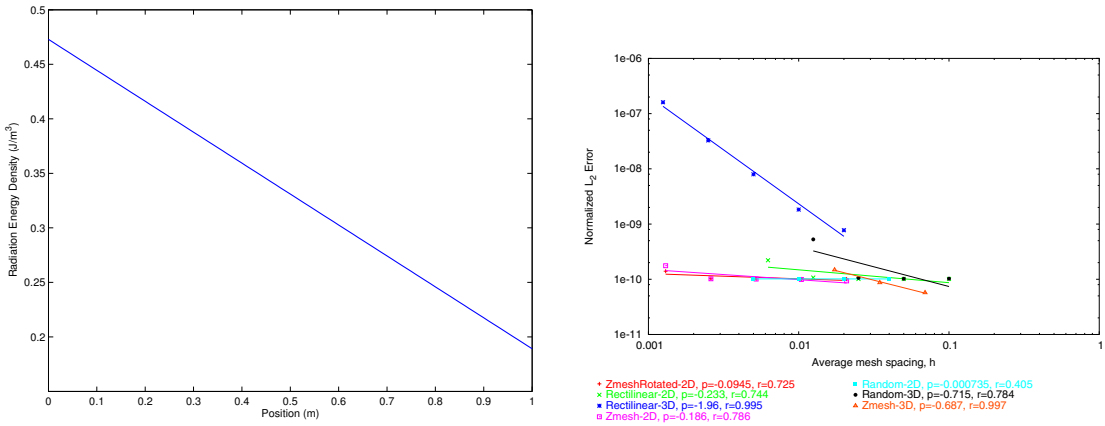

(a) Analytic Solution (b) Convergence Study

Figure 3.1. Steady state solution in a slab with the Dirichlet condition $E(0) = B(T = 5000\,\mathrm{K})$ and the vacuum condition at $x_r = 1\,\mathrm{m}$ with $\sigma_t = \sigma_s = 1\,\mathrm{m}^{-1}$. This second order diffusion method should get this exactly, so there is no expected convergence.

3.3.1.1 Dirichlet and Vacuum

If we set the left boundary with a Dirichlet boundary condition $E(0) = B(T)$ and a vacuum boundary at $x_r = 1$, we get

$$E(x) = B(T)\left(1 - \frac{1}{1+2D}x\right) = B(T)\left(1 - \frac{3\sigma_t}{3\sigma_t + 2}x\right) \tag{3.3.7}$$

Figure 3.1 shows the solution to this problem for a specific set of parameters.

3.3.1.2 Source and Albedo

If we have a source boundary at $x_l = 0$ and an albedo boundary at $x_r = 1$ we get

$$E(x) = B(T)\frac{(\alpha-1)x + 1 - \alpha + 2D(1+\alpha)}{1 - \alpha + 4D} \tag{3.3.8}$$

or

$$E(x) = B(T)\frac{(\alpha-1)x + 1 - \alpha + 2D(1+\alpha)}{1 - \alpha + 4D} \tag{3.3.9}$$

If $\alpha = 1$, we have a reflective boundary and

$$E(x) = B(T). \tag{3.3.10}$$

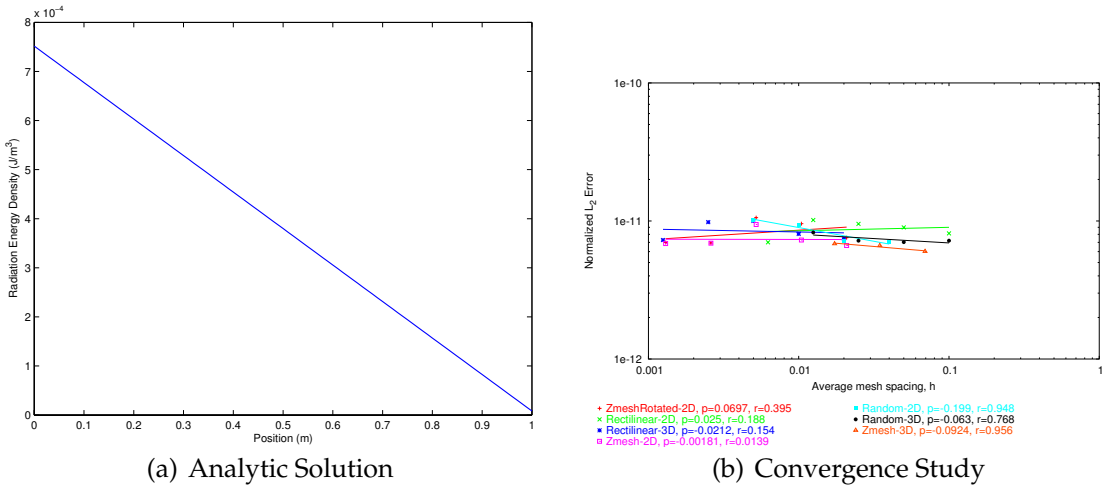

(a) Analytic Solution (b) Convergence Study

Figure 3.2. Steady state solution in a slab with the source condition $F_{\text{in}}(0) = B(T = 1000\,\text{K})/4$ and the albedo condition at $x_r = 1\,\text{m}$ with $\alpha = 0.25$ and $\sigma_t = \sigma_s = 100\,\text{m}^{-1}$. This second order diffusion method should get this exactly, so there is no expected convergence.

If $\alpha = 0$, we have a vacuum boundary and

$$E(x) = B(T)\frac{1 + 2D - x}{1 + 4D} \tag{3.3.11}$$

Figure 3.2 shows the solution to this problem for a specific set of parameters.

3.3.2 Absorption and Scattering

We can reintroduce absorption to test that term as well as the diffusion operator in Eq. 3.2.1. In steady state we have the simplified diffusion equation

$$\frac{\partial^2 E}{\partial x^2} - 3\sigma_t\sigma_a E = 0. \tag{3.3.12}$$

Eq. 3.3.12 implies that $E(x)$ has the form

$$E(x) = a\,\mathrm{e}^{\lambda x} + b\,\mathrm{e}^{-\lambda x} \tag{3.3.13}$$

where

$$\lambda = \frac{1}{L} = \sqrt{3\sigma_t\sigma_a} \tag{3.3.14}$$

where L is the characteristic length of the problem (sometimes called the diffusion length). The derivative of $E(x)$ is

$$\frac{\partial E}{\partial x} = a\lambda\,\mathrm{e}^{\lambda x} - b\lambda\,\mathrm{e}^{-\lambda x} \tag{3.3.15}$$

Inserting the assumed solution into the boundary conditions gives us

$$\mathcal{A}_r(a\,\mathrm{e}^{\lambda x_r} + b\,\mathrm{e}^{-\lambda x_r}) - \mathcal{B}_r D(a\lambda\,\mathrm{e}^{\lambda x_r} - b\lambda\,\mathrm{e}^{-\lambda x_r}) = \mathcal{C}_r \tag{3.3.16}$$

$$\mathcal{A}_l(a\,\mathrm{e}^{\lambda x_l} + b\,\mathrm{e}^{-\lambda x_l}) + \mathcal{B}_l D(a\lambda\,\mathrm{e}^{\lambda x_l} - b\lambda\,\mathrm{e}^{-\lambda x_l}) = \mathcal{C}_l \tag{3.3.17}$$

Solving for a and b for arbitrary boundary conditions yields

$$a = \frac{\mathcal{C}_l\,\mathrm{e}^{\lambda x_l}(\mathcal{A}_r + \lambda D\mathcal{B}_r) - \mathcal{C}_r\,\mathrm{e}^{\lambda x_r}(\mathcal{A}_l - \lambda D\mathcal{B}_l)}{\mathrm{e}^{2\lambda x_l}(\mathcal{A}_l + \lambda D\mathcal{B}_l)(\mathcal{A}_r + \lambda D\mathcal{B}_r) - \mathrm{e}^{2\lambda x_r}(\mathcal{A}_l - \lambda D\mathcal{B}_l)(\mathcal{A}_r - \lambda D\mathcal{B}_r)} \tag{3.3.18}$$

$$b = \frac{\mathrm{e}^{\lambda(x_l+x_r)}[\mathcal{C}_r\,\mathrm{e}^{\lambda x_l}(\mathcal{A}_l + \lambda D\mathcal{B}_l) - \mathcal{C}_l\,\mathrm{e}^{\lambda x_r}(\mathcal{A}_r - \lambda D\mathcal{B}_r)]}{\mathrm{e}^{2\lambda x_l}(\mathcal{A}_l + \lambda D\mathcal{B}_l)(\mathcal{A}_r + \lambda D\mathcal{B}_r) - \mathrm{e}^{2\lambda x_r}(\mathcal{A}_l - \lambda D\mathcal{B}_l)(\mathcal{A}_r - \lambda D\mathcal{B}_r)}. \tag{3.3.19}$$

3.3.2.1 Dirichlet and Vacuum Boundaries

For the specific case when on the left ($x_l = 0$) we have a vacuum boundary and on the right we have a Dirichlet boundary $E(x_r) = B(T)$, the coefficients a and b in Eq. 3.3.15 are

$$a = B(T)\frac{1 + 2\lambda D}{\mathrm{e}^{\lambda x_r}(1 + 2\lambda D) - \mathrm{e}^{-\lambda x_r}(1 - 2\lambda D)} \tag{3.3.20}$$

$$b = -B(T)\frac{1 - 2\lambda D}{\mathrm{e}^{\lambda x_r}(1 + 2\lambda D) - \mathrm{e}^{-\lambda x_r}(1 - 2\lambda D)} \tag{3.3.21}$$

Figure 3.3 shows the solution to this problem for a specific set of parameters.

3.3.2.2 Source and Albedo Boundaries

If instead we have on the left ($x_l = 0$) an albedo boundary and on the right (x_r) a source boundary, the coefficients in Eq. 3.3.15 are

$$a = B(T)\frac{1 - \alpha + 2\lambda D(1 + \alpha)}{8\lambda D\cosh\lambda x_r + 2(1 - \alpha + 4\lambda^2 D^2(1 + \alpha))\sinh\lambda x_r} \tag{3.3.22}$$

$$b = B(T)\frac{\alpha - 1 + 2\lambda D(1 + \alpha)}{8\lambda D\cosh\lambda x_r + 2(1 - \alpha + 4\lambda^2 D^2(1 + \alpha))\sinh\lambda x_r}. \tag{3.3.23}$$

For $\alpha = 1$ we get

$$a = b = B(T)\frac{1}{2\cosh\lambda x_r + 4\lambda D\sinh\lambda x_r}. \tag{3.3.24}$$

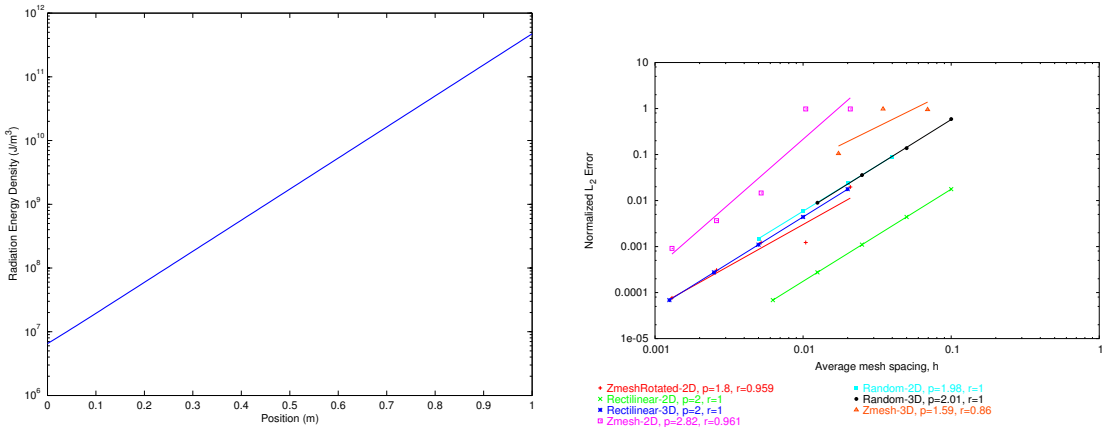

(a) Analytic Solution (b) Convergence Study

Figure 3.3. Steady state solution in a slab with the Dirichlet condition $E(1\,\mathrm{m}) = B(T = 5.0\mathrm{e}6\,\mathrm{K})$ and the vacuum condition at $x_r = 0\,\mathrm{m}$ with $\sigma_s = 1\,\mathrm{m}^{-1}$ and $\sigma_a = 6\,\mathrm{m}^{-1}$.

This makes sense since we must be symmetric about the origin. For $\alpha = 0$ we get

$$a = B(T)\frac{1 + 2\lambda D}{8\lambda D \cosh \lambda x_r + (2 + 8\lambda^2 D^2)\sinh \lambda x_r} \tag{3.3.25}$$

$$b = B(T)\frac{-1 + 2\lambda D}{8\lambda D \cosh \lambda x_r + (2 + 8\lambda^2 D^2)\sinh \lambda x_r} \tag{3.3.26}$$

Figure 3.4 shows the solution to this problem for a specific set of parameters.

3.4 Steady Steady Cylindrical and Spherical Problems

One dimensional problems in curvilinear coordinates can be used to test the two and three dimensional versions of the code. These problems are one material with a source boundary condition on the outside of the cylinder or sphere. Both absorption and scattering will be included.

3.4.1 A Cylinder

In cylindrical coordinates, the one dimensional diffusion equation is

$$\frac{1}{r}\frac{\partial}{\partial r}\frac{r}{3\sigma_t}\frac{\partial}{\partial r}E = \sigma_a E. \tag{3.4.1}$$

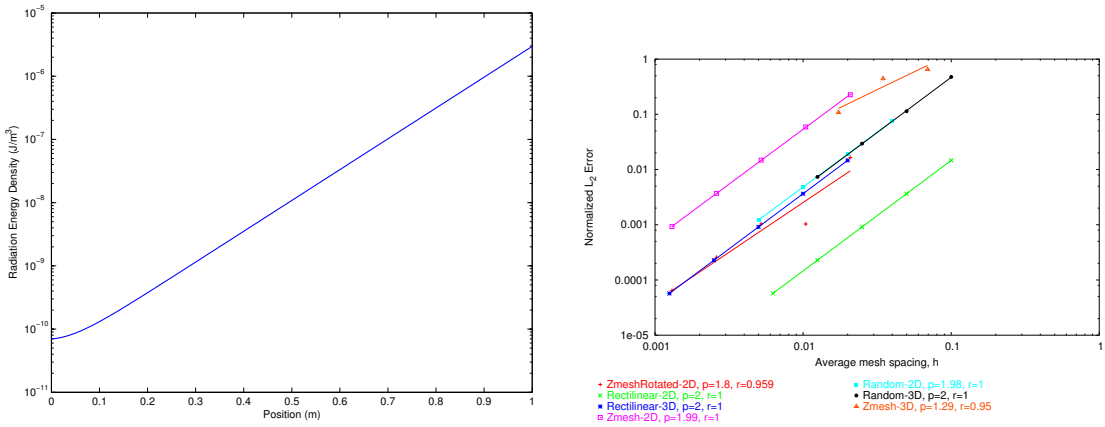

(a) Analytic Solution (b) Convergence Study

Figure 3.4. Steady state solution in a slab with the source condition $F_{\text{in}}(1\,\text{m}) = B(T = 300\,\text{K})/4$ and the albedo condition at $x_r = 0\,\text{m}$ with $\alpha = 0.75$, $\sigma_s = 1\,\text{m}^{-1}$ and $\sigma_a = 6\,\text{m}^{-1}$.

We will impose the source boundary condition a some radius r_0, namely

$$-\frac{1}{2}E(r_0) + D\frac{\partial E(r_0)}{\partial r} = -\frac{1}{2}B(T). \tag{3.4.2}$$

In the center, the energy density must be finite. Expanding the derivative in Eq. 3.4.1 yields

$$r\frac{\partial^2}{\partial r^2}E + \frac{\partial}{\partial r}E = r\lambda^2 E. \tag{3.4.3}$$

The generic solution to this is

$$E(r) = \frac{a}{\sqrt{\pi}}\,\mathrm{K}_0(\lambda r) + b\,\mathrm{I}_0(\lambda r) \tag{3.4.4}$$

where $\mathrm{I}_n(x)$ is the modified Bessel function of the first kind and $\mathrm{K}_n(x)$ is the modified Bessel function of the second kind. Since the energy density must remain finite, we must have $a = 0$ since $\lim_{r\to 0}\mathrm{K}_0(r) = \infty$. Using $a = 0$, the derivative of $E(r)$ is then

$$\frac{\partial E(r)}{\partial r} = b\lambda\,\mathrm{I}_1(\lambda r) \tag{3.4.5}$$

The source boundary implies

$$b\left[\mathrm{I}_0(\lambda r_0) + 2\lambda D\,\mathrm{I}_1(\lambda r_0)\right] = B(T) \tag{3.4.6}$$

So finally

$$E(r) = \frac{B(T)}{\mathrm{I}_0(\lambda r_0) + 2\lambda D\,\mathrm{I}_1(\lambda r_0)}\,\mathrm{I}_0(\lambda r) \tag{3.4.7}$$

Figure 3.5 shows the solution to this problem for a specific set of parameters.

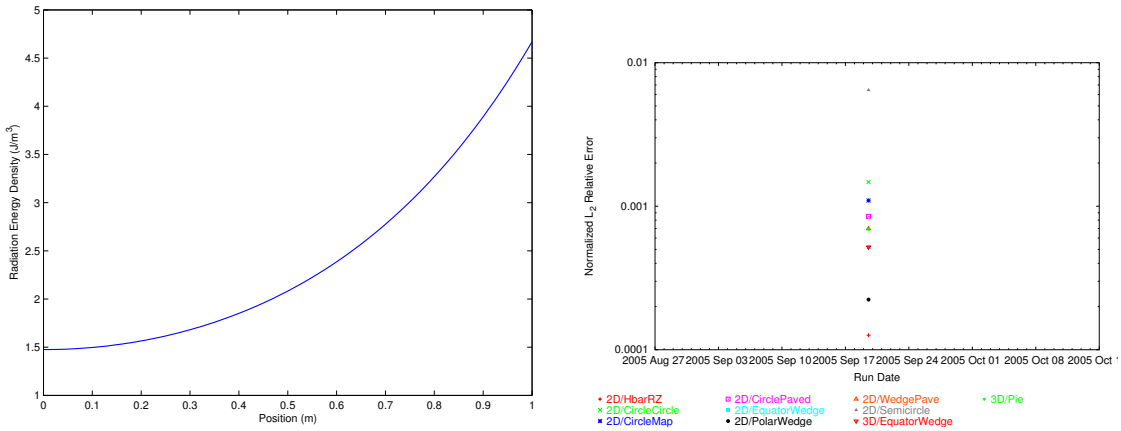

(a) Analytic Solution (b) Error History

Figure 3.5. Steady state solution in a cylinder with the source condition at $r_0 = 1\,\mathrm{m}$ of $B(T = 10000\,\mathrm{K})$ with $\sigma_s = 1\,\mathrm{m}^{-1}$ and $\sigma_a = 1\,\mathrm{m}^{-1}$. A convergence study with this problem still needs to be set up and done.

3.4.2 A Sphere

In spherical coordinates, the one dimensional diffusion equation becomes

$$-\frac{1}{\rho^2}\frac{\partial}{\partial\rho}\rho^2\frac{\partial}{\partial\rho}E = -\lambda^2 E, \tag{3.4.8}$$

where ρ is the distance from the origin. The source boundary condition imposed at ρ_0 is

$$-\frac{1}{2}E(\rho_0) - D\frac{\partial E(\rho_0)}{\partial\rho} = -\frac{1}{2}B(T). \tag{3.4.9}$$

Expanding the derivative in Eq. 3.4.8 yields

$$\rho^2\frac{\partial^2}{\partial\rho^2}E + 2\rho\frac{\partial}{\partial\rho}E = \lambda^2\rho^2 E. \tag{3.4.10}$$

The generic solution of this equation is

$$E(\rho) = a\frac{\cosh(\lambda\rho)}{\rho} + b\frac{\sinh(\lambda\rho)}{\rho}. \tag{3.4.11}$$

Since the solution must remain finite, which implies that $a = 0$ because

$$\lim_{\rho\to 0}\frac{\cosh(\lambda\rho)}{\rho} = \infty. \tag{3.4.12}$$

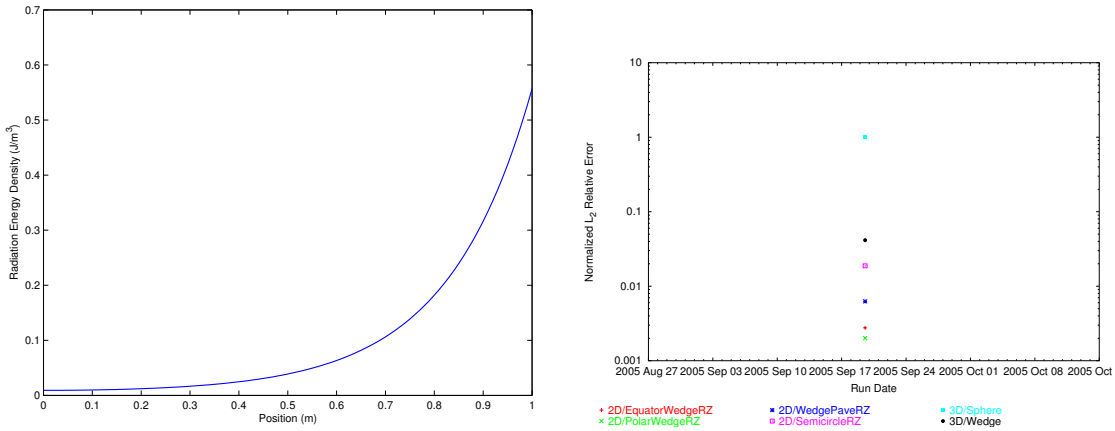

(a) Analytic Solution (b) Error History

Figure 3.6. Steady state solution in a sphere with the source condition at $r_0 = 1\,\mathrm{m}$ of $B(T = 6000\,\mathrm{K})$ with $\sigma_s = 2\,\mathrm{m}^{-1}$ and $\sigma_a = 3\,\mathrm{m}^{-1}$. A convergence study with this problem still needs to be set up and done.

Inserting the generic solution into the source boundary condition gives us

$$b\left[\frac{\sinh(\lambda\rho_0)}{\rho_0} + 2D\left(\frac{\lambda\cosh(\lambda\rho_0)}{\rho_0} - \frac{\sinh(\lambda\rho_0)}{\rho_0^2}\right)\right] = B(T). \tag{3.4.13}$$

And finally we can solve for the energy density as a function of radius,

$$E(\rho) = B(T)\frac{\rho_0}{\sinh(\lambda\rho_0) + 2D\left(\lambda\cosh(\lambda\rho_0) - \frac{\sinh(\lambda\rho_0)}{\rho_0}\right)}\frac{\sinh(\lambda\rho)}{\rho}. \tag{3.4.14}$$

Figure 3.6 shows the solution to this problem for a specific set of parameters.

3.5 External Sources

The problems in this section test the external source term in the diffusion equation.

3.5.1 Constant Uniform Source: Constant Solution

Consider infinite slab with a constant, uniform source and absorption opacity. Eq. 3.2.1 implies

$$E = \frac{1}{c\sigma_a}S \tag{3.5.1}$$

Alternatively, coupled to the material equation, we expect

$$E = B(T_m) = aT_m^4. \tag{3.5.2}$$

This test can be run with periodic, reflective, and Dirichlet boundary conditions, as well as both with and without the flux limiter.

3.5.2 Constant Uniform Source: One Dimensional Quadratic Solution

Consider a slab with vacuum boundaries and a uniform source of photons. The governing diffusion equation, without absorption, in this case is

$$\frac{\partial^2}{\partial x^2} E = -\frac{3\sigma_t}{c} S \tag{3.5.3}$$

The generic solution is

$$E(x) = ax^2 + bx + d \tag{3.5.4}$$

Inserting this into the diffusion equation gives us the value of the coefficient a, namely

$$a = -\frac{3\sigma_t}{2c} S \tag{3.5.5}$$

Vacuum boundaries at x_l and x_r helps us determine the other two coefficients. Inserting the generic solution into the boundary conditions gives us

$$-(ax_r^2 + bx_r + d) - \frac{2}{3\sigma_t}(2ax_r + b) = 0 \tag{3.5.6}$$

$$-(ax_l^2 + bx_l + d) + \frac{2}{3\sigma_t}(2ax_l + b) = 0 \tag{3.5.7}$$

After solving for b and d and simplifying, the final form of the energy density is

$$E(x) = \frac{S}{c}\left[(x_r - x_l) + \frac{3\sigma_t}{2}(x - x_l)(x_r - x)\right]. \tag{3.5.8}$$

Since we have a second order method, we expect to get this solution exactly for all meshes, regardless of mesh spacing.

Figure 3.7 shows the solution to this problem for a specific set of parameters.

3.5.3 Varying Source

In a slightly more complicated case, we will allow a spatially varying source such that the governing equation is

$$\frac{\partial^2}{\partial x^2} E = -\frac{3\sigma_t}{c} S_0 \, \mathrm{e}^{-Ax}. \tag{3.5.9}$$

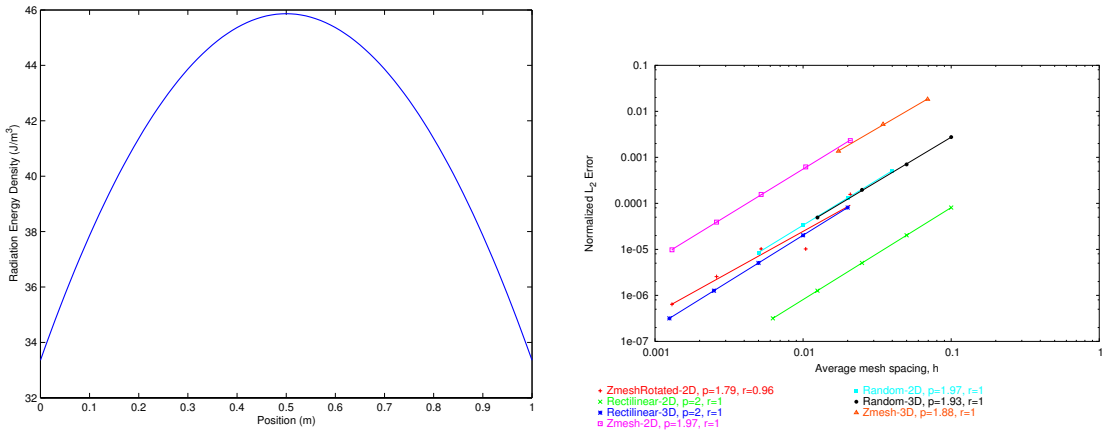

(a) Analytic Solution (b) Convergence Study

Figure 3.7. Steady state solution in a slab with a uniform source of $S = 1 \times 10^{10}\,\mathrm{W/m^3}$ and $\sigma_t = \sigma_s = 1\,\mathrm{m}^{-1}$.

We will impose Dirichlet boundary conditions on each side of the slab so that

$$E(0) = E_0 \tag{3.5.10}$$

$$E(1) = E_1. \tag{3.5.11}$$

The solution for the energy density is

$$E(x) = E_0 + (E_1 - E_1)x + \frac{3\sigma_t S_0}{cA^2}\left[1 - \mathrm{e}^{-Ax} - x\left(1 - \mathrm{e}^{-A}\right)\right]. \tag{3.5.12}$$

3.6 Two Material Steady State Problems

These tests involve a system with two distinct materials. The solution is essentially a solution of two problems, one in each material. At the material interface, the energy density, E, and the energy flux, $\mathbf{n} \cdot \mathbf{F}$, must be continuous across the material interface. Since the boundary conditions are tested elsewhere, we will use Dirichlet boundaries on the problems.

In all of the following problems, $E^l(x_l) = E_0$, $E^l(x_i) = E^r(x_i)$ and $E^r(x_r) = E_1$, where x_l, x_i, and x_r are the left, interface, and right boundaries respectively. The left (or inner) slab has material properties σ_a^l and σ_t^l. The right (or outer) slab has material properties σ_a^r and σ_t^r.

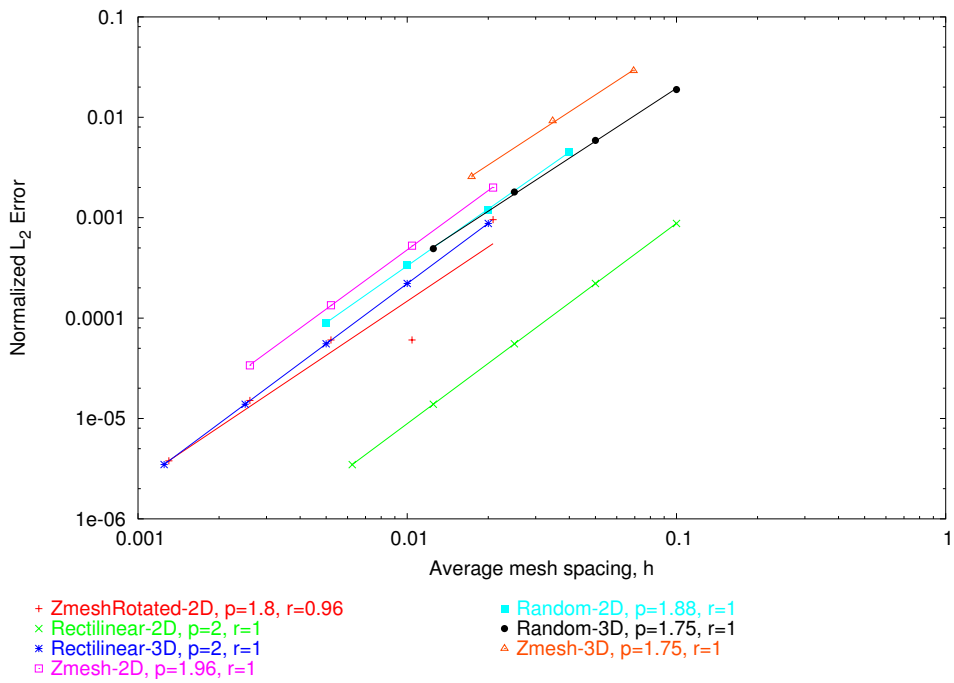

Figure 3.8. Convergence rates of the absolute relative error on various meshes for the nonuniform source problem with $\sigma_t = \sigma_s = 1.0$, $S_0 = 1.0e10$, $A = 10$, $E_0 = B(5000)$, and $E_1 = B(10000)$.

3.6.1 Cartesian With Only Scattering

In one dimensional Cartesian coordinates with $\sigma_a = 0$, we have the two general solutions for the energy density in the left and right materials, respectively:

$$E^l(x) = a_l x + b_l \tag{3.6.1}$$

$$E^r(x) = a_r x + b_r \tag{3.6.2}$$

Applying the Dirichlet boundary conditions along with the interface conditions gives us a linear system to solve for the constants a_l, a_r, b_l, and b_r, namely

$$a_l x_l + b_l = E_0 \tag{3.6.3}$$

$$a_r x_r + b_r = E_1 \tag{3.6.4}$$

$$a_l x_i + b_l = a_r x_i + b_r \tag{3.6.5}$$

$$-\frac{1}{3\sigma_t^l} a_l = -\frac{1}{3\sigma_t^r} a_r. \tag{3.6.6}$$

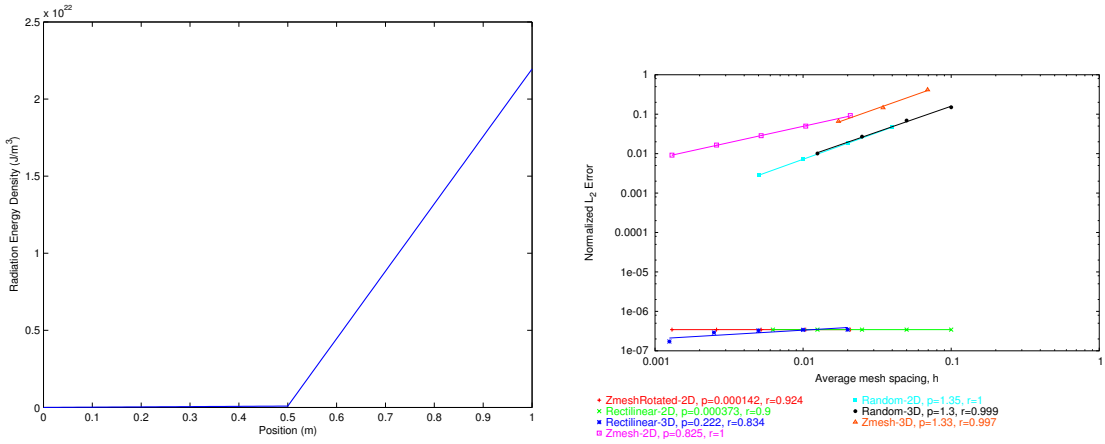

(a) Analytic Solution (b) Convergence Study

Figure 3.9. Steady state solution in a two material slab with the Dirichlet conditions $E(0) = 0$ and $E(1\,\mathrm{m}) = B(200\,\mathrm{keV})$ with $\sigma_s^l = 0.02\,\mathrm{m}^{-1}$, $\sigma_s^r = 5.0\,\mathrm{m}^{-1}$, and $x_i = 0.5\,\mathrm{m}$. These parameters were chosen to test a thick material followed by a near vacuum. This method should get this solution exactly, so there is no expected convergence on the regular meshes. There is some error in mixed material cells, however, so there is first order convergence on skewed or randomized meshes.

Solving for the coefficients yields

$$a_r = -(E_0 - E_1)\frac{\sigma_t^r}{\sigma_t^l(x_i - x_l) + \sigma_t^r(x_r - x_i)} \tag{3.6.7}$$

$$a_l = -(E_0 - E_1)\frac{\sigma_t^l}{\sigma_t^l(x_i - x_l) + \sigma_t^r(x_r - x_i)} \tag{3.6.8}$$

$$b_r = E_1 + (E_0 - E_1)\frac{\sigma_t^r x_r}{\sigma_t^l(x_i - x_l) + \sigma_t^r(x_r - x_i)} \tag{3.6.9}$$

$$b_l = E_0 + (E_0 - E_1)\frac{\sigma_t^l x_l}{\sigma_t^l(x_i - x_l) + \sigma_t^r(x_r - x_i)} \tag{3.6.10}$$

Figure 3.9 shows the solution to this problem for a specific set of parameters.

3.6.2 Cartesian With Scattering and Absorption

With absorption reintroduced, in one dimensional Cartesian coordinates we have the following two general solutions for the energy density in the left and right

materials:

$$E^l(x) = a_l \, \mathrm{e}^{\lambda_l x} + b_l \, \mathrm{e}^{-\lambda_l x} \tag{3.6.11}$$

$$E^r(x) = a_r \, \mathrm{e}^{\lambda_r x} + b_r \, \mathrm{e}^{-\lambda_r x} \tag{3.6.12}$$

The Dirichlet boundary conditions and the interface conditions impose four constraints that we can use to determine the parameters, namely

$$E^l(x_l) = E_l \tag{3.6.13}$$

$$E^r(x_r) = E_r \tag{3.6.14}$$

$$E^l(x_i) = E^r(x_i) \tag{3.6.15}$$

$$\frac{1}{\sigma_t^l}\frac{\partial E^l(x_i)}{\partial x} = \frac{1}{\sigma_t^r}\frac{\partial E^r(x_i)}{\partial x}. \tag{3.6.16}$$

Applying these conditions yields the following matrix equation for the unknown parameters:

$$\begin{bmatrix} \mathrm{e}^{\lambda_l x_l} & \mathrm{e}^{-\lambda_l x_l} & 0 & 0 \\ 0 & 0 & \mathrm{e}^{\lambda_r x_r} & \mathrm{e}^{-\lambda_r x_r} \\ \mathrm{e}^{\lambda_l x_i} & \mathrm{e}^{-\lambda_l x_i} & -\mathrm{e}^{\lambda_r x_i} & -\mathrm{e}^{-\lambda_r x_i} \\ \frac{\lambda_l}{\sigma_t^l}\mathrm{e}^{\lambda_l x_i} & -\frac{\lambda_l}{\sigma_t^l}\mathrm{e}^{-\lambda_l x_i} & -\frac{\lambda_r}{\sigma_t^r}\mathrm{e}^{\lambda_r x_i} & \frac{\lambda_r}{\sigma_t^r}\mathrm{e}^{-\lambda_r x_i} \end{bmatrix} \begin{bmatrix} a_l \\ b_l \\ a_r \\ b_r \end{bmatrix} = \begin{bmatrix} E_l \\ E_r \\ 0 \\ 0 \end{bmatrix}. \tag{3.6.17}$$

This is solved numerically for the coefficients that are then used in Eq. 3.6.12.

Figure 3.10 shows the solution to this problem for a specific set of parameters.

3.6.3 One Vacuum Material

While not well defined in a vacuum, the diffusion approximation is frequently used in this regime because it is cheap to compute, so this needs to be tested as well. We can extend the problem in Section 3.3.1.1 to include a vacuum region in the problem. The answer in the slab should remain the same, as well as all tallies, since we're simply adding on a vacuum region outside the vacuum boundary. The solution to this will be a bit like the two material solution; we will ignore the fact that the opacity is zero for a while.

In Section 3.3.1.1 there was a Dirichlet boundary at x_l and a vacuum boundary at x_r. In the augmented problem the vacuum region will extend from $x_r \leq x \leq x_v$, with a vacuum boundary at x_v. The boundary and interface conditions are

$$E_m(x_l) = B(T) = E_l \tag{3.6.18}$$

$$E_m(x_r) = E_v(x_r) \tag{3.6.19}$$

$$\frac{1}{3\sigma_m}\frac{\partial E_m}{\partial x}(x_r) = \frac{1}{3\sigma_v}\frac{\partial E_v}{\partial x}(x_r) \tag{3.6.20}$$

$$-\frac{1}{2}E_v(x_v) - \frac{1}{3\sigma_v}\frac{\partial E_v}{\partial x}(x_v) = 0, \tag{3.6.21}$$

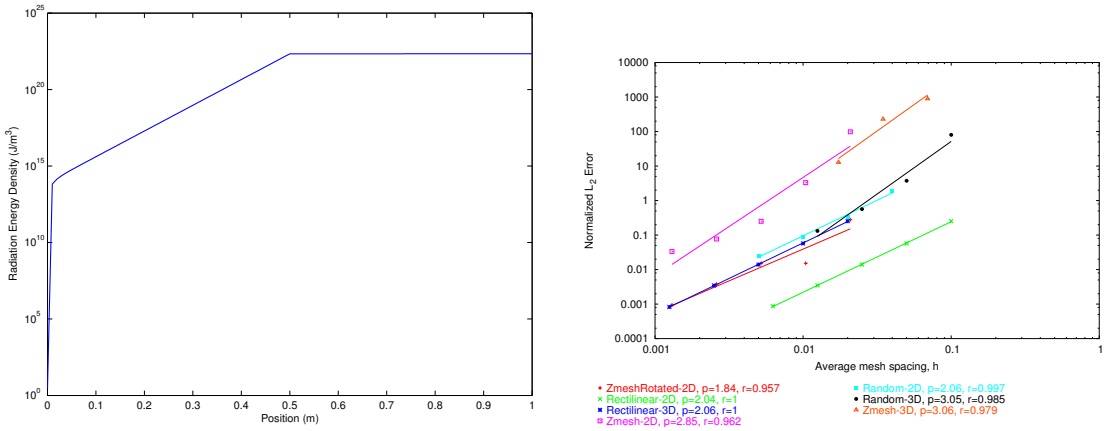

(a) Analytic Solution (b) Convergence Study

Figure 3.10. Steady state solution in a two material slab with the Dirichlet conditions $E(0) = 0$ and $E(2\,\mathrm{m}) = B(200\,\mathrm{keV})$ with $\sigma_s^l = 5\,\mathrm{m}^{-1}$, $\sigma_a^l = 20\,\mathrm{m}^{-1}$, $\sigma_s^r = 0.01\,\mathrm{m}^{-1}$, and $\sigma_a^r = 0.01\,\mathrm{m}^{-1}$. These parameters were chosen to test an optically thin material followed by a thick one. The excessive convergence rates of about $O(3)$ are only because there were problems in converging the solution on the coarse meshes. The reason for this is currently unknown.

where the m and v subscripts indicate quantities in the material and vacuum, respectively. The general solutions are

$$E_m(x) = a_m x + b_m \tag{3.6.22}$$

$$E_v(x) = a_v x + b_v \tag{3.6.23}$$

Applying Eq. 3.6.18 implies that $b_m = E_l$, if $x_l = 0$. We get the following linear system for the remaining coefficients

$$a_m x_r - a_v x_r - b_v = -E_l \tag{3.6.24}$$

$$\sigma_v a_m - \sigma_m a_v = 0 \tag{3.6.25}$$

$$3\sigma_v(a_v x_v + b_v) + 2a_v = 0 \tag{3.6.26}$$

The solution is

$$a_m = -E_l \frac{3\sigma_m}{2 + 3\sigma_m x_r + 3\sigma_v(x_v - x_r)} \tag{3.6.27}$$

$$b_m = E_l \tag{3.6.28}$$

$$a_v = -E_l \frac{3\sigma_v}{2 + 3\sigma_m x_r + 3\sigma_v(x_v - x_r)} \tag{3.6.29}$$

$$b_v = E_l \frac{2 + 3\sigma_v x_v}{2 + 3\sigma_m x_r + 3\sigma_v(x_v - x_r)} \tag{3.6.30}$$

or if $\sigma_v = 0$, we get

$$a_m = -E_l \frac{3\sigma_m}{2 + 3\sigma_m x_r} \tag{3.6.31}$$

$$b_m = E_l \tag{3.6.32}$$

$$a_v = 0 \tag{3.6.33}$$

$$b_v = E_l \frac{2}{2 + 3\sigma_m x_r} \tag{3.6.34}$$

and finally

$$E_m(x) = E_l \left(1 - \frac{3\sigma_m}{2 + 3\sigma_m x_r} x\right) \tag{3.6.35}$$

$$E_v(x) = 2E_l \frac{1}{2 + 3\sigma_m x_r} \tag{3.6.36}$$

Indeed, Eq. 3.6.35 is the same as Eq. 3.3.7 if $x_r = 1$. In the vacuum, the radiation is not "free streaming", or beam-like, but rather the flux is determined by what leaves the boundary of the material through Eq. 3.6.20. The flux throughout the problem is

$$F = \frac{cE_l}{2 + 3\sigma_m x_r} \tag{3.6.37}$$

Figure 3.11 shows the solution in Eq. 3.6.35 and Eq. 3.6.36 for a given set parameters.

3.7 Time Dependent Problems

All of the tests so far have been time independent. The two problem here are pulsed sources in a slab geometry. The first problem is a infinitesimally thin plane source, which tends to be difficult to implement numerically. The second problem is a slab source of finite thickness slab source, which can be simulated much easier.

3.7.1 A Plane Source

In in one dimensional Cartesian geometry without sources, the diffusion equation, Eq. 3.2.1, is

$$\frac{1}{c}\frac{\partial E}{\partial t} - \frac{1}{3\sigma_t}\frac{\partial^2 E}{\partial x^2} = -\sigma_a E. \tag{3.7.1}$$

In an infinite medium, the initial condition is

$$E(r, t = 0) = E_0 \delta(x), \tag{3.7.2}$$

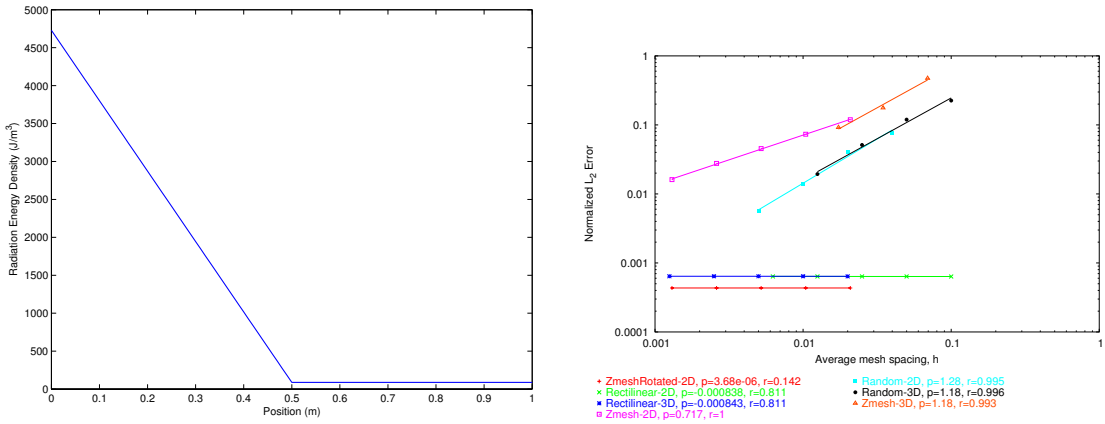

(a) Analytic Solution (b) Convergence Study

Figure 3.11. A problem with a void region. The material region on the right extends from $x = 0$ to $x = 0.5\,\mathrm{m}$ with $\sigma_s = 70\,\mathrm{m}^{-1}$ and $\sigma_a = 0$. The vacuum region extends from $x = 0.5\,\mathrm{m}$ to $x = 1\,\mathrm{m}$. A vacuum boundary condition is applied at $x = 1$ and a Dirichlet boundary condition on the left of $E(0) = B(50000\,\mathrm{K})$

where E_0 is a total energy and $E_0\delta(x)$ is an energy density. This initial condition is equivalent to a pulsed source. Performing a Laplace transform on Eq. 3.7.1 yields

$$s\hat{E} - E_0\delta(x) - \frac{c}{3\sigma_t}\frac{\partial^2 \hat{E}}{\partial x^2} = -c\sigma_a\hat{E} \tag{3.7.3}$$

where

$$\hat{E}(x,s) = \int_0^\infty \mathrm{e}^{-st}E(x,t)\,\mathrm{d}t \quad \text{and} \quad E(x,t) = \frac{1}{2\pi i}\int_{c-i\infty}^{c+i\infty} \mathrm{e}^{-st}\hat{E}(x,s)\,\mathrm{d}s. \tag{3.7.4}$$

Fourier transforming Eq. 3.7.3 yields

$$s\tilde{E} - \frac{E_0}{\sqrt{2\pi}} + \frac{ck^2}{3\sigma_t}\tilde{E} = -c\sigma_a\tilde{E} \tag{3.7.5}$$

where

$$\tilde{E}(k,s) = \frac{1}{\sqrt{2\pi}}\int_{-\infty}^{\infty} \mathrm{e}^{-ikx}\hat{E}(x,s)\,\mathrm{d}x \quad \text{and} \quad \hat{E}(x,s) = \frac{1}{\sqrt{2\pi}}\int_{-\infty}^{\infty} \mathrm{e}^{ikx}\tilde{E}(k,s)\,\mathrm{d}k \tag{3.7.6}$$

We can easily solve Eq. 3.7.5 for $\tilde{E}$, namely

$$\tilde{E} = \frac{E_0}{\sqrt{2\pi}(s + \frac{ck^2}{3\sigma_t} + c\sigma_a)} \tag{3.7.7}$$

Performing first the inverse Laplace transform then the inverse Fourier transform yields

$$E(x,t) = E_0\sqrt{\frac{3\sigma_t}{4\pi ct}}\,\mathrm{e}^{-c\sigma_a t}\,\mathrm{e}^{-\frac{3\sigma_t x^2}{4ct}} \tag{3.7.8}$$

Note that this is a Gaussian that both spreads out, due to the scattering, and decays, due to the absorption, in time.

3.7.2 A Slab Source

We can use the plane source solution of Eq. 3.7.8 as Green's functions to build a slab source of finite thickness. Assuming that the energy density is initially E_0 in the range $-x_0 \leq x \leq x_0$, we can integrate multiple plane sources at each location in this range to get the total energy density for the slab source, namely

$$E(x,t) = \int_{-x_0}^{x_0} E_0\sqrt{\frac{3\sigma_t}{4\pi ct}}\,\mathrm{e}^{-c\sigma_a t}\,\mathrm{e}^{-\frac{3\sigma_t (x-x')^2}{4ct}}\,\mathrm{d}x'. \tag{3.7.9}$$

Performing the integration we get

$$E(x,t) = \frac{E_0}{2}\,\mathrm{e}^{-c\sigma_a t}\left[\mathrm{erf}\left(a(x+x_0)\right) - \mathrm{erf}\left(a(x-x_0)\right)\right] \tag{3.7.10}$$

where $a = \sqrt{\frac{3\sigma_t}{4ct}}$. For $x_0 = 0.1$ and $a \geq 6.666$, $E(x,t)$ is numerically zero.

3.7.2.1 A Nicer Solution

The slab source problem is difficult to analyze because the energy density is very small (or even zero) in some parts of the problem some of the time. If we assume that there is no absorption, we can get a nonzero solution everywhere. Without the source, any arbitrary energy density, E_1 is also a solution in the infinite medium. Because this is a linear problem, we can add that to Eq. 3.7.10 to get

$$E(x,t) = \frac{E_0}{2}\left[\mathrm{erf}\left(a(x+x_0)\right) - \mathrm{erf}\left(a(x-x_0)\right)\right] + E_1 \tag{3.7.11}$$

Even with this addition, there are still some difficulties with this problem. Specifically, the discontinuity in the initial conditions makes it difficult to converge the problem, and we may not be in the asymptotic regime, making the order of convergence not valid.

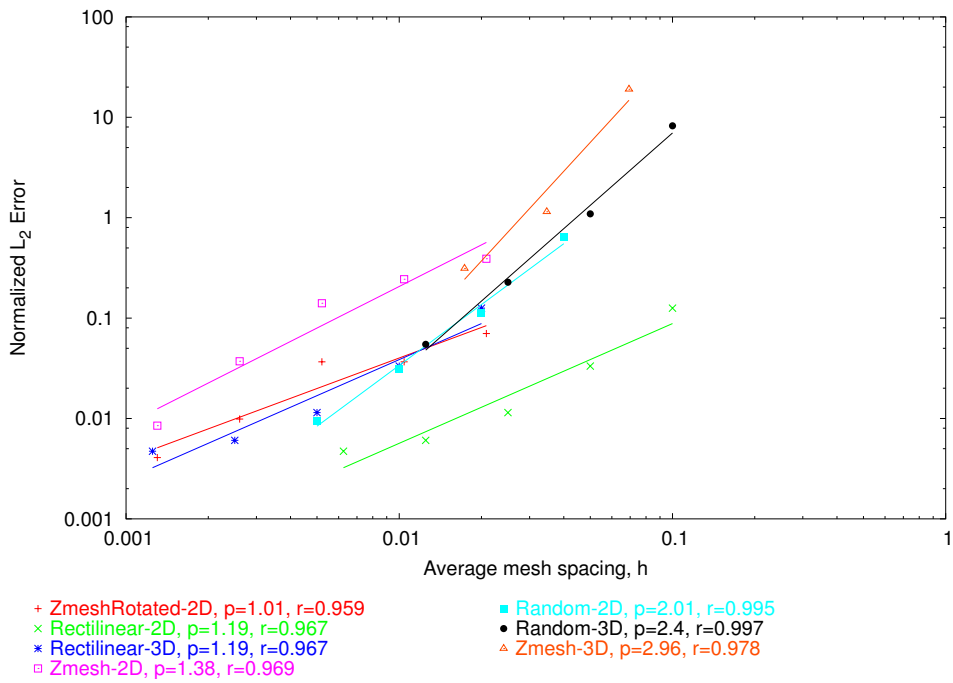

Figure 3.12. Pulsed slab source problem. The discontinuity in the initial conditions makes it difficult to converge the problem, and we may not be in the asymptotic regime, making the order of convergence not valid.

3.8 Polynomial Solutions

In Sections 3.5.1, 3.3.1, and 3.5.2 we have already shown constant, linear, and quadratic solutions, but only in one dimension aligned with the coordinate system and mesh. If we use the same system parameters as before, for example steady state without absorption for the linear case, we can get other polynomial solutions. If we pick the constants in the solutions, we can drive the problem by setting Dirichlet boundary conditions. This is a very simplified view of [17].

3.8.1 Constant

In an infinite medium with constant material properties, the radiation temperature should be also be uniform and the same as the material temperature.

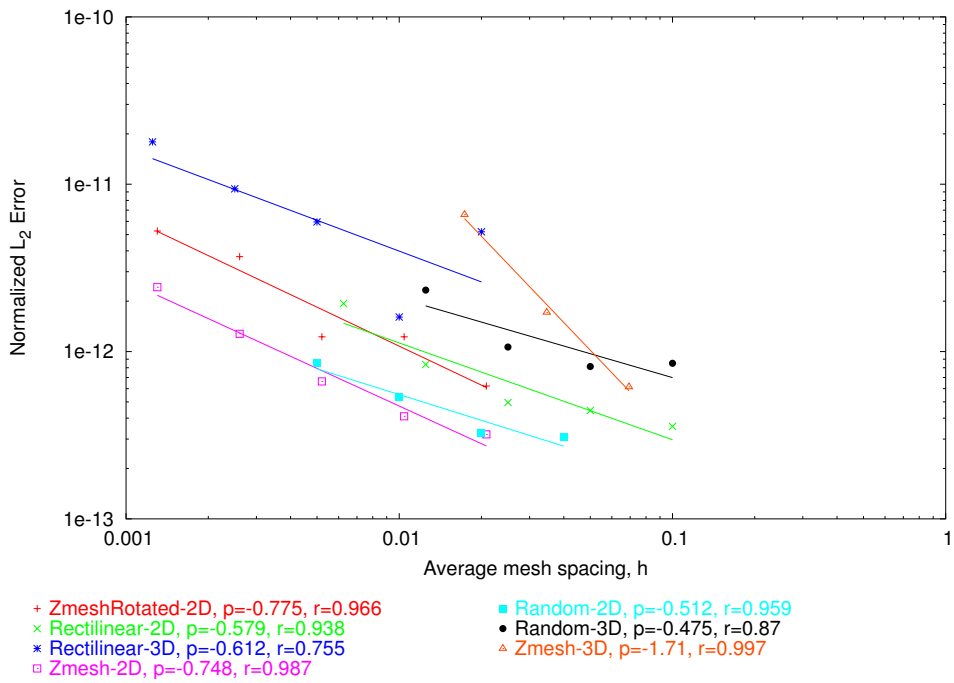

Figure 3.13. Uniform infinite medium problem. This second order diffusion method should get this exactly within the linear solver tolerance, so there is no expected convergence.

3.8.2 Linear

Extending Section 3.3.1 to three dimensions, the steady state diffusion equation without absorption looks like

$$\nabla^2 E = 0. \tag{3.8.1}$$

This has a linear solution

$$E = \mathbf{a} \cdot \mathbf{x} + b. \tag{3.8.2}$$

We can pick the values for $\mathbf{a}$ and b so that on the domains of interest the solution stays positive.

3.8.3 Quadratic

In three dimensions with only scattering and a source, the appropriate diffusion equation is

$$\nabla^2 E = -\frac{3\sigma_t}{c} S. \tag{3.8.3}$$

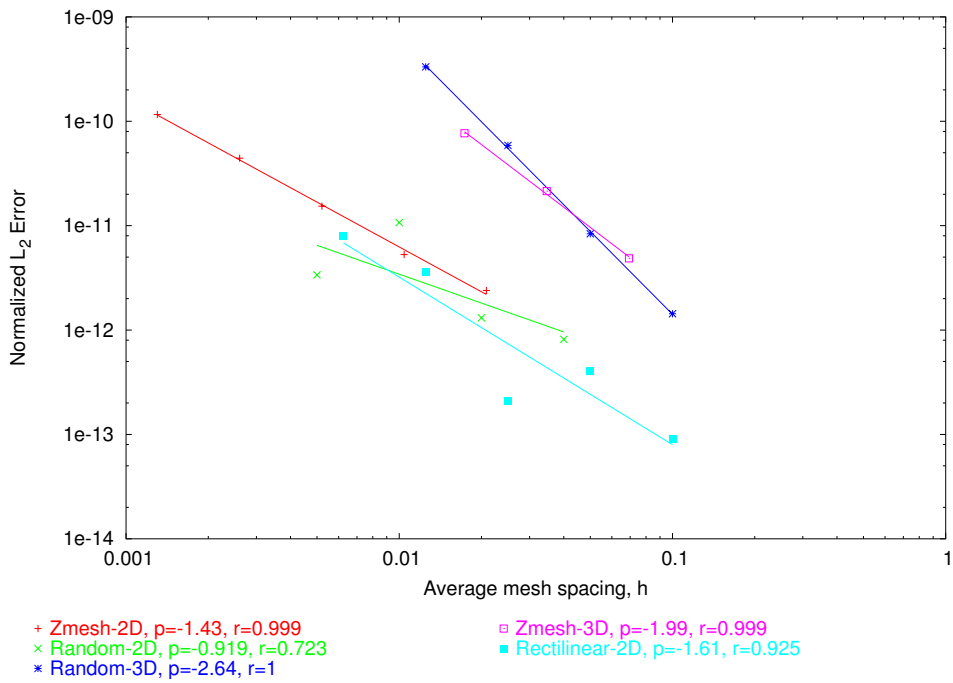

Figure 3.14. Linear problem with Dirichlet boundary conditions. This second order diffusion method should get this exactly within the linear solver tolerance, so there is no expected convergence.

The general solution to this is

$$E = ax^2 + by^2 + c'z^2 + dxy + eyz + fxz + gx + hy + iz + k \tag{3.8.4}$$

We can pick the constants, a through k, so that on the meshes that we will use, the energy density stays positive. Additionally we have the constraint that

$$2(a + b + c') = -\frac{3\sigma_t}{c}S. \tag{3.8.5}$$

If we arbitrarily set $b = 2a$ and $c' = 3a$, we get

$$a = -\frac{\sigma_t}{4c}S, \tag{3.8.6}$$

Setting $d = e = f = g = h = i = 0$ yields

$$E = -\frac{\sigma_t S}{4c}(x^2 + 2y^2 + 3z^2) + k \tag{3.8.7}$$

If we want a positive energy density over $-1 < x, y, z < 1$, then

$$k > \frac{3\sigma_t S}{2c}. \tag{3.8.8}$$

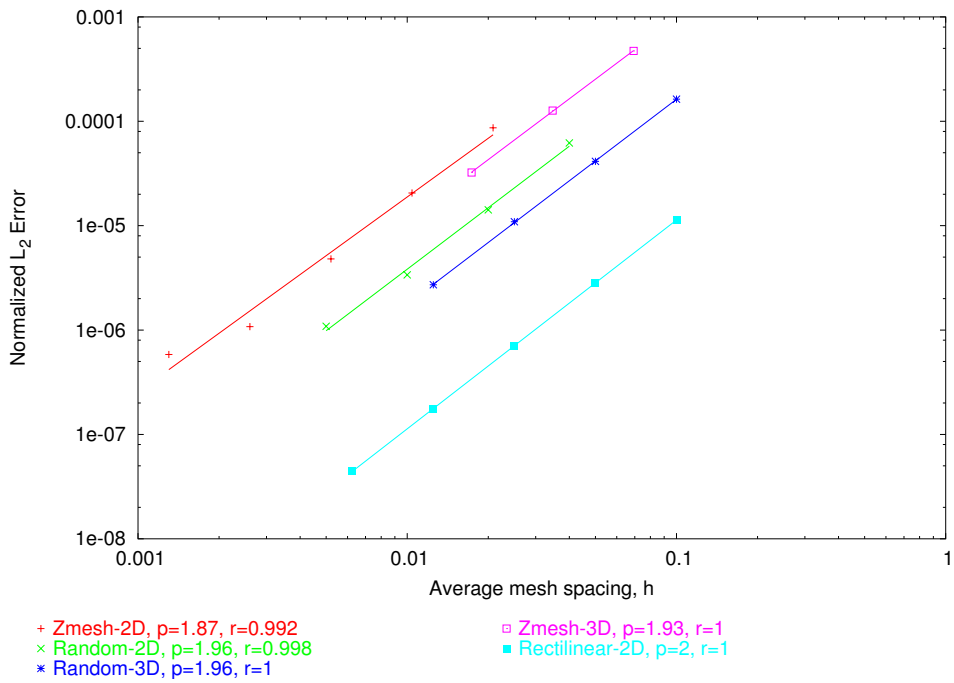

Figure 3.15. Quadratic problem with Dirichlet boundary conditions.

3.9 Manufactured Solutions

The diffusion equation can only be solved analytically for relatively simple problems, but one would like to verify the code is working on more complicated (and realistic) problems as well. The Method of Manufactured Solutions (MMS) is a relatively simple way to test the code on very complicated problems[25, 15, 20]. The idea is to assume some function for the solution, for example the solution varies linearly with space. The assumed solution is then inserted into the equation, and the equation is solved for the external source that is needed to support that solution. This source is then used as input into the code, and the code should recover the solution that you assumed.

A key part of doing MMS is to convergence studies of the code; even if the errors in the code are of a reasonable magnitude, if the code does not converge at the expected rate, there may be an error. Salari[15] recommends a test problem where all features of the code are tested simultaneously. While this is important, simpler tests are also useful in pinpointing problems in the code.

The error[15] of a given solution can be computed using an L_2 norm of the

relative error integrated over the entire domain, namely

$$\varepsilon = \sqrt{\frac{1}{V}\int_D \left(\frac{E_{\text{code}} - E_{\text{analytic}}}{E_{\text{analytic}}}\right)^2 \mathrm{d}V} \tag{3.9.1}$$

On a regular grid where all the zones are the same size, the volume integral can be replaced by a summation solution at the computational points (nodes, zone centers, etc.) using

$$\varepsilon = \sqrt{\frac{1}{N}\sum_{i=1}^{N}\left(\frac{f(\mathbf{x}_i) - \tilde{F}_i}{\tilde{f}(\mathbf{x}_i}\right)^2}, \tag{3.9.2}$$

where N is the number of grid points, $f(\mathbf{x}_i)$ is the exact solution, and $\tilde{F}_i$ and the simulated result, at all the grid points, $\mathbf{x}_i$. Eq. 3.9.2 is only valid for regular grids and is not used here.

Once in the asymptotic regime, the order of accuracy p can be computed with as few as two simulations using

$$p = \frac{\log \frac{\varepsilon_{\text{course}}}{\varepsilon_{\text{fine}}}}{\log \frac{\Delta x_{\text{course}}}{\Delta x_{\text{fine}}}}, \tag{3.9.3}$$

where Δx is a characteristic grid length.

Four main aspects of the code have not been tested by the simple problems in the previous sections. These include the flux limiters, material coupling, arbitrarily varying material properties, and photon energy dependence. One problem will be devised to test each of these along with fifth problem that will test all features of the code at once.

3.9.1 A Flux Limiter Test

Staring with Eq. 3.2.1 with cold, constant, uniform materials, we can solve for the source term

$$S_r = c\left(\sigma_a E - \nabla \cdot D \nabla E\right) \tag{3.9.4}$$

A Gaussian shaped solution in space as a function of radius is not one that the diffusion equation approximation will get exactly correct and tests the multidimensional features of the code, But manipulating a Gaussian solution in Eq. 3.9.4, namely

$$E_{\text{FL}} = E_0\, \mathrm{e}^{-\kappa r'^2}, \tag{3.9.5}$$

is relatively straight forward. Here, r' is the distance from the origin, and the exact form depends on the coordinate system. For two dimensional Cartesian coordinates, we define a cylindrically symmetric solution, where

$$r' = r = \sqrt{x^2 + y^2}. \tag{3.9.6}$$

The two dimensional Cartesian and cylindrical versions of the code can be used to compute the cylindrically symmetric solutions. We can also define a spherically symmetric solution, where

$$r' = \rho = \sqrt{x^2 + y^2 + z^2} = \sqrt{r^2 + z^2}, \tag{3.9.7}$$

which can be used to test the two dimensional cylindrical and the three dimensional Cartesian versions of the code.

Inserting these into Eq. 3.9.4 for regular diffusion yields

$$S_{\text{3D POD}} = c\left[\sigma_a + \frac{2\kappa}{3\sigma_t}(3 - 2\rho^2\kappa)\right] E_{\text{FL}} \tag{3.9.8}$$

and

$$S_{\text{2D POD}} = c\left[\sigma_a + \frac{4\kappa}{3\sigma_t}(1 - r^2\kappa)\right] E_{\text{FL}}. \tag{3.9.9}$$

Using the Larsen 2 flux limiter instead, gives us

$$S_{\text{3D L2}} = c\left[\sigma_a + \frac{16\rho^2\kappa^3(1 - \rho^2\kappa) + 18\kappa(3 - 2\rho^2\kappa)\sigma_t^2}{(4\rho^2\kappa^2 + 9\sigma_t^2)^{3/2}}\right] E_{\text{FL}}. \tag{3.9.10}$$

and

$$S_{\text{2D L2}} = c\left[\sigma_a + \frac{8r^2\kappa^3(1 - 2r^2\kappa) + 36\kappa(1 - r^2\kappa)\sigma_t^2}{(4r^2\kappa^2 + 9\sigma_t^2)^{3/2}}\right] E_{\text{FL}}. \tag{3.9.11}$$

For the Larsen limiter, we can write down a metric for the amount of flux limiting that is being done, namely

$$C_1 = \frac{|\nabla E|}{E 3\sigma_t} = \frac{2\kappa r}{3\sigma_t}. \tag{3.9.12}$$

At $r = 0$ the limiter is turned off. At some arbitrarily large value, say $C_1 = 100$, it is almost completely flux limited. Eq. 3.9.12 can be used to choose a consistent set of problem parameters that tests the entire range of the flux limiter.

3.9.2 Coupling to a Uniform Material

In thermal radiation transport, the radiation energy density is coupled to the material through the following equations

$$\frac{\partial E}{\partial t} - \frac{c}{3\sigma_t}\nabla^2 E = c\sigma_a(B(T) - E) + S \tag{3.9.13}$$

$$\rho C_v \frac{\partial T}{\partial t} = -c\sigma_a(B(T) - E), \tag{3.9.14}$$

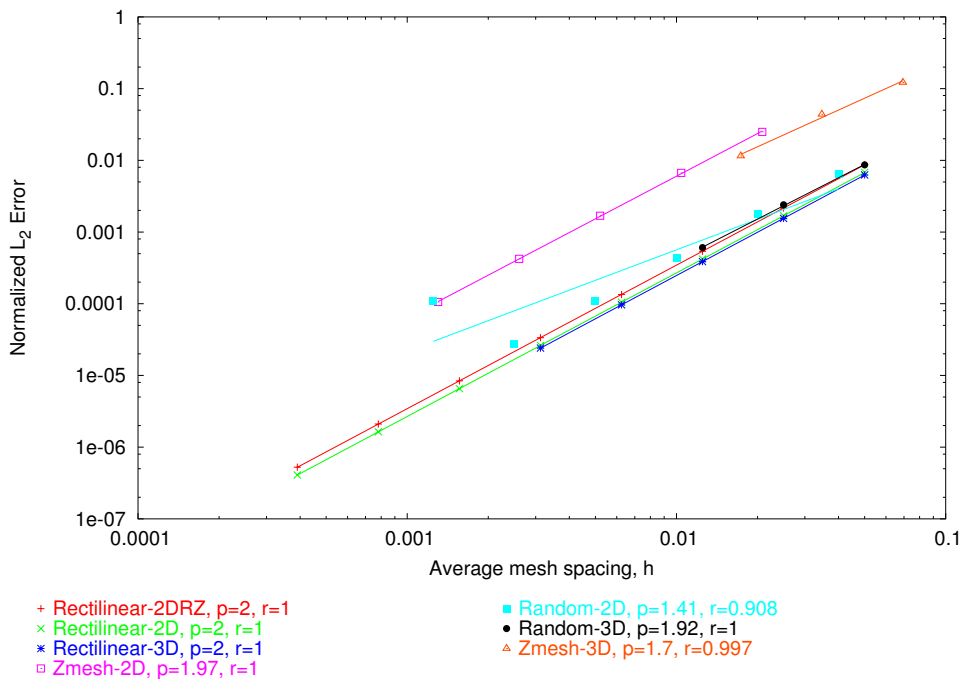

Figure 3.16. Regular diffusion MMS test.

where T is the material temperature, and $B(T)$ is the black body function. Instead of solving for T, we'd like to change variables to $B(T) = aT^4$, assuming one group diffusion. With a change of variables, Eq. 3.9.14 then becomes

$$\frac{\rho C_v}{4aT^3}\frac{\partial B}{\partial t} = -c\sigma_a(B - E). \tag{3.9.15}$$

We will now assume the solution for B to be

$$B_{\text{MC}}(\mathbf{x}, t) = aT_0\, \mathrm{e}^{-\tau t - \kappa r^2}, \tag{3.9.16}$$

where $r = |\mathbf{x}|$; equivalently, the material temperature is

$$T(\mathbf{x}, t) = T_0\, \mathrm{e}^{-\frac{1}{4}(\tau t + \kappa r^2} \tag{3.9.17}$$

Inserting this into Eq. 3.9.15 and solving for E yields

$$E_{\text{MC}}(\mathbf{x}, t) = \left[1 - \frac{\rho C_v \tau}{4ac\sigma_a T^3}\right] B_{\text{MC}}(\mathbf{x}, t) \tag{3.9.18}$$

In order to simplify taking the derivatives on E_{MC} in Eq. 3.9.13, we would like to make the multiplier in Eq. 3.9.19 to be constant in space. This can be done by

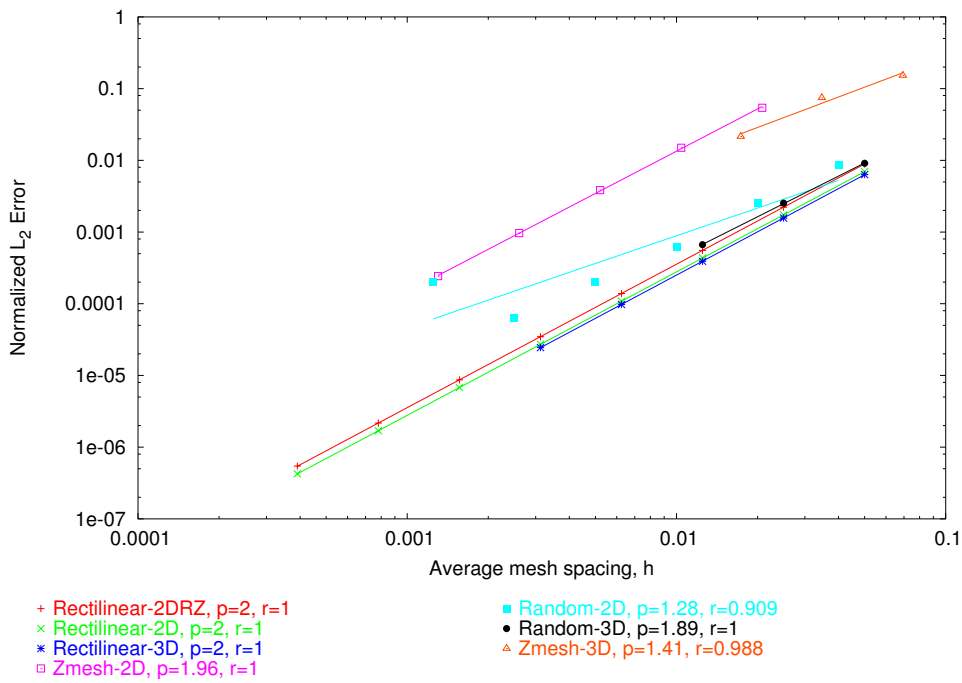

Figure 3.17. Larsen-2 flux limiter MMS test.

choosing $\rho C_v = \alpha T^3$; This form of the specific heat is used by Pomraning in several of his test problems. With this, Eq. 3.9.18 becomes

$$E_{\text{MC}}(\mathbf{x}, t) = \left[1 - \frac{\alpha\tau}{4ac\sigma_a}\right] B_{\text{MC}}(\mathbf{x}, t). \tag{3.9.19}$$

The results are very similar to the last section, with the addition of a time derivative term in the source. For regular diffusion we get

$$S_{\text{3D POD}} = c\left[\sigma_a - \frac{\tau}{c} + \frac{2\kappa}{3\sigma_t}(3 - 2\rho^2\kappa)\right] E_{\text{MC}} \tag{3.9.20}$$

and

$$S_{\text{2D POD}} = c\left[\sigma_a - \frac{\tau}{c} + \frac{4\kappa}{3\sigma_t}(1 - r^2\kappa)\right] E_{\text{MC}}. \tag{3.9.21}$$

We need to choose these parameters so that the coupling between the equations is strong enough. To do that, we'd like the terms in the inhomogeneous source in Eq. 3.9.13 to be roughly the same magnitude. For 3D regular diffusion, the inhomogeneous source is

$$S_{\text{inhomogeneous}} = \left(\left[\sigma_a - \frac{\tau}{c} + \frac{2\kappa}{3\sigma_t}(3 - 2\rho^2\kappa)\right]\left[1 - \frac{\alpha\tau}{4ac\sigma_a}\right] + \sigma_a\left[\frac{\alpha\tau}{4ac\sigma_a}\right]\right) B_{\text{MC}}(\mathbf{x}, t) \tag{3.9.22}$$

Setting these terms equal implies

$$\frac{\left[\sigma_a - \frac{\tau}{c} + \frac{2\kappa}{3\sigma_t}(3 - 2r^2\kappa)\right]\left[1 - \frac{\alpha\tau}{4ac\sigma_a}\right]}{\left[\frac{\alpha\tau}{4ac}\right]} \approx 1 \tag{3.9.23}$$

or

$$\left[1 - \frac{\tau}{c\sigma_a} + \frac{2\kappa}{3\sigma_t\sigma_a}(3 - 2r^2\kappa)\right]\left[\frac{4ac\sigma_a}{\alpha\tau} - 1\right] \approx 1. \tag{3.9.24}$$

We would also like the radiation energy density to be positive, which implies

$$0 < \frac{\alpha\tau}{4ac\sigma_a} < 1. \tag{3.9.25}$$

Finally, we would also like to have the flux limiter, if we were using one, to vary significantly, so C_1 in Eq. 3.9.12 should be chosen large enough.

We now have three equations to help us choose our constants, namely

$$\frac{2\kappa r}{3\sigma_t} = C_1 \tag{3.9.26}$$

$$\frac{\alpha\tau}{4ac\sigma_a} = C_2 \tag{3.9.27}$$

$$\left[1 - \frac{\tau}{c\sigma_a} + \frac{2\kappa}{3\sigma_t\sigma_a}(3 - 2r^2\kappa)\right]\left[\frac{4ac\sigma_a}{\alpha\tau} - 1\right] = C_3, \tag{3.9.28}$$

where $0 < C_2 < 1$ and $C_3 \approx 1$. Nature determines a and c. We choose $C_1 = 10$, $C_2 = \frac{1}{4}$, $C_3 = \frac{1}{2}$, $\kappa = 5$, and $\alpha = 3.026306806045420251 \times 10^{-14}$. ($\alpha$ is chosen to be the same in the Su-Olsen benchmarks, and is a multiple of the black body constant.) Solving for σ_a, σ_t, and τ in Eq. 3.9.26 through Eq. 3.9.28 yields

$$\sigma_t = \frac{2r\kappa}{3C_1} \tag{3.9.29}$$

$$\sigma_a = \frac{\frac{\alpha}{4a}C_1(C_2 - 1)(3 - 2r^2\kappa)}{C_2 r(C_2 - 1) - r\frac{\alpha}{4a}(C_2 + C_2C_3 - 1)} \tag{3.9.30}$$

$$\tau = \frac{cC_1C_2(C_2 - 1)(3 - 2r^2\kappa)}{C_2 r(C_2 - 1) - r\frac{\alpha}{4a}(C_2 + C_2C_3 - 1)}. \tag{3.9.31}$$

For the chosen set of parameters at $r = 1$, we get $\sigma_t = \frac{1}{3}$, $\sigma_a = 120$, and $\tau = 9 \times 10^{11}$. This implies that $\sigma_s = \sigma_t - \sigma_a < 0$, which is unphysical, but since σ_s never appears in the equations, this doesn't matter. Nothing about a manufactured solution or its problem specification needs to be physical, but traps in the code that test for certain physical conditions should not be activated.

This problem can be run both single and multigroup, as well as with logically different materials, from the code's point of view, even if all the materials behave the same. It is also possible, without modification, to use a varying absorption

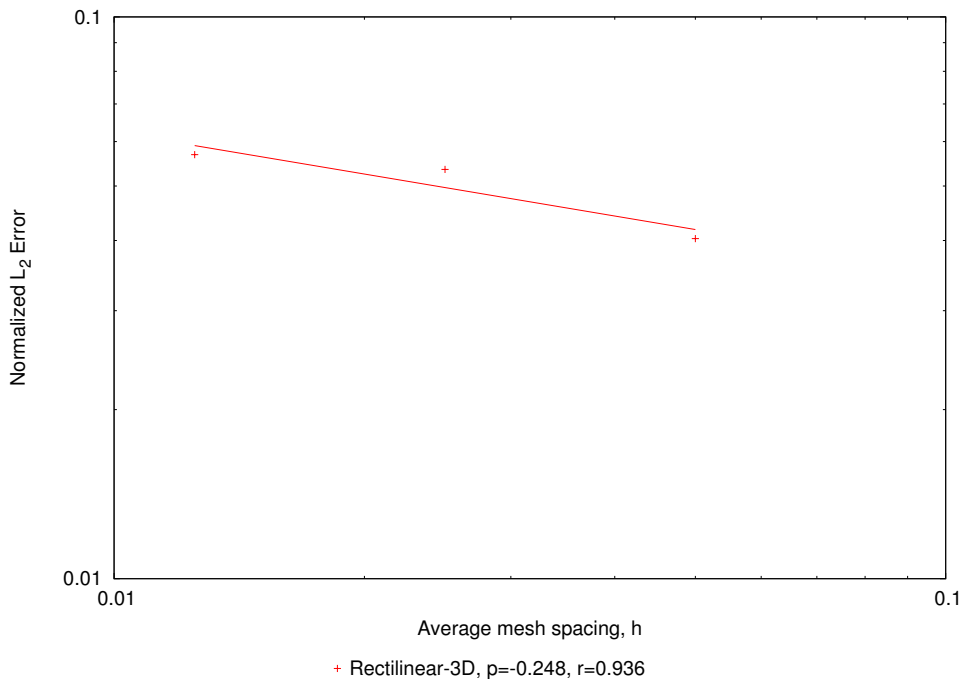

Figure 3.18. Radiation energy density results in a MMS test with coupling to a uniform material using regular diffusion. This problem does not converge as expected and is still be investigated.

opacity while holding the total cross section constant. While this does not test the flux limiter's dependence on varying materials, it does test the material coupling in that situation.

This problem does not converge as expected and is still be investigated.

3.9.3 Nonuniform Opacities

The assumed solution to the energy density is similar to the last section, namely

$$E_{\mathrm{NO}}(\mathbf{x}, t) = A\,\mathrm{e}^{-\tau t - \kappa r^2}, \tag{3.9.32}$$

and the total opacity has the following form

$$\sigma_t(r) = \sigma_a(r) = \sigma_0\,\mathrm{e}^{\lambda r}, \tag{3.9.33}$$

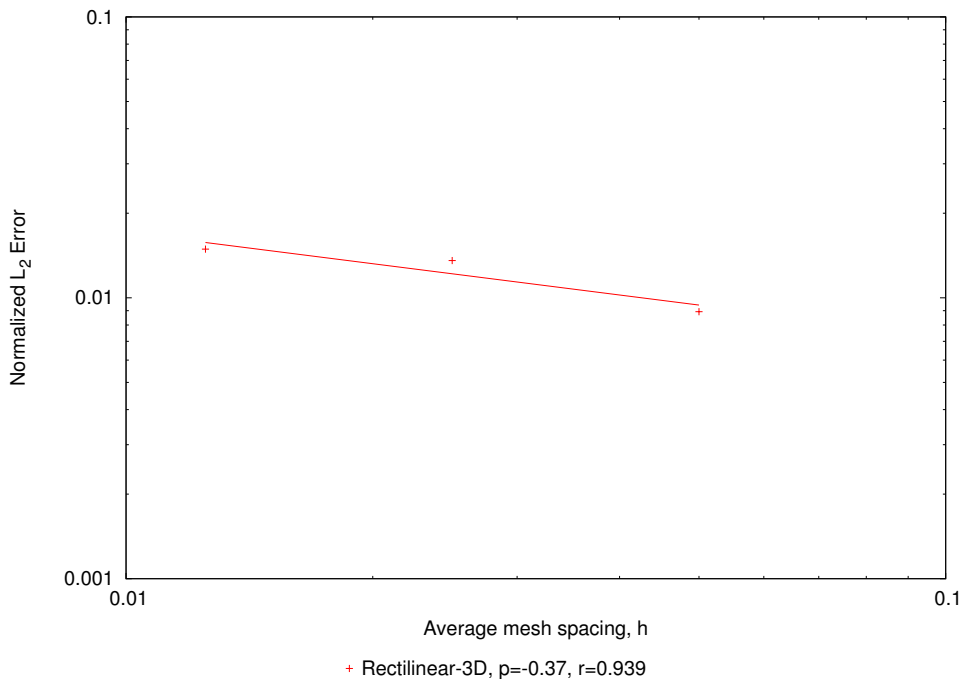

Figure 3.19. Material temperature results in a MMS test with coupling to a uniform material using regular diffusion. This problem does not converge as expected and is still be investigated.

where σ_0 and λ are arbitrary parameter that can be used to adjust the shape of the flux limiting parameter,

$$\chi = \frac{2\kappa r}{3\sigma_0}\,\mathrm{e}^{-\lambda r}. \tag{3.9.34}$$

Again, it is important to test the entire range of the flux limiter, namely $0 < \chi < 100$. Some parameters that do this are $\kappa = 10$, $\lambda = 8$, $\sigma_0 = 0.005$ on the range $0 < r < 1$.

Inserting the same assumed energy density and this opacity into the diffusion equation without material coupling, we get sources needed to support it. For regular diffusion

$$S_{\text{3D POD}} = c\left[\sigma_0\,\mathrm{e}^{\lambda\rho} - \frac{\tau}{c} - \frac{2\kappa}{3\sigma_0\,\mathrm{e}^{\lambda\rho}}\left(2\rho^2\kappa + \lambda\rho - 3\right)\right] E_{\text{NO}} \tag{3.9.35}$$

and

$$S_{\text{2D POD}} = c\left[\sigma_0\,\mathrm{e}^{\lambda r} - \frac{\tau}{c} - \frac{2\kappa}{3\sigma_0\,\mathrm{e}^{\lambda r}}\left(2r^2\kappa + \lambda r - 2\right)\right] E_{\text{NO}} \tag{3.9.36}$$

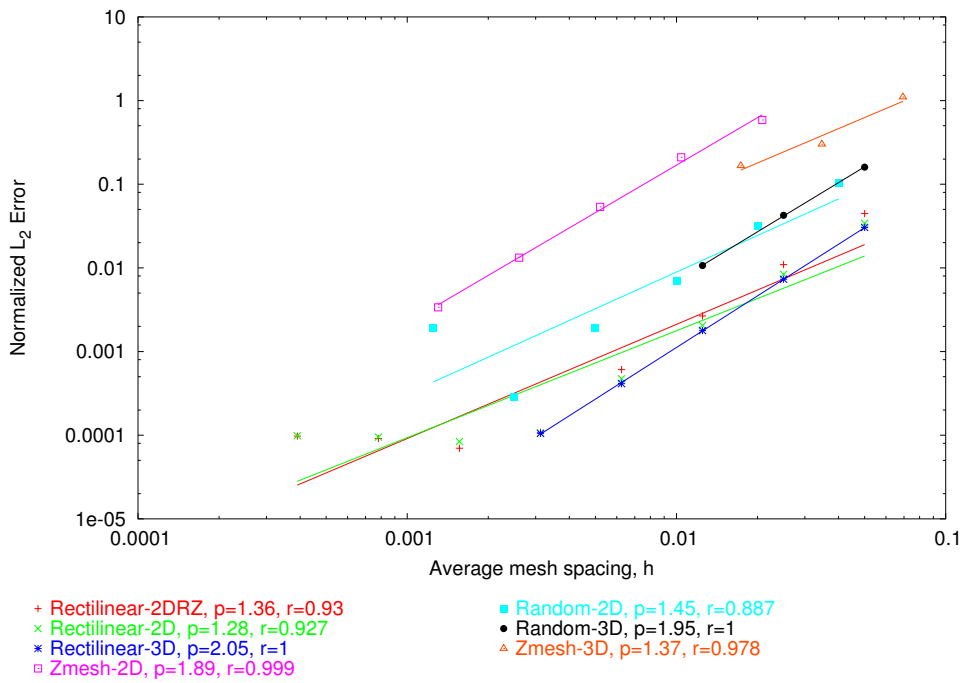

Figure 3.20. MMS test with spatially varying opacities and regular diffusion.

For the Larsen 2 flux limiter, we get

$$S_{\text{3D L2}} = c\left[\sigma_0\,\mathrm{e}^{\lambda\rho} - \frac{\tau}{c} + \frac{16\rho^2\kappa^2(\kappa-\rho^2\kappa^2) + 18\sigma_0^2\,\mathrm{e}^{2\lambda\rho}(3\kappa - 2\rho^2\kappa^2 - \rho\lambda\kappa)}{\left(4\rho^2\kappa^2 + 9\sigma_0^2\,\mathrm{e}^{2\lambda\rho}\right)^{3/2}}\right] E_{\text{NO}} \tag{3.9.37}$$

and

$$S_{\text{2D L2}} = c\left[\sigma_0\,\mathrm{e}^{\lambda r} - \frac{\tau}{c} + \frac{8r^2\kappa^2(\kappa-2r^2\kappa^2) + 18\sigma_0^2\,\mathrm{e}^{2\lambda r}(2\kappa - 2r^2\kappa^2 - r\lambda\kappa)}{\left(4r^2\kappa^2 + 9\sigma_0^2\,\mathrm{e}^{2\lambda r}\right)^{3/2}}\right] E_{\text{NO}} \tag{3.9.38}$$

3.9.4 Multigroup

We'll assume the following form of the energy density:

$$E_{\text{MG}}(t,\varepsilon) = E_0\,\mathrm{e}^{-\tau t - \alpha\varepsilon - \kappa\rho^2}. \tag{3.9.39}$$

We will also assume an opacity with the following form:

$$\sigma_t = \sigma_a = \sigma_0 \, \mathrm{e}^{-\beta\varepsilon}, \tag{3.9.40}$$

where $0 < \beta < \alpha$. Inserting these into Eq. 2.1.1 and solving for the source in the plane diffusion, three dimensional case without material coupling gives us a result very similar to Eq. 3.9.8

$$S_{\text{3D MG}} = E_0 \, \mathrm{e}^{-\tau t - \kappa\rho^2} \left[-\tau \, \mathrm{e}^{-\alpha\varepsilon} + c\sigma_0 \, \mathrm{e}^{-(\alpha+\beta)\varepsilon} + \frac{2\kappa c}{3\sigma_0}(3 - 2\rho^2\kappa) \, \mathrm{e}^{-(\alpha-\beta)\varepsilon} \right] \tag{3.9.41}$$

We can integrate this source over an energy group g, with $\varepsilon_g \leq \varepsilon < \varepsilon_{g+1}$ to get

$$\begin{aligned} S_{\text{3D MG},g} = E_0 \, \mathrm{e}^{-\tau t - \kappa\rho^2} \Bigg[& c\sigma_0 \frac{\mathrm{e}^{-(\alpha+\beta)\varepsilon_g} - \mathrm{e}^{-(\alpha+\beta)\varepsilon_{g+1}}}{\alpha+\beta} \\ & + \frac{2\kappa c}{3\sigma_0}(3 - 2\rho^2\kappa) \frac{\mathrm{e}^{-(\alpha-\beta)\varepsilon_g} - \mathrm{e}^{-(\alpha-\beta)\varepsilon_{g+1}}}{\alpha-\beta} \\ & - \tau \frac{\mathrm{e}^{-\alpha\varepsilon_g} - \mathrm{e}^{-\alpha\varepsilon_{g+1}}}{\alpha} \Bigg] \end{aligned} \tag{3.9.42}$$

Similarly for two dimensions we find

$$\begin{aligned} S_{\text{2D MG},g} = E_0 \, \mathrm{e}^{-\tau t - \kappa r^2} \Bigg[& c\sigma_0 \frac{\mathrm{e}^{-(\alpha+\beta)\varepsilon_g} - \mathrm{e}^{-(\alpha+\beta)\varepsilon_{g+1}}}{\alpha+\beta} \\ & + \frac{4\kappa c}{3\sigma_0}(1 - r^2\kappa) \frac{\mathrm{e}^{-(\alpha-\beta)\varepsilon_g} - \mathrm{e}^{-(\alpha-\beta)\varepsilon_{g+1}}}{\alpha-\beta} \\ & - \tau \frac{\mathrm{e}^{-\alpha\varepsilon_g} - \mathrm{e}^{-\alpha\varepsilon_{g+1}}}{\alpha} \Bigg] \end{aligned} \tag{3.9.43}$$

Normally there is an approximation in the multigroup equations because the exact spectrum of the energy density is unknown and usually approximated with a Plank spectrum. Since we know the energy density spectrum, we can compute an exact group average opacity that will make the group equations exact, namely

$$\sigma_{a,g} = \frac{\int_{\varepsilon_g}^{\varepsilon_{g+1}} \sigma_a E_{\text{MG}} \, \mathrm{d}\varepsilon}{\int_{\varepsilon_g}^{\varepsilon_{g+1}} E_{\text{MG}} \, \mathrm{d}\varepsilon} = \sigma_0 \left[\frac{\alpha}{\alpha+\beta} \right] \left[\frac{\mathrm{e}^{-(\alpha+\beta)\varepsilon_g} - \mathrm{e}^{-(\alpha+\beta)\varepsilon_{g+1}}}{\mathrm{e}^{-\alpha\varepsilon_g} - \mathrm{e}^{-\alpha\varepsilon_{g+1}}} \right]. \tag{3.9.44}$$

Similarly, the Rosseland mean opacity is

$$\sigma_{r,g} = \left[\frac{\int_{\varepsilon_g}^{\varepsilon_{g+1}} \frac{1}{\sigma_t} E_{\text{MG}} \, \mathrm{d}\varepsilon}{\int_{\varepsilon_g}^{\varepsilon_{g+1}} E_{\text{MG}} \, \mathrm{d}\varepsilon} \right]^{-1} = \sigma_0 \left[\frac{\alpha-\beta}{\alpha} \right] \left[\frac{\mathrm{e}^{-\alpha\varepsilon_g} - \mathrm{e}^{-\alpha\varepsilon_{g+1}}}{\mathrm{e}^{-(\alpha-\beta)\varepsilon_g} - \mathrm{e}^{-(\alpha-\beta)\varepsilon_{g+1}}} \right]. \tag{3.9.45}$$

The group-wise energy density is

$$E_{\text{MG},g} = E_0 \, \mathrm{e}^{-\tau t - \kappa\rho^2} \left[\frac{\mathrm{e}^{-\alpha\varepsilon_g} - \mathrm{e}^{-\alpha\varepsilon_{g+1}}}{\alpha} \right]. \tag{3.9.46}$$

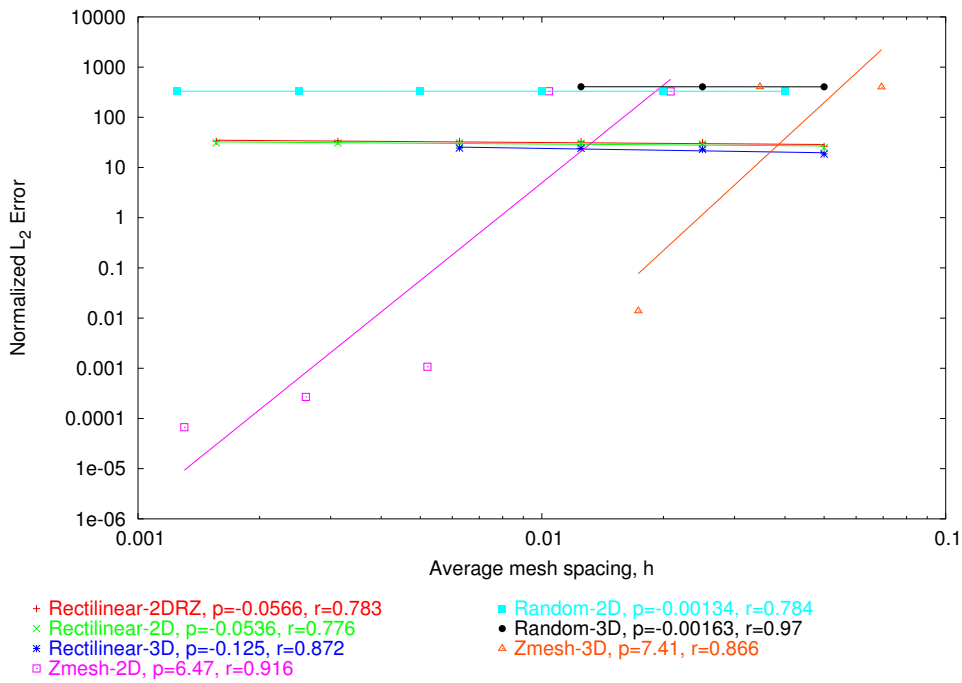

Figure 3.21. MMS test of the multigroup equations integrating all groups. Because of the opacities, the higher groups are optically thin, and an automatic diffusion coefficient limiter kicks in to keep the matrix well-conditions. This causes it to diverge from the correct answer, however.

There are two main limitations with this test. The first is the fact that this spectrum and opacity are far from what is typically used in the the code. The second is that it does not couple with the material, and consequently the groups are not coupled to each other. Running the test that does couple with the material in multigroup mode alleviates some of this concern, but not entirely because that opacity doesn't change with energy.

3.10 Transport Tests

The IMC should stay in equilibrium with a material in a box uniformly filled with a material at a given temperature. The radiation temperature should be the same as the material temperature. This is mostly a test of energy conservation, but many parts of the code need to be working in order for this to work. We will also check convergence of the radiation temperature field to the known solution as the num-

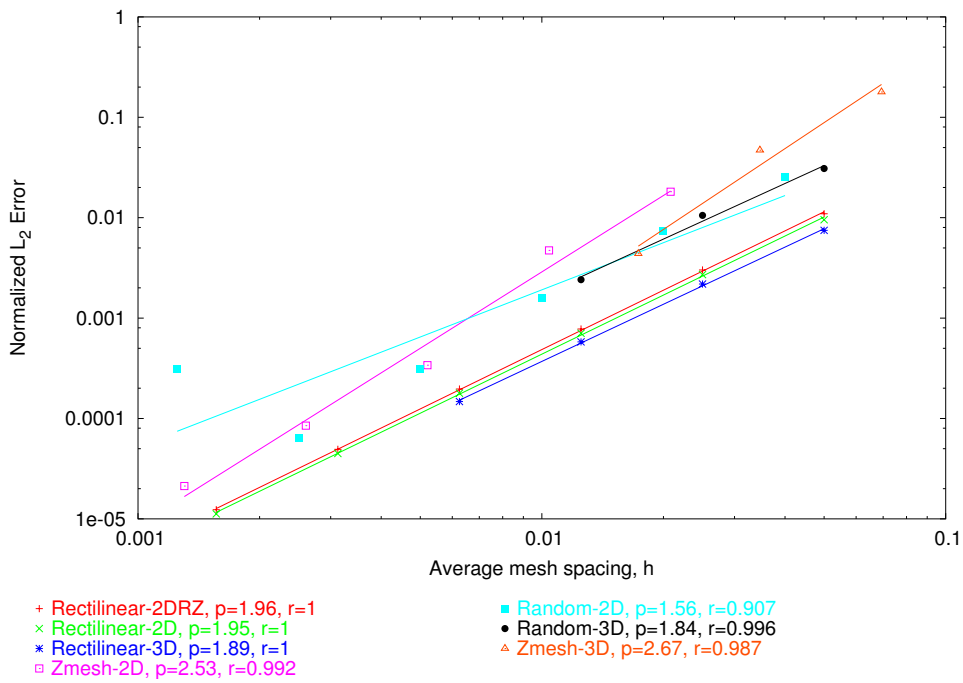

Figure 3.22. MMS of Multigroup, looking at only the second group's results. Without the influence of the thin groups, this converges as expected.

ber of photons increases. The convergence should be

$$\varepsilon = \frac{C}{\sqrt{N}} \tag{3.10.1}$$

where ε is the error in the simulation, C is some constant, and N is the number of photons.

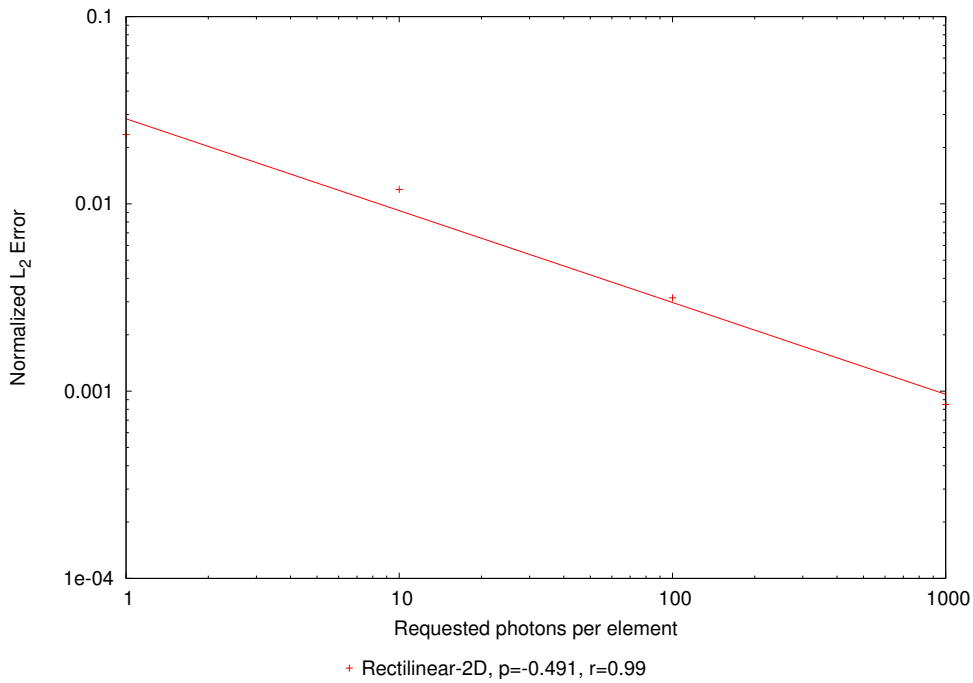

Figure 3.23. A hot, uniform box calculated using Implicit Monte Carlo. As the number of particles (N) increases, the error should be proportional to $1/\sqrt{N}$.

3.11 Meshes

Since most of the analytic solutions are one dimensional, each problem is run on different meshes to stress the solution method. Below, in Figures 3.24-3.25 each of the meshes is shown.

3.12 Conclusions and Future Work

The tests outlined above verify that the radiation diffusion package in ALEGRA is mostly working correctly. There are a few cases where the linear solver failed to converge, creating erroneous results. This behavior still needs to be investigated, but several fixes and new features are being implemented by the Trilinos team that may address these issues.

Currently these tests are only being run one way. Different things can be done as sanity checks to increase the confidence in the code. These include:

- Fill mesh with varying degrees of two (or more) materials that are really the same, should get one material answer. This should be both all cells uniformly filled with different volume fractions as well as something like a a pie shape inserted on a square mesh. This could test any number of materials per element. Each fraction of material should behave the same as the other parts in the element.
- Fill mesh with varying degrees of multiple materials that are different, should get same as average value. I'm not so sure about the material response here.
- Use periodic boundaries.
- Also compute analytic flux tallies across various surfaces and compare to the code.
- Run some diffusive problems with the IMC. It should be possible to get the diffusion result. Boundary differences between diffusion and IMC probably limit this to infinite medium or MMS solutions.
- Wave-like problem with "real" specific heats and opacities as a function of temperature. Since this is one of the primary modes of running the code, it would be good to develop a test for it.

Many benchmark problems have been described in the literature. Most are analytic solutions to one-dimensional problems, and suffer many of the same limitations as the earlier problems in this document. The manufactured solutions tests

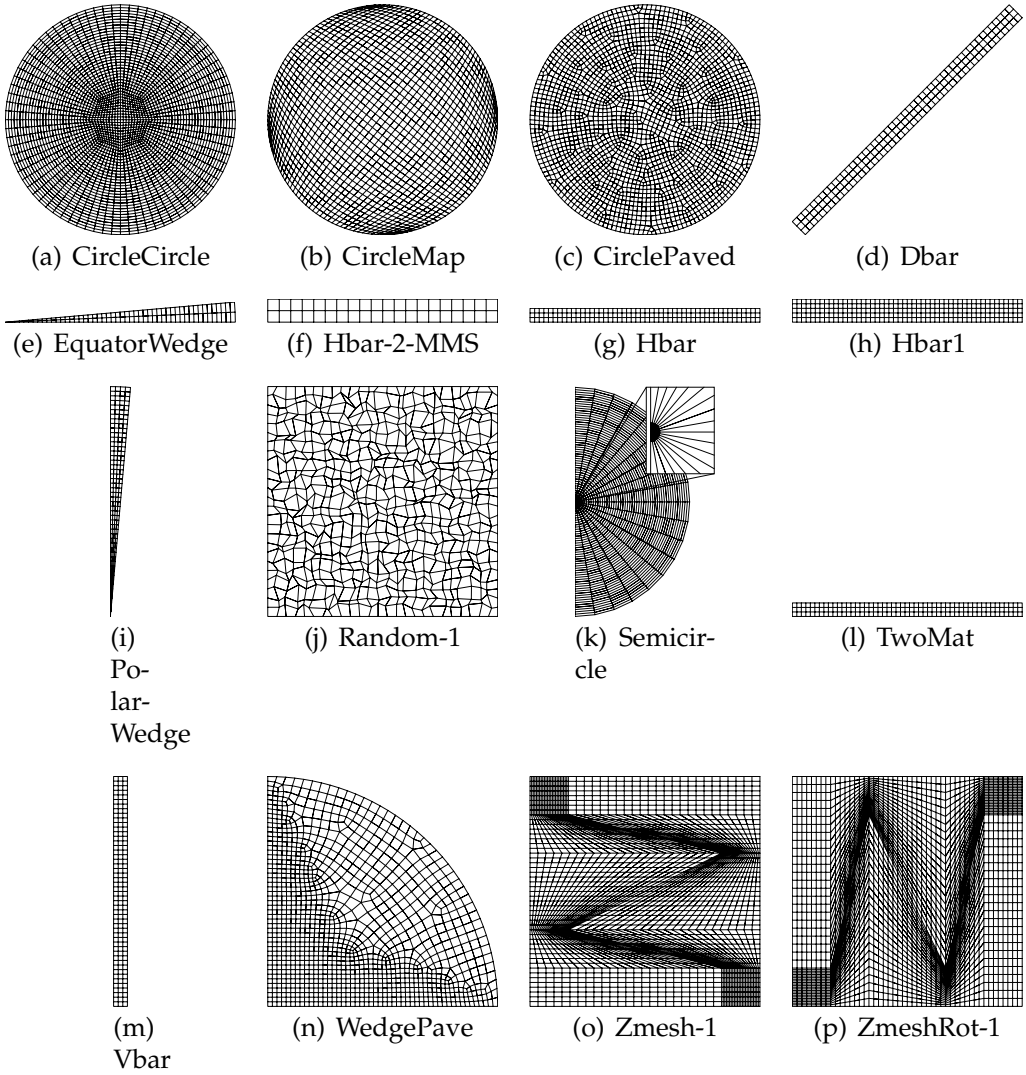

Figure 3.24. Two Dimensional Meshes

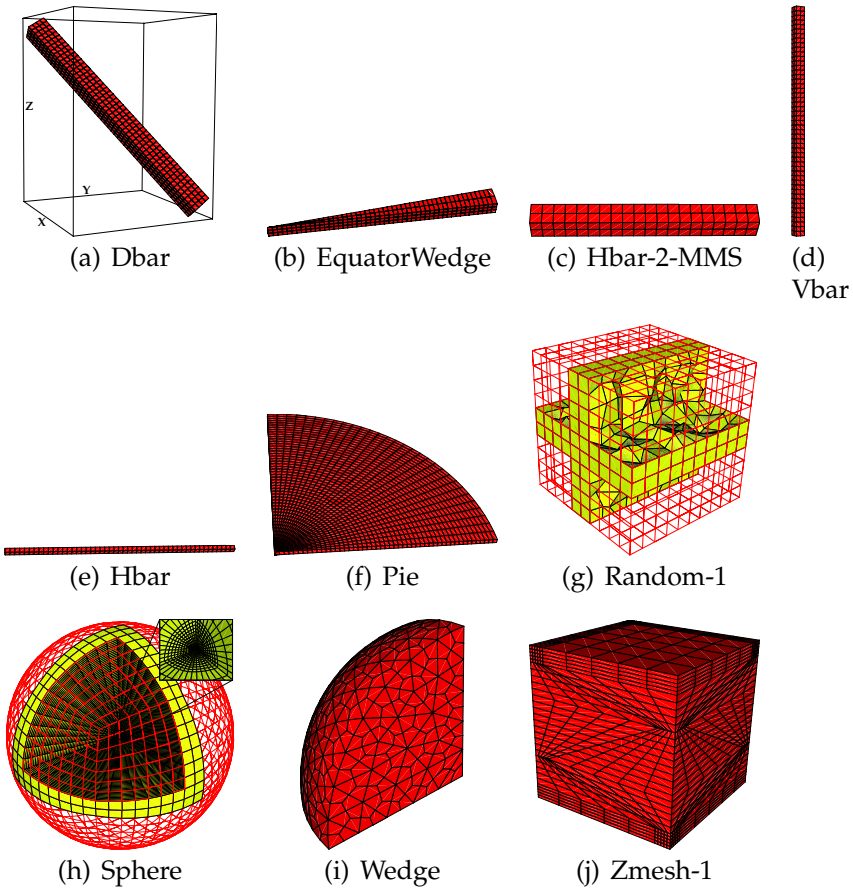

(a) Dbar (b) EquatorWedge (c) Hbar-2-MMS (d) Vbar

(e) Hbar (f) Pie (g) Random-1

(h) Sphere (i) Wedge (j) Zmesh-1

Figure 3.25. Three Dimensional Meshes, part 1.

in Section 3.9 are more comprehensive than most these problems, from a software implementation point of view. These tests may be more physical problems that improve the confidence level of the code on particular problems. The tests are:

- Su-Olson Marshak [30], an analytic solution to the diffusion equation coupled to the material with a very unphysical form for the specific heat.
- Su-Olson Source region [31], a diffusion and transport solution to a source-driven problem that is coupled to the material temperature.
- So-Olson Picket Fence [32], a multigroup test with an analytic answer.
- Frank Graziani at LLNL is working on a different multigroup benchmark test.
- Barry Ganapol has developed many benchmarks, and are mostly solution of transport equation.[9, 11, 10]

Chapter 4

Spherical Harmonics

Riemann solvers have been extensively researched as methods for the numerical solution of problems in computational fluid dynamics (CFD). [1] These methods respect the finite propagation speed and non-dissipative nature of hyperbolic conservation laws (e.g. the Euler equations or the transport equation). The success of Riemann solver based finite volume schemes in the CFD community has spurred the research into the application of these methods for radiation transport [4, 5, 6, 8]. These methods performed well in capturing steep-gradients, and [4, 5, 6] utilized explicit time integration while [8] solves steady-state problems.

The development of implicit time-integration methods for Riemann solvers became the next logical step in developing practical computer codes. However, one obstacle in this endeavor is the nonlinear nature of high resolution Riemann solvers, a characteristic that arises out of the necessity that slope reconstruction be nonlinear to achieve better than first order accuracy. To accomplish implicit time integration, it is therefore necessary to solve a system of nonlinear equations at each time step. Solving nonlinear systems seems somewhat of a bugbear in the transport community and some have even suggested that Riemann solvers were inherently explicit [34]. Due to the advent of Newton-Krylov methods [16] it is now possible to efficiently solve nonlinear systems. Using one such method we have developed an implicit Riemann solver for time-dependent transport.

We also have investigated the properties of Riemann solvers in problems of a "diffusive" nature, that is, in problems where scattering interactions dominate. At steady-state these problems are described by an elliptic diffusion equation, which is an approximation to the full transport equation in the limit of asymptotically small absorption and small sources. In radiation transport the steady-state solution to diffusive problems varies on a length scale characterized by the diffusion length $L = 1/\sqrt{3\Sigma_t\Sigma_a}$ which is much larger than a mean-free-path $1/\Sigma_t$. As is well known,

[1] See [18] for a detailed discussion

time dependent diffusion is governed by a parabolic equation, and that, unlike hyperbolic problems, parabolic equations are characterized by infinite propagation speed of information. They are also characterized by dissipation: they produce smooth solutions even from non-smooth sources and initial data.

This presents a challenge: Riemann solvers are specifically designed to solve hyperbolic equations and to upwind information flow at finite speed in a minimally dissipative way. Riemann solvers will give good results for cells that are on the order of $1/\Sigma_t$ or smaller, but to resolve the solution in a diffusive problem a cell on the order of L should be sufficient. For robustness we would hope that a Riemann solver would capture this diffusive solution on a spatial grid that only resolves the diffusion length L. A method that has this robustness property is said to have a diffusion limit.

We will show that the standard Roe-type Riemann solver for the P_n equations does *not* have a diffusion limit. Because of this a mean-free path must be resolved to obtain a good steady solution even in diffusive problems. An asymptotic analysis of the problem reveals that the main impediment to a diffusion limit in a Riemann solver is the numerical dissipation present in the scheme. This grid-size-dependent dissipation is present in a Riemann solver to make it upwinded and thus maintain the proper physics of finite propagation speed, and hence stability. However, the collisional interactions that in transport physics dominate the diffusion limit represent another type of dissipation. The number of particles traveling in a given direction is reduced by collisions. We propose a method that recovers the diffusion limit by systematically scaling out the numerical dissipation in regions where scattering collisions dominate. The result is a hybrid method that is a Riemann solver when the grid resolves a mean-free-path, but which becomes a centered difference method when when the grid is large. With the use of this scaling, a proper diffusion limit exists for the modified Roe-type Riemann solver.

4.1 The Discretization of the P_n equations

4.1.1 The P_n Equations

The equations we seek to solve are the one-dimensional, one-speed P_n equations with isotropic scatter

$$\begin{gathered}\frac{1}{c}\frac{\partial\psi_0}{\partial t}+\frac{\partial}{\partial x}\left(B_1\psi_1\right)+\Sigma_a\psi_0=\frac{Q}{2\sqrt{\pi}}\\ \frac{1}{c}\frac{\partial\psi_1}{\partial t}+\frac{\partial}{\partial x}\left(A_{l-1}\psi_{l-1}+B_{l+1}\psi_{l+1}\right)+\Sigma_t\psi_l=0 \qquad l=1\ldots n\\ \psi_{n+1}=0.\end{gathered} \tag{4.1.1}$$

The moments, ψ_l are defined as

$$\psi_l = \int_{-1}^{1} Y_l^0 \psi(x,\mu) d\mu \tag{4.1.2}$$

$$Y_l^0(\mu) = \sqrt{\frac{2l+1}{4\pi}} P_l(\mu), \tag{4.1.3}$$

where ψ is the angular flux and P_l is the lth Legendre polynomial. Also,

$$A_l = \sqrt{\frac{(l+1)^2}{(2l+3)(2l+1)}} \tag{4.1.4}$$

$$B_l = \sqrt{\frac{l^2}{(2l+1)(2l-1)}}, \tag{4.1.5}$$

and c is the particle speed, Σ_a, Σ_t are the absorption and total cross-sections, and Q is the inhomogeneous source. We can also write Eq. (4.1.1) as

$$\frac{1}{c}\frac{\partial \psi}{\partial t} + \mathbf{A}\frac{\partial \psi}{\partial x} + \mathbf{S}\psi = \mathbf{Q} \tag{4.1.6}$$

with ψ the $n+1$ length vector of moments ψ_l, $\mathbf{Q}$ is a vector of length $n+1$, and $\mathbf{A}$ and $\mathbf{S}$ are $(n+1)\times(n+1)$ matrices.

4.1.2 Cell-Averaged Equations and Riemann Solver

Integrating Eq. (4.1.6) over a spatial cell and dividing by the cell width yields

$$\frac{1}{c}\frac{\partial \psi_i}{\partial t} + \mathbf{A}\frac{\psi_{i+1/2} - \psi_{i-1/2}}{\Delta x} + \mathbf{S}\psi_i = \mathbf{Q}_i, \tag{4.1.7}$$

where

$$\psi_i = \frac{1}{\Delta x}\int_{x_i-\Delta x}^{x_i+\Delta x} \psi dx. \tag{4.1.8}$$

Notice that the terms involving $\psi_{i\pm 1/2}$ are not cell-averaged quantities, in fact these are the values at the cell interfaces. Finding expressions for these terms, which represent the flow of information from cell to cell, as functions of cell averaged quantities is the heart of a Riemann solver. To find these values in terms of cell-averaged quantities we exactly solve a simpler problem. This problem is the Riemann problem in which ψ is treated as an initial constant on each side of the cell interface. Its exact solution [2] gives

$$\mathbf{A}\psi_{i+1/2} = \sum_{\lambda_k>0} \lambda_k \mathbf{l_k}\cdot\psi_i \mathbf{r_k} + \sum_{\lambda_k<0} \lambda_k \mathbf{l_k}\cdot\psi_{i+1}\mathbf{r_k}. \tag{4.1.9}$$

[2]For a thorough discussion of the solution to the Riemann problem in cases such as this see [2].

where the λ_k are the eigenvalues of $\mathbf{A}$, with left and right eigenvectors $\mathbf{l}_k$, $\mathbf{r}_k$ respectively. Notice that this solution is up-winded – positive eigenvalues move information from the left to the right and negative eigenvalues from the right to the left. We can also rewrite Eq. (4.1.9) as

$$\mathbf{A}\psi_{i+1/2} = \frac{1}{2}\mathbf{A}\left(\psi_{i+1} + \psi_i\right) - \frac{1}{2}\sum_{\lambda_k} |\lambda_k| \mathbf{l}_k \cdot \left(\psi_{i+1} - \psi_i\right) \mathbf{r}_k \tag{4.1.10}$$

When Eq. (4.1.10) is introduced into Eq. (4.1.7) the equation will appear to be a centered difference approximation to the spatial derivative with some added dissipation.

4.1.3 Slope Reconstruction

Equation 4.1.10 will yield a first-order accurate spatial method. To get a higher-order method we will reconstruct the solution using linear interpolation within a cell to have a better estimate of the solution at the cell boundary in Eq. (4.1.10). We seek to prevent the introduction of artificial oscillations into the solution, hence a nonlinear method must be used to calculate the slope within a cell to achieve better than first order accuracy. This is a statement of Godunov's Theorem [18]. The method we use comes from van Leer [33], and on a uniform mesh the equation for each element of ψ_i is

$$\psi_{l,i\pm 1/2} = \psi_{l,i} \pm \frac{\Delta x}{2} m_i, \tag{4.1.11}$$

where the slope m_i is computed as

$$m_i = \frac{|m_-|m_+ + m_-|m_+|}{|m_+| + |m_-|}, \tag{4.1.12}$$

with

$$m_- = \frac{\psi_{l,i} - \psi_{l,i-1}}{\Delta x} \tag{4.1.13}$$

$$m_+ = \frac{\psi_{l,i} - \psi_{l,i-1}}{\Delta x}. \tag{4.1.14}$$

Now Eq. 4.1.10 becomes

$$\begin{aligned} \mathbf{A}\psi_{i+1/2} =& \frac{1}{2}\mathbf{A}\left(\psi_{i+1} - \frac{\Delta x}{2}\mathbf{m}_{i+1} + \psi_i + \frac{\Delta x}{2}\mathbf{m}_i\right) \\ &- \frac{1}{2}\sum_{\lambda_k} |\lambda_k| \mathbf{l}_k \cdot \left(\psi_{i+1} - \frac{\Delta x}{2}\mathbf{m}_{i+1} - \psi_i + \frac{\Delta x}{2}\mathbf{m}_i\right) \mathbf{r}_k. \end{aligned} \tag{4.1.15}$$

The way $\mathbf{m}$ is calculated ensures that artificial extrema are not introduced at the cell interface. Also notice that the only difference between Eq. 4.1.10 and Eq. 4.1.15 are the "$\mathbf{m}$" terms. This is only a small correction to the first-order scheme, a fact that we shall take advantage of in our implementation.

4.1.4 Time Integration

Time integration was handled using the backward Euler method in which Eq. 4.1.7 becomes

$$\frac{1}{c}\frac{\psi_i^{j+1}-\psi_i^j}{\Delta t}+\frac{1}{\Delta x}\mathbf{A}\left(\psi_{i+1/2}^{j+1}-\psi_{i+1/2}^{j+1}\right)=-\mathbf{S}\psi_i^{j+1}+\mathbf{Q}_i^{j+1}, \tag{4.1.16}$$

The first-order spatial scheme given by Eq. 4.1.10 presents a system of linear equations that must be solved at each time step. This system is block tridiagonal and asymmetric with the blocks being square matrices of size $(n+1)$. The high resolution scheme that results from using Eq. 4.1.15 in Eq. 4.1.16 is a *nonlinear* system of equations. Each equation in the system can be represented as a linear part (the same linear operator from the first-order scheme) plus a nonlinear part that contains the slope reconstruction.

4.2 Implementation

The above scheme was implemented in the computer code ROOSTER (Riemann, Object-Oriented Solver for the Transport of Energetic Radiation). This is an object oriented code written in `C++` using the Trilinos solver library [14] available from Sandia National Laboratories. Trilinos' AztecOO package was used to solve the linear systems of the first-order scheme using the Generalized Minimal Residual (GMRES) method. AztecOO is able to exploit the block tri-diagonal nature of this system.

For the nonlinear system arising from the high resolution scheme, the NOX package of Trilinos is used. Specifically, the system is solved using a matrix-free Newton-Krylov method. This method does not require the specification of the Jacobian of the nonlinear system, instead the Jacobian is approximated by finite differences. The nonlinear system is solved efficiently by preconditioning the system with the matrix from the first-order system. This is an ideal preconditioner because the high-resolution scheme is basically a correction to that first-order system – hence the inverse of the linear system is a good approximate to the inverse of the nonlinear system. Using this preconditioner causes the solution time of the nonlinear system to be comparable to that of the linear system.

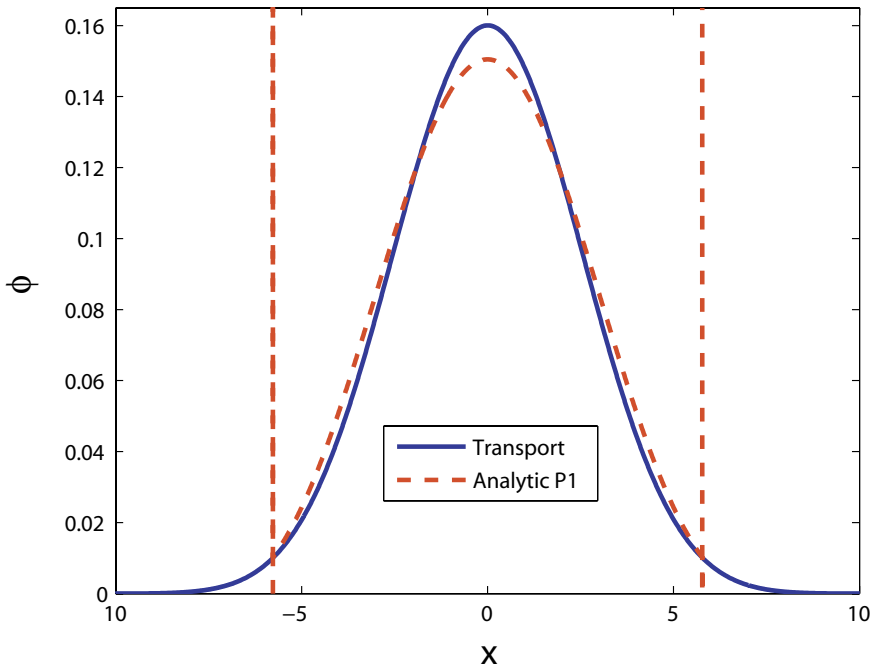

Figure 4.1. The scalar flux for the first test problem at $T = 10$ after the initial pulse

4.3 Test Problems

4.3.1 Plane Source

The first test problem solved using ROOSTER involved a purely scattering medium, $\Sigma_s = \Sigma_t = 1$ in which at time $t = 0$ a plane pulse of particles is emitted at the origin (i.e. a problem with initial condition $\psi_0(x, t = 0) = \delta(x)$). This problem has an analytic transport solution due to Ganapol [9] and an analytic P_1 solution from Brunner [2]; both solutions can be seen in Figure 4.3.1.

This problem presents a numerical method with a mare's nest of difficulties. Early in time the P_n solution is a series of delta function spikes moving away from the origin, but as time progresses a smooth solution representing the collided particles grows in the middle of the domain. Hence, a numerical scheme must capture both steep gradients (the spikes) and smooth regions. Also the method must move the uncollided particles at the appropriate speed.

Table 4.1. Material Layout in Reed's Problem

Vacuum Boundary	Scattering Region		Vacuum	Absorber	Strong Source	Reflecting Boundary
	$\Sigma_a = 0.1$ $\Sigma_s = 0.9$			$\Sigma_a = 5$ $\Sigma_s = 0$ $S = 0$	$\Sigma_a = 50$ $\Sigma_s = 0$ $S = 50$	
	$S = 0$ $\Delta x = 2$	$S = 1$ $\Delta x = 2$	$\Delta x = 2$	$\Delta x = 1$	$\Delta x = 2$	

4.3.2 Reed's Problem

The other test problem is known as Reed's problem [27], this is a multi-material problem with a steady-state solution. The problem set up is detailed in Table 4.3.2. This problem features very distinct material types and provides a way to assess a method's ability to handle the interfaces between dissimilar media.

4.4 Results

4.4.1 Plane Source Problem

Figures 4.2 and 4.3 give representative high resolution results from calculations we have performed on the plane source problem using the high-resolution scheme. In these figures CFL is an abbreviation of the Courant-Friedrichs-Lewy number given by CFL $\equiv c\Delta t/\Delta x$, with the so-called CFL limit being CFL ≤ 1 for stability in explicit schemes.

Figure 4.2 demonstrates that the computed P_1 scalar flux is converging, as expected, to a solution that captures the analytic P_1 solution in the middle region of the problem, but even for large CFL $= 50$ the numerical solution captures the exact solution away from the P_1 wavefront. The front of the wave of particles with speed $\pm\sqrt{(1/3)}$ – which is captured in the analytic solution by a delta function – is not advected at the proper speed with large time steps. This is not an artifact from the Riemann solver, rather it arises from the time integration scheme, as can be seen in [2]. In this reference results for the same problem using explicit time integration have the wave fronts moving at the appropriate speeds. Increasing the size of the time step beyond the CFL limit moves particles at the wrong speeds. This effect is seen in Fig. 4.2, in which we see that as Δt is reduced (CFL decreases for Δx fixed) the wave-front tracks the correct location more accurately.

Figure 4.3(a) gives results from a P_5 calculation at $T = 10$ after the pulse. Results for time steps much smaller than ten give good agreement with the transport

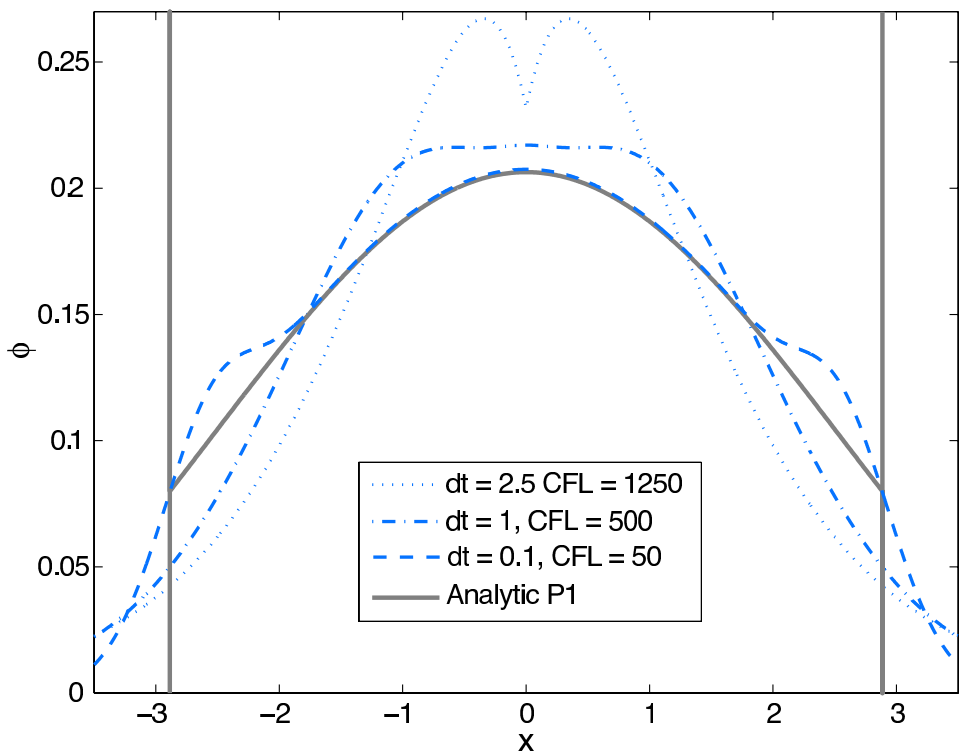

Figure 4.2. Results of P_1 calculations $T = 5$ after the initial pulse of particles is introduced

solution. As the size of the time step becomes on the order of ten, the error in the middle of the problem grows and the effect of moving particles at the wrong speeds becomes apparent. The error convergence as the time step is decreased is also demonstrated in this figure. The linear convergence on a logarithmic scale (seen in Fig. 4.3(b)) suggests that the time integration scheme is converging linearly in Δt – the expected result for the backward Euler method.

4.4.2 Reed's Problem

Steady state problems are solved in ROOSTER using what is colloquially referred to as "time-stepping to steady state." An initial condition is given and this condition is propagated forward in time until the solution converges (i.e. the difference in solution vectors between successive time steps is sufficiently small). The results for steady state calculations using the high resolution spatial scheme on Reed's problem are given in Fig. 4.4. These are P_7 solutions obtained using the high resolution spatial scheme and $\Delta t = 10$ for various Δx values. Here we see that our method is able to handle the sharp changes in solution behavior at the material interfaces and the solution is fairly insensitive to increasing the spatial grid size.

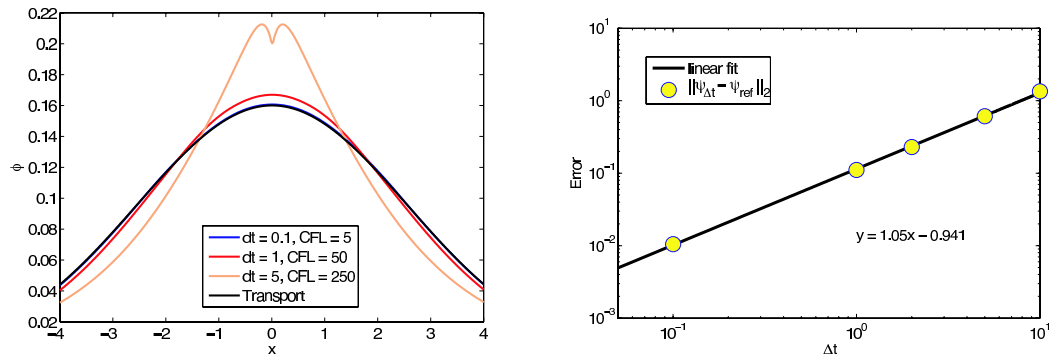

(a) The scalar flux for different values of Δt.

(b) Error convergence as a function of Δt; ψ_{ref} was calculated with $\Delta t = 0.01$.

Figure 4.3. Results from P_5 solution at $T = 10$ after pulse

Also, in Fig. 4.4 the S_8 solution using the multidimensional multi-balance method [13] is shown. The agreement of the solutions suggests that the implicit Riemann solver is converging to the correct solution.

Figure 4.5(a) shows the solution to Reed's problem at $T = 1$. The initial condition had all moments set to zero and steady state solution "grows" out of this. The only region where the solution is sensitive to the size of the time step is the region with non-negligible scattering. This suggests that the scattering source (which is ignored in deriving the Riemann solver) becomes important with large Δt and affects the solution in this area. Finally, Fig. 4.5(b) shows that the method is first-order in time.

4.5 The P_n equations and Riemann discretization

Just to recall our notation, consider the one-speed transport equation with speed c, isotropic scattering, and isotropic source

$$\frac{1}{c}\frac{\partial \psi}{\partial t} + \mu \frac{\partial \psi}{\partial x} + \Sigma_t \psi = \frac{\Sigma_s}{2} \int_{-1}^{1} \psi \, d\mu + \frac{Q}{4\pi} \,. \tag{4.5.1}$$

Here the total and scattering cross sections are Σ_t and Σ_s, respectively, Q is the total source strength (particles per length cubed per second), and all quantities depend only on the one spatial variable x.

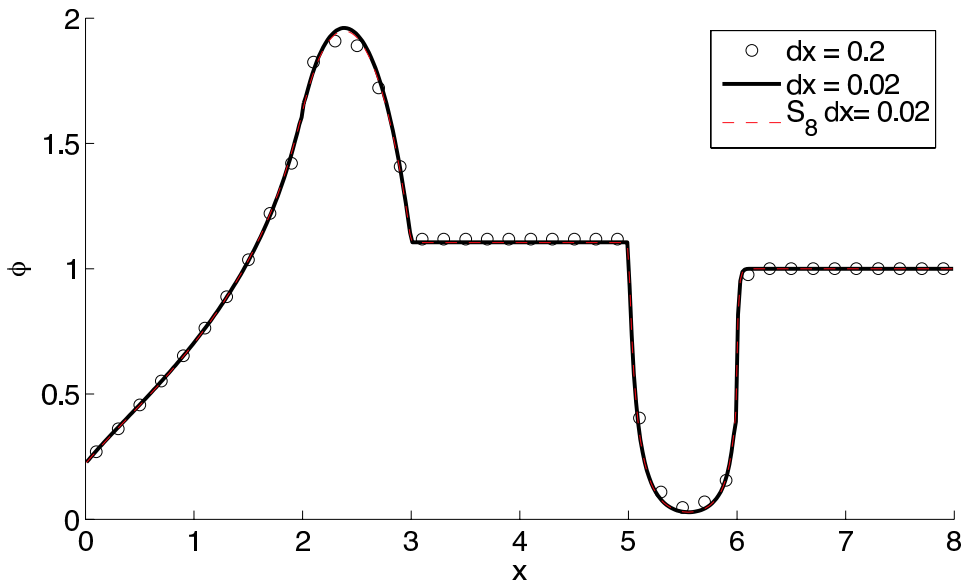

Figure 4.4. Steady state results from Reed's problem

We normalize the spherical harmonics Y_l^m as in Bell & Glassstone [1],

$$Y_l^m(\mu,\varphi) = (-1)^m \sqrt{\frac{2l+1}{4\pi}\frac{(l-m)!}{(l+m)!}} P_l^m(\mu) e^{im\varphi} \tag{4.5.2}$$

$$P_l^m(\mu) = (-1)^m \frac{(1-x^2)^{m/2}}{2^l\, l!}\frac{d^{l+m}}{dx^{l+m}}(x^2-1)^l \tag{4.5.3}$$

and define the moments

$$\psi_l = 2\pi \int_{-1}^{1} Y_l^0(\mu)\psi(x,\mu)\, d\mu\,. \tag{4.5.4}$$

The one-group, one-dimensional spherical harmonic or P_n equations with isotropic scatter are then

$$\begin{gathered} \frac{1}{c}\frac{\partial \psi_0}{\partial t} + \frac{\partial}{\partial x}\left(B_1\psi_1\right) + \Sigma_a\psi_0 = \frac{Q}{2\sqrt{\pi}} \\ \frac{1}{c}\frac{\partial \psi_l}{\partial t} + \frac{\partial}{\partial x}\left(A_{l-1}\psi_{l-1} + B_{l+1}\psi_{l+1}\right) + \Sigma_t\psi_l = 0 \\ \psi_{n+1} = 0, \end{gathered} \tag{4.5.5}$$

with $l = 1 \ldots n$. Here

$$A_l = \sqrt{\frac{(l+1)^2}{(2l+3)(2l+1)}} \tag{4.5.6}$$

$$B_l = \sqrt{\frac{l^2}{(2l+1)(2l-1)}}\,, \tag{4.5.7}$$

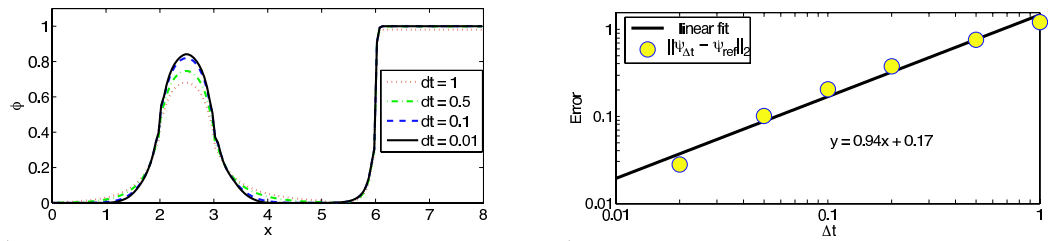

(a) The scalar flux for different values of Δt; cell width is $\Delta x = 0.05$.

(b) Error convergence as a function of Δt; ψ_{ref} was calculated with $\Delta t = 0.01$.

Figure 4.5. Time dependent results from Reed's problem at $T = 1$

and note that in our normalization $\psi_0 = \sqrt{\pi}\int_{-1}^{1}\psi(x,\mu)\,d\mu$ and $\phi = 2\pi\int_{-1}^{1}\psi\,d\mu = 2\sqrt{\pi}\psi_0$. When we wish to write the P_n equations more compactly we will write them as

$$\frac{1}{c}\frac{\partial}{\partial t}\psi + \frac{\partial}{\partial x}\mathbf{A}\psi = -\mathbf{S}\psi + \mathbf{Q}, \tag{4.5.8}$$

where we have collapsed the A and B coefficients into the matrix $\mathbf{A}$, all the interaction cross-sections are in the diagonal matrix $\mathbf{S}$, $\mathrm{diag}(\mathbf{S}) = [\Sigma_a, \Sigma_t, \Sigma_t, \ldots]^T$ and $\mathbf{Q} = [Q/(2\sqrt{\pi}), 0, 0, \ldots]^T$ contains the source terms. Here ψ is a vector of angular moments ascending through l.

The first-order-in-space Riemann discretization of Eq. 4.5.5 [18, 2] is of the form

$$\frac{1}{c}\frac{\partial}{\partial t}\psi_i + \mathbf{A}\frac{(\psi_{i+1} - \psi_{i-1})}{2\Delta x} - |\mathbf{\Lambda}|\,(\psi_{i+1} - 2\psi_i + \psi_{i-1}) = -\mathbf{S}\psi_i + \mathbf{Q}_i(t)\,. \tag{4.5.9}$$

Here ψ_i is a vector of angular moments ascending through l averaged over spatial cell i, and

$$|\mathbf{\Lambda}| = \sum_{k=0}^{n}\mathbf{r}_k|\lambda_k|\mathbf{l}_k\,, \tag{4.5.10}$$

where we denote the kth right and left eigenvectors (normalized so $\mathbf{l}_k\,\mathbf{r}_k = 1$) and eigenvalues of $\mathbf{A}$ by $\mathbf{r}_k, \mathbf{l}_k$, and λ_k respectively. The index k is selected to start at zero because it corresponds to the index l of the spherical harmonics. This discretization is upwinded along each characteristic direction of the system and first order accurate in space. A high-resolution scheme, second order in space, requires a nonlinear limited averaging process resulting in a significantly more complex form for the equations. This higher order scheme is described by [4, 6, 2, 18]. We are more interested in the properties of the discretization in the diffusive limit, and so will content ourselves with the simpler first order discretization in the analysis of the next section.

4.6 Diffusion properties of the P_n equations

Since we study the spherical harmonic equations, we wish to understand their properties in the diffusion limit.

Let us begin by exploring a diffusion-like solution of the transport equation.[3] Suppose that we have a linear-in-space source $Q = qx$ for some constant q, and we seek a solution of the transport equation that is linear in space x and linear in the direction cosine μ. Substituting $\psi(x, \mu) = ax + b\mu$ into Eq. 4.5.1 we find

$$\mu a + \Sigma_t(ax + b\mu) = x\Sigma_s a + x\frac{q}{4\pi}\,. \tag{4.6.1}$$

From this we find $a = q/(4\pi\Sigma_a)$ and $b = -a/\Sigma_t$, and thus

$$\psi(x, \mu) = \frac{q}{4\pi\Sigma_a}\left[x - \frac{\mu}{\Sigma_t}\right] \tag{4.6.2}$$

is a special solution of the one-speed transport equation with constant cross-sections and a linear-in-space isotropic source.

This solution is interesting because it satisfies Fick's law: in particular, it has

$$\phi = 2\pi\int_{-1}^{1}\psi\,d\mu = \frac{q}{\Sigma_a}x \qquad \text{a linear in space scalar flux, and} \tag{4.6.3}$$

$$J = 2\pi\int_{-1}^{1}\mu\psi\,d\mu = -\frac{q}{3\Sigma_a\Sigma_t} = -\frac{1}{3\Sigma_t}\frac{\partial\phi}{\partial x} \qquad \text{a constant current satisfying Fick's law}\,. \tag{4.6.4}$$

Because of this property it has been suggested that a numerical scheme for the transport equation should capture this solution [13, 17] at least in the diffusion limit. A method that can produce these linear solutions is said to be linear solution preserving (LSP). We will see later that the Roe-type Riemann solver for the P_n equations is LSP, and so is the modified Riemann solver that we propose in this paper.

4.6.1 Linear solution of the P_n equations

We should like to know if the P_n equations capture the linear-in-space, linear-in-direction cosine solution just described in Eq. 4.6.2. For that solution we can im-

[3] This is a simple exercise in the method of manufactured solutions, a technique first suggested by Lingus [20]

mediately compute that

$$\psi_0 = \frac{qx}{2\Sigma_a\sqrt{\pi}} \tag{4.6.5}$$

$$\psi_1 = -\frac{q}{2\Sigma_a\Sigma_t\sqrt{3\pi}} \tag{4.6.6}$$

$$\psi_l = 0 \qquad l > 1\,. \tag{4.6.7}$$

Noting that $A_0 = B_1 = 1/\sqrt{3}$, and substituting these into Eqs. 4.5.5 along with $Q = qx$ we discover that they do indeed satisfy the P_n equations. Therefore the P_n equations have the special solution that represents Fick's law.

In order for a numerical scheme to capture this solution it is necessary only that the derivative in the zeroth moment equation map a constant to zero (so it must be at least zeroth order accurate) and the derivative in the first moment equation must map a linear function to a constant of the correct value (so it must be at least first order accurate). These not very demanding conditions will guarantee that a method for the P_n equations will capture the linear-in-space and linear-in-direction cosine solution of the P_n equations. We will note below that the Riemann solver for the P_n equations does have these properties.

We also note in passing that because of the rotational invariance of the spherical harmonic equations, they will in fact have an entire family of linear-in-space and linear-in-direction cosine solutions resulting from rotations of the special x-dependent solution just displayed.

4.6.2 Asymptotic Analysis of the P_n equations

To investigate the diffusive limit of the P_n equations, and numerical methods for them, we want to examine their solution when scattering dominates over absorption namely, $\Sigma_t \gg \Sigma_a$, and when time variation is negligible, $\partial\psi_l/\partial t \approx 0$. To do this we divide Σ_t by a small, positive parameter ϵ and multiply Σ_a, Q and $\partial/\partial t$ by ϵ as well, resulting in

$$\begin{gathered}
\frac{\epsilon}{c}\frac{\partial\psi_0}{\partial t} + \frac{\partial}{\partial x}\left(B_1\psi_1\right) + \epsilon\Sigma_a\psi_0 = \epsilon\frac{Q}{2\sqrt{\pi}} \\
\frac{\epsilon}{c}\frac{\partial\psi_l}{\partial t} + \frac{\partial}{\partial x}\left(A_{l-1}\psi_{l-1} + B_{l+1}\psi_{l+1}\right) + \frac{\Sigma_t}{\epsilon}\psi_l = 0 \\
\psi_{n+1} = 0\,.
\end{gathered} \tag{4.6.8}$$

We also then postulate a asymptotic expansion for ψ_l given by

$$\psi_l \sim \sum_{j=0}^{\infty} \epsilon^j \psi_l^{(j)}(x,t)\,, \quad \epsilon \to 0\,. \tag{4.6.9}$$

Next, we present a theorem on the asymptotic behavior of the P_n equations that we will want to recapture with our modified Riemann solver.

Theorem 1. *Let $\Sigma_t > 0$. Then for the asymptotic expansion Eq. 4.6.9 to satisfy the scaled P_n equations, Eq. 4.6.8, we must have $\psi_l^{(j)} = 0$ for $l > j$. In other words, $\psi_l = O(\epsilon^l)$. Furthermore, the solution satisfies Fick's law at leading order,*

$$\psi_1^{(1)} = -A_0 \frac{\partial \psi_0^{(0)}}{\partial x} \tag{4.6.10}$$

and

$$\frac{1}{c}\frac{\partial \psi_0^{(0)}}{\partial t} - \frac{\partial}{\partial x}\frac{A_0 B_1}{\Sigma_t}\frac{\partial \psi_0^{(0)}}{\partial x} + \Sigma_a \psi_0^{(0)} = \frac{Q}{2\sqrt{\pi}} \tag{4.6.11}$$

Proof by induction. Substituting Eq. 4.6.9 into Eq. 4.6.8 yields

$$\begin{gathered}
\sum_{j=1}^{\infty} \epsilon^j \frac{1}{c}\frac{\partial \psi_0^{(j)}}{\partial t} + \sum_{j=0}^{\infty} \epsilon^j \frac{\partial}{\partial x}\left(B_1 \psi_1^{(j)}\right) + \sum_{j=1} \epsilon^j \Sigma_a \psi_0^{(j-1)} = \epsilon \frac{Q}{2\sqrt{\pi}} \\
\sum_{j=1}^{\infty} \epsilon^j \frac{1}{c}\frac{\partial \psi_l^{(j)}}{\partial t} + \sum_{j=0}^{\infty} \epsilon^j \frac{\partial}{\partial x}\left(A_{l-1}\psi_{l-1}^{(j)} + B_{l+1}\psi_{l+1}^{(j)}\right) + \sum_{j=-1}^{\infty} \epsilon^j \Sigma_t \psi_l^{(j+1)} = 0 \\
\sum_{j=0}^{\infty} \epsilon^j \psi_{n+1}^{(j)} = 0,
\end{gathered} \tag{4.6.12}$$

with $l = 1 \ldots n$. Gathering terms of order ϵ^{-1} yields $\psi_l^{(0)} = 0$ for $l > 0$. Gathering terms of order ϵ^0 yields

$$\frac{\partial}{\partial x}\left(B_1 \psi_1^{(0)}\right) = 0 \tag{4.6.13}$$

$$\frac{\partial}{\partial x}\left(A_{l-1}\psi_{l-1}^{(0)} + B_{l+1}\psi_{l+1}^{(0)}\right) + \Sigma_t \psi_l^{(1)} = 0 \tag{4.6.14}$$

$$\psi_{n+1}^{(0)} = 0\,. \tag{4.6.15}$$

Since $\psi_1^{(0)} = 0$, Eq. 4.6.13 is automatically satisfied. Eq. 4.6.14 for $l = 1$ implies $A_0 \partial \psi_0^{(0)}/\partial x + \Sigma_t \psi_1^{(1)} = 0$, which is Fick's law. Also since $\psi_l^{(0)} = 0$ for $l > 0$, Eq. 4.6.14 for $l > 1$ implies $\psi_l^{(1)} = 0$ for $l > 1$.

Repeating the exercise for terms of order ϵ^1 we will discover that

$$\frac{1}{c}\frac{\partial \psi_0^{(0)}}{\partial t} + \frac{\partial}{\partial x}\left(B_1 \psi_1^{(1)}\right) + \Sigma_a \psi_0^{(0)} = \frac{Q}{2\sqrt{\pi}} \tag{4.6.16}$$

$$\frac{1}{c}\frac{\partial \psi_l^{(0)}}{\partial t} + \frac{\partial}{\partial x}\left(A_{l-1}\psi_{l-1}^{(1)} + B_{l+1}\psi_{l+1}^{(1)}\right) + \Sigma_t \psi_l^{(2)} = 0 \tag{4.6.17}$$

$$\psi_{n+1}^{(1)} = 0\,. \tag{4.6.18}$$

Equation 4.6.16 combines with Fick's law to give us the time-dependent diffusion equation for $\psi_0^{(0)}$. From Eq. 4.6.17 with $l > 2$, and using $\psi_l^{(1)} = 0$ for $l > 1$, we see that $\psi_l^{(2)} = 0$ for $l > 2$. Thus we begin to build up an induction on the order j to show that $\psi_l^{(j)} = 0$ for $l > j$.

Suppose that there is a value j such that for all values $j' \leq j$ we know $\psi_l^{(j')} = 0$ for $l > j'$. We need only consider $j > 2$ since we have already established this for $j \leq 2$. Gathering terms of order ϵ^j we have

$$\frac{1}{c}\frac{\partial \psi_0^{(j-1)}}{\partial t} + \frac{\partial}{\partial x}\left(B_1 \psi_1^{(j)}\right) + \Sigma_a \psi_0^{(j-1)} = 0 \tag{4.6.19}$$

$$\frac{1}{c}\frac{\partial \psi_l^{(j-1)}}{\partial t} + \frac{\partial}{\partial x}\left(A_{l-1}\psi_{l-1}^{(j)} + B_{l+1}\psi_{l+1}^{(j)}\right) + \Sigma_t \psi_l^{(j+1)} = 0 \tag{4.6.20}$$

$$\psi_{n+1}^{(j)} = 0\,. \tag{4.6.21}$$

Using $\psi_l^{(j-1)} = 0$ for $l > j-1$ and $\psi_{l-1}^{(j)} = 0$ for $l-1 > j$, and hence $\psi_l^{(j)} = 0$ and $\psi_{l+1}^{(j)} = 0$ for $l-1 > j$, with Eq. 4.6.20 for $l > j+1$ therefore implies that $\Sigma_t \psi_l^{(j+1)} = 0$, and hence $\psi_l^{(j+1)} = 0$ for $l > j+1$. This completes the induction.

□

Note that $A_0 B_1 = 1/3$, and also recalling that $\phi = 2\sqrt{\pi}\psi_0$ we see from Eq. 4.6.11 that the scalar flux ϕ satisfies the time dependent diffusion equation to leading order in ϵ. This proof shows that the diffusion limit of the P_n equations is connected to the angular moments of order l being of order ϵ^l, and in the correct Fick's law arising at first order in the expansion.

4.7 Diffusion properties of the Riemann discretization

We now want to explore the Riemann solver discretization in the diffusion limit. We first consider the linear-in-space and linear-in-direction cosine solution, which in the discrete form should be

$$\psi_{0,i} = \frac{q\; i\Delta x}{2\Sigma_a\sqrt{\pi}} \tag{4.7.1}$$

$$\psi_{1,i} = -\frac{q}{2\Sigma_a\Sigma_t\sqrt{3\pi}} \tag{4.7.2}$$

$$\psi_{l,i} = 0 \qquad l > 1\,. \tag{4.7.3}$$

We wish to see if this solution satisfies Eq. 4.5.9. For this solution we immediately have $(\psi_{0,i+1} - \psi_{0,i-1})/2\Delta x = q/(2\Sigma_a\sqrt{\pi})$, $(\psi_{l,i+1} - \psi_{l,i-1})/2\Delta x = 0$ for $l > 0$, and

$\psi_{i+1} - 2\psi_i + \psi_{i-1} = 0$. With these observations it is easy to conclude that this linear-in-space and linear-in-direction cosine solution is an exact solution of the Riemann discretized P_n equations. This really was inevitable from the first order accuracy of the discretization.

However, even though the Riemann discretized P_n equations have this exact diffusion-like solution (which exactly satisfies Fick's law, you will recall), it does not have a good diffusion limit. Introducing the same scaling in ϵ as for Theorem 1 we write the Riemann discretized equations as

$$\frac{\epsilon}{c}\frac{d\psi_i}{dt} + \mathbf{A}\frac{(\psi_{i+1} - \psi_{i-1})}{2\Delta x} - |\mathbf{\Lambda}|\left(\psi_{i+1} - 2\psi_i + \psi_{i-1}\right) = \\ - \begin{pmatrix} \epsilon\Sigma_a & 0 & 0 & \dots \\ 0 & \Sigma_t/\epsilon & 0 & \dots \\ 0 & 0 & \Sigma_t/\epsilon & \\ \vdots & \vdots & & \ddots \end{pmatrix} \psi + \begin{pmatrix} \epsilon Q/(2\sqrt{\pi}) \\ 0 \\ 0 \\ \vdots \end{pmatrix}, \quad (4.7.4)$$

We once again use the asymptotic expansion $\psi_{l,i} \sim \sum_{j=0}^{\infty} \epsilon^j \psi_{l,i}^{(j)}(t)$ and have the following unfortunate theorem which says the Riemann solver has a poor diffusion limit.

Theorem 2. *Using $\psi_{l,i} \sim \sum_{j=0}^{\infty} \epsilon^j \psi_{l,i}^{(j)}(t)$ in Eq. 4.7.4 with $\Sigma_t > 0$ we must have $\psi_1^{(0)} = 0$ and $\psi_{0,i+1}^{(0)} - 2\psi_{0,i}^{(0)} + \psi_{0,i-1}^{(0)} = 0$, so $\psi_{0,i}^{(0)}$ does* not *satisfy a discrete diffusion equation.*

Proof. Considering first terms of order ϵ^{-1}, we get contributions only from the right hand side and when $\Sigma_t \neq 0$; these terms imply $\psi_{l,i}^{(0)} = 0$, and in particular $\psi_1^{(0)} = 0$, yielding the first claim of the theorem.

Moving on to terms of order ϵ^0 we have

$$\mathbf{A}\frac{\psi_{i+1}^{(0)} - \psi_{i-1}^{(0)}}{2\Delta x} - |\mathbf{\Lambda}|\left(\psi_{i+1}^{(0)} - 2\psi_i^{(0)} + \psi_{i-1}^{(0)}\right) = \begin{pmatrix} 0 & 0 & 0 & \dots \\ 0 & \Sigma_t & 0 & \dots \\ 0 & 0 & \Sigma_t & \\ \vdots & \vdots & & \ddots \end{pmatrix} \psi_i^{(1)}. \quad (4.7.5)$$

This appears to have many terms, but in fact we already know that only $\psi_{0,i}^{(0)}$ is non-zero, and all other $\psi_{l,i}^{(0)} = 0$ for $l > 0$, and so most of the terms on the left are zero. So consider only the first row

$$|\mathbf{\Lambda}|_{0,0}\left(\psi_{0,i+1}^{(0)} - 2\psi_{0,i}^{(0)} + \psi_{0,i-1}^{(0)}\right) = 0 \quad (4.7.6)$$

where $|\mathbf{\Lambda}|_{0,0}$ denotes the first row, first column of $|\mathbf{\Lambda}|$, which corresponds to $l = 0$, explaining the zero indexes. So, in order to establish the theorem we need only show that $|\mathbf{\Lambda}|_{0,0} \neq 0$.

Going back to Eq. 4.5.10, $|\mathbf{\Lambda}| = \sum_{k=0}^{n} \mathbf{r}_k |\lambda_k| \mathbf{l}_k$, Brunner & Holloway [5, 6] have previously derived the eigenvectors and eigenvalues of $\mathbf{A}$, and from these results one can construct $|\mathbf{\Lambda}|_{0,0}$ and see that it is non-zero. Alternately, noting that $B_{l+1} = A_l$ we see that $\mathbf{A}$ is symmetric, hence $\mathbf{r}_k = \mathbf{l}_k$. Every term in the sum for $|\mathbf{\Lambda}|$ is therefore non-negative, and if the first element of $\mathbf{r}_k$ corresponding to a non-zero eigenvalue λ_k is non-zero, then $|\mathbf{\Lambda}|_{0,0} > 0$. This is easy to discover from the structure of $\mathbf{A}$, which has a zero diagonal and non-zeros on the first super and sub-diagonals. If the first element of an eigenvector is zero then, for a non-zero eigenvalue, the second element is zero. And if the first and second elements are zero, the third must be, and so on down the line. Hence the first element of the eigenvector cannot be zero, so $|\mathbf{\Lambda}|_{0,0} > 0$ and the theorem is proved. □

So, at first order in ϵ we discover the equation for the leading order scalar flux $\psi_{0,i}$ is

$$\psi_{0,i+1} - 2\psi_{0,i} + \psi_{0,i-1} = 0\,, \tag{4.7.7}$$

hence the *Götterdämmerung*[4] of the standard Riemann solver in the diffusion limit. This equality tells us that the leading order terms will not satisfy the correct diffusion equation. We see this be noting that Eq. 4.7.7 is (within a constant factor) a finite-difference Laplacian. This Laplacian being zero tells us the leading order terms are linear in space and satisfy an erroneous diffusion equation $\nabla^2 \psi_0^{(0)} = 0$.

4.8 Modified Riemann Solver in the Diffusive Limit

Riemann solvers were designed to add just the right amount of dissipation to make the advective terms of a problem upwinded and stable. They treat an idealized problem (one in which there are no sources or sinks) exactly and use the solution to this problem to determine the amount of flow across a cell interface. In problems where the advection of information dominates this is the correct approach. Transport problems have terms that act as sources, namely collisional interactions and inhomogeneous source terms. When the mean free path of the particles is resolved in a numeric scheme, the Riemann solver's added dissipation is the correct amount. However, this dissipation dominates for large cell sizes, so that when a mean free path is not resolved and the particle streaming is not the dominant process in the cell, the dissipation is incorrect.

To address this problem we suggest that the Riemann dissipation be scaled out as the cell size relative to a mean free path grows. In particular we suggest that the dissipation matrix $|\mathbf{\Lambda}|$ be multiplied by $\left[1 + (\Sigma_s \Delta x)^2\right]^{-1}$, where $\Sigma_s = \Sigma_t - \Sigma_a$

[4]Properly translated into English, *Götterdämmerung*, means "twilight of the gods" and denotes the turbulent and complete downfall of a regime or institution. The word is the mistranslation into German of the Old Norse *ragnarok* (which means "fate of the gods") and its most famous usage is by Richard Wagner as the title for the finale of *The Ring of the Nibelung*.

is the scattering cross-section. This scaling allows the dissipation to be largely unchanged when the cell size is smaller than a scattering mean free path, but also reduces the dissipation acutely when the cell size is larger than the scattering mean free path. This has the effect of effectively making $|\mathbf{\Lambda}|_{0,0} = O(\epsilon^2)$ as $\epsilon \to 0$ in the proof of Theorem 2, and thereby this "diffusion correction" removes the problem.

This scaling factor obeys

$$\frac{1}{1 + (\Sigma_t/\epsilon - \epsilon\Sigma_a)^2 \Delta x^2} \sim \begin{cases} 1 & \epsilon \to \infty \\ \frac{\epsilon^2}{\Sigma_s^2 \Delta x^2} & \epsilon \to 0\,. \end{cases} \tag{4.8.1}$$

Using this scaling the order $1/\epsilon$ equations still yield

$$\psi_{l,i}^{(0)} = 0 \tag{4.8.2}$$

for $l > 0$. But the order 1 equations now state

$$\psi_{1,i}^{(1)} = \frac{-1}{2\Delta x \Sigma_t \sqrt{3}} \left(\psi_{0,i+1}^{(0)} - \psi_{0,i-1}^{(0)} \right), \tag{4.8.3}$$

which recalls Fick's law. Finally, the order ϵ equations give

$$\frac{1}{c}\frac{d\psi_{0,i}^{(0)}}{dt} - \frac{1}{3\Sigma_t}\left(\frac{\psi_{0,i+2}^{(0)} - 2\psi_{0,i}^{(0)} + \psi_{0,i-2}^{(0)}}{4\Delta x} \right) + \Sigma_a \psi_{0,i}^{(0)} = \frac{Q_i}{2\sqrt{\pi}}\,. \tag{4.8.4}$$

This is a discrete diffusion equation with the correct diffusion coefficient $D = 1/3\Sigma_t$. The effect of the scaled dissipation is to convert the solver from an upwinded Riemann solver when computational cells are on the order of a mean-free-path or smaller, into a cell-centered diffusion solver when cells are many scattering mean-free-paths thick.

It should be noted that this diffusion equation is discretized on a mesh that is of size $2\Delta x$, rather than on the mesh of size Δx. As written this limit is therefore yielding two diffusion equations, one on even numbered mesh cells, and one on odd numbered cells. This arises because in the first-order Riemann solver all quantities are effectively cell-centered. However, as we will show in the results of the next section, we have not seen a problem with this in practice because the nonlinear interpolation used in a high-resolution Riemann solver does couple neighboring cells in this limit.

We also note that the scaling of the Riemann dissipation term could have been of the form $\left[1 + (\frac{\Sigma_t}{\epsilon}\Delta x)^2\right]^{-1}$ based on Σ_t rather than Σ_s. Our thinking, however, was that for a mesh that contains large cells in a strong absorber we should continue to upwind the solution, rather than allow it to become a centered difference scheme. However, in problems of thermal radiative transfer the absorption/reëmission process behaves as effective scattering. In this case the scaling factor using Σ_t would be appropriate.

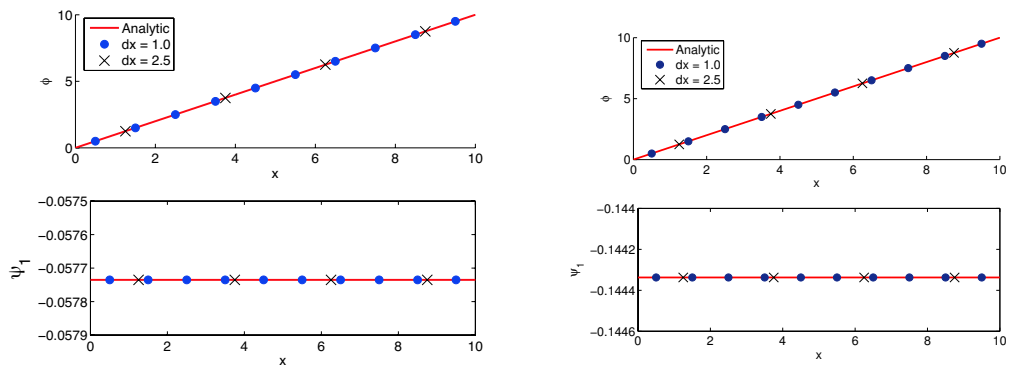

(a) The standard Riemann solver solution where $\Sigma_t = 10, \Sigma_a = 0.1$: ϕ should have a slope of 1 and ψ_1 should be $-\frac{1}{10\sqrt{3}} \approx -0.057735$.

(b) The standard Riemann solver solution where $\Sigma_t = 4, \Sigma_a = 3$: ϕ should have a slope of 1 and ψ_1 should be $-\frac{1}{4\sqrt{3}} \approx -0.14434$.

Figure 4.6. The scalar flux and first moments for the standard Riemann solver for the linear source problem (cf. Sec. 4.6)

4.9 Computational demonstrations

4.9.1 Preserving Linear Solutions

The ability of the Riemann solver to be LSP both with and without the diffusion correction is shown in Figs. 4.6 and 4.7. These problems had a source $q = \Sigma_a$ (cf. Eq. (4.6.2)). The linearity in both space and angle is captured both with and without the diffusion correction. Also, it is evident that the Riemann solver is LSP in both diffusive and non-diffusive regimes.

4.9.2 Diffusion Correction

We now turn to results detailing the effectiveness of the diffusion correction suggested in Sec. 4.8. Both steady state and time-dependent problems will be used to explore the properties of the diffusion-corrected Riemann solver with the high resolution spatial scheme.

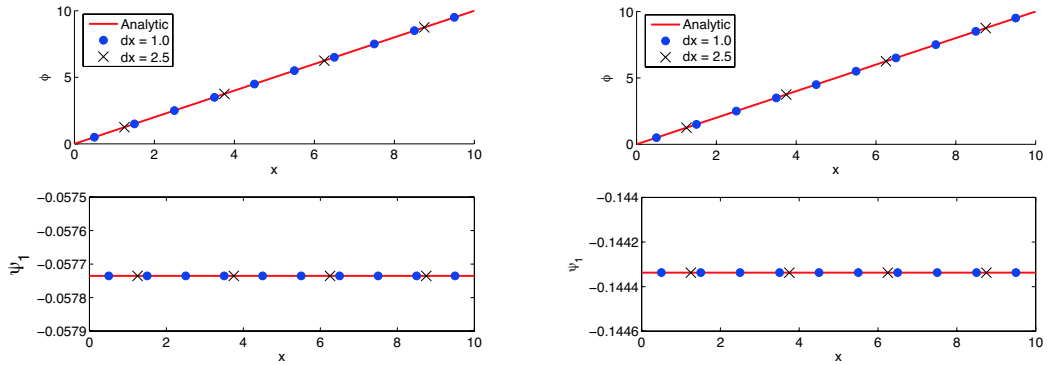

(a) The modified Riemann solver solution where $\Sigma_t = 10, \Sigma_a = 0.1$: ϕ should have a slope of 1 and ψ_1 should be $-\frac{1}{10\sqrt{3}} \approx -0.057735$.

(b) The modified Riemann solver solution where $\Sigma_t = 4, \Sigma_a = 3$: ϕ should have a slope of 1 and ψ_1 should be $-\frac{1}{4\sqrt{3}} \approx -0.14434$.

Figure 4.7. The scalar flux and first moments for the diffusion-corrected Riemann solver for the linear source problem

4.9.2.1 Steady State Problems

Figure 4.8 presents results from a P_5 steady state calculation both with and without the diffusion correction. The problem has an incident beam at $x = 0$, a strong absorbing region from $x = 0$ to $x = 2$ and a strong scattering region from $x = 2$ to $x = 7$. In the scattering region, where the diffusion approximation is valid, the uncorrected method (Fig. 4.8(b)) gives different solutions for different mesh spacings. With the correction added to the dissipation term, the solution does not vary significantly with changes in the cell size. Even for cells that are large compared to a mean-free-path the method with a proper diffusion limit still yields correct results as seen in Fig. 4.8(a).

Figure 4.9 shows a problem of a uniform source embedded in a diffusive material with vacuum boundary conditions. Only resolving the diffusion length, the modified Riemann solver produces a nearly identical solution to the result calculated with a mesh that resolves a mean free path. The standard Riemann solver causes the height of the solution "plateau" and the boundary layer to be incorrect when the mean free path is not resolved.

Another steady state problem used to test the diffusion correction is a modified version of Reed's problem [28]. The problem was modified to make the diffusive region in the problem optically thick. This was in an attempt to gage the ability of the diffusion correction in problems with a variety of materials. The results in Fig. 4.10 show that in the diffusion correction does indeed improve the calculated flux

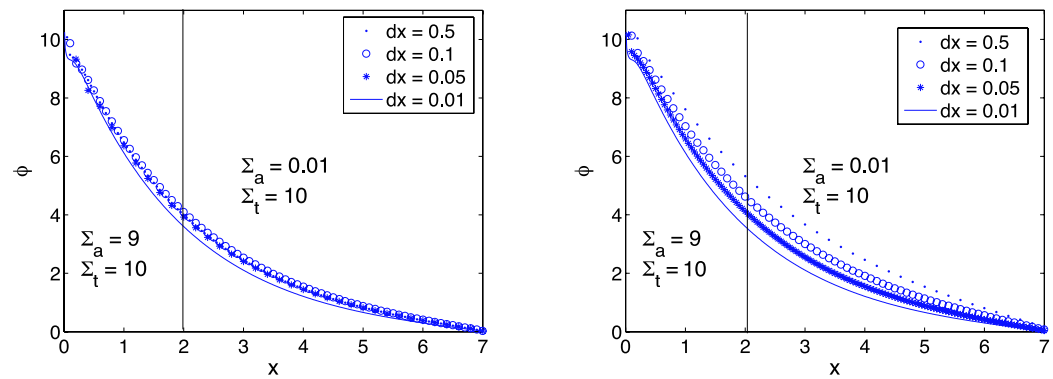

(a) The solution using the diffusion-corrected Riemann solver

(b) The solution using the standard Riemann solver without the diffusion correction

Figure 4.8. The P_5, steady state solution with incident beam on the left, and two regions: a strong absorber and a strong scatterer

in the diffusive region. Moreover, the solution in the strong source and absorber regions is nearly identical. There does appear to be an issue in the void region. The scalar flux is too high. This is most likely due to effects at the interface between the diffusive region and the void – an issue not explored in this paper.

4.9.2.2 Time Dependent Problems

The diffusion correction is also effective in time-dependent problems. One problem used to test the correction places a plane pulse of particles at the center of a medium dominated by scattering ($\Sigma_t = 10, \Sigma_s = 9.9$). The differences between the corrected solution and the standard Riemann solver are noteworthy. Figures 4.11 and 4.12 show the P7 and P1 solutions to this problem at $t = 35$ after the pulse with $\Delta t = 0.5$. The lack of a diffusion limit in the unaltered Riemann solver leads to very different solutions with different spatial grids. Figures 4.11(b) and 4.12(b) show that the width of the pulse in the solution artificially spreads as Δx increases in the solution without the diffusion correction. The fact that the diffusion correction behaves the same both in the P_1 approximation and the P_7 approximation is demonstrated by these figures. This is manifest in the fact that the standard Riemann solver solutions are similar for both P_1 and P_7 and the diffusion corrected solutions are similar for both angular approximations (i.e. Fig. 4.11(b) is similar to Fig. 4.12(b) and Fig. 4.11(a) is similar to Fig. 4.12(a)).

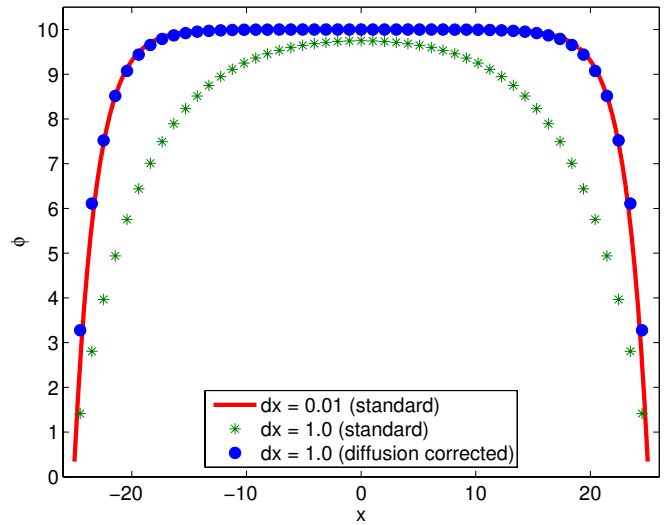

Figure 4.9. The P_1, steady-state solution to a uniform source problem with $Q = \frac{1}{2\pi}$ and $\Sigma_a = 0.01, \Sigma_t = 10$

4.10 Conclusions and Future Work

We have presented an implicit Riemann solver for one-dimensional P_n transport. A high resolution spatial scheme is considered with an implicit time integration method. To make the method both implicit in time and high resolution in space a system of nonlinear equations must be solved at each time step. We accomplish this using a matrix-free Newton-Krylov method that is preconditioned by the linear system from the first-order spatial discretization. Results from two test problems – one steady state and the other time independent – demonstrate the capabilities of this method. For time-dependent problems, computations that violate the CFL limit still agree with analytic solutions and even far beyond the CFL limit good qualitative agreement can be seen. In the steady state test problem, results obtained by ROOSTER were in almost exact agreement with state-of-the-art S_n results. For transients before the steady state, there is sensitivity to the size of the time step in regions with significant scattering. It is conjectured that this is due to the fact that our Riemann solver ignored sources (both collisional and prescribed) in its derivation.

The authors plan to explore the extension of this implicit Riemann solver to multiple dimensions and unstructured grids. Along the way capabilities to solve radiative transfer problems (i.e. problems of photon transport where absorption and reëmission from the background media is taken into account) will also be added to the method.

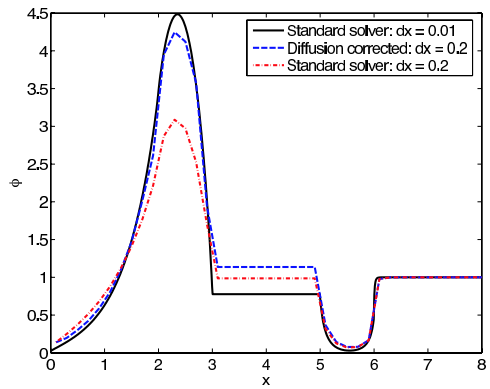

Figure 4.10. The solution to the modified Reed's problem.

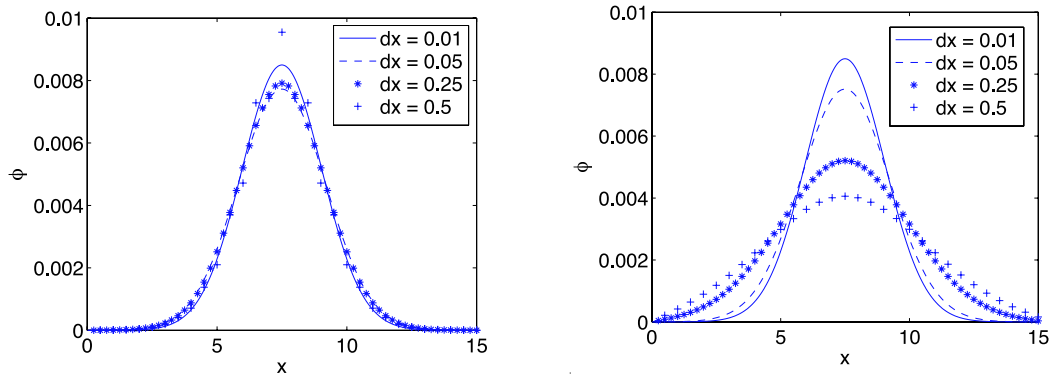

(a) The solution from the modified Riemann solver

(b) The standard Riemann solver solution

Figure 4.11. The P7 solution at $t = 35$ after the initial pulse of particles

In the context of diffusive problems using the Riemann solver developed, this research gave new insight into the behavior of this method. The LSP property was shown for the P_n equations both analytically and in numerical simulations using the standard Riemann solver previously implemented for radiation transport problems. We then showed that despite being LSP, the standard Riemann solver discretization does *not* have a diffusion limit. The dissipation introduced by the Riemann solver to make the differencing scheme stable requires spatial resolution of a particle mean free path.

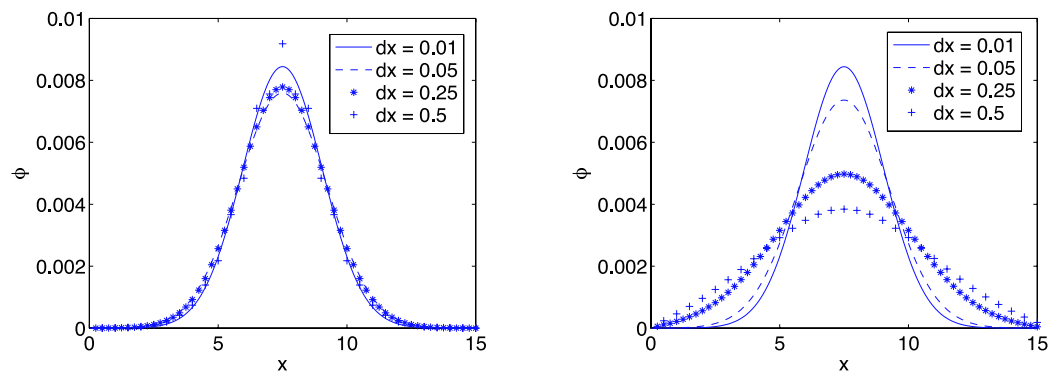

(a) The solution from the modified Riemann solver

(b) The standard Riemann solver solution

Figure 4.12. The P1 solution at t=35 after the initial pulse of particles

References

[1] G. I. Bell and S. Glasstone. *Nuclear Reactor Theory*. Krieger, 1970. ISBN 0-88275-790-3.

[2] T. A. Brunner. *Riemann Solvers for Time-Dependent Transport Based on the Maximum Entropy and Spherical Harmonics Closures*. Ph.D. thesis, University of Michigan, 2000.

[3] T. A. Brunner. "Forms of Approximate Radiation Transport." Tech. Rep. SAND2002-1778, Sandia National Laboratories, Jul 2002.

[4] T. A. Brunner and J. P. Holloway. "One-Dimensional Riemann Solvers and the Maximum Entropy Closure." *Journal of Quantitative Spectroscopy and Radiative Transfer*, vol. 69, pp. 543–566, 2001.

[5] T. A. Brunner and J. P. Holloway. "Two Dimensional Time Dependent Riemann Solvers for Neutron Transport." In "M&C 2001 Salt Lake City," American Nuclear Society, September 2001.

[6] T. A. Brunner and J. P. Holloway. "Two-dimensional time dependent Riemann solvers for neutron transport." *Journal of Computational Physics*, vol. 210(1), pp. 386–399, NOV 2005.

[7] B. A. Clark. "Computing multigroup radiation integrals using polylogarithm-based methods." *Journal of Computational Physics*, vol. 70(2), pp. 311 – 29, JUN 1987.

[8] M. Eaton, C. C. Pain, C. de Oliveira, and A. Goddard. "A High-Order Riemann Method for the Boltzmann Transport Equation." In "Nuclear Mathematical and Computational Sciences: A Century in Review; A Century Anew," American Nuclear Society, Gatlinburg, Tennesee, April 2003.

[9] B. D. Ganapol. "Solution of the One-Group Time-Dependent Neutron Transport Equation in and Infinite Medium by Polynomial Reconstruction." *Nuclear Science and Engineering*, vol. 92, pp. 272–279, 1986.

[10] B. D. Ganapol. *Homogeneous Infinite Media Time-Dependent Analytic Benchmarks for X-TM Transport Methods Development*. Los Alamos National Laboratory, Mar 1999.

[11] B. D. Ganapol and K. L. Peddicord. "The Generation of Time-Dependent Neutron Transport Solutions in Infinite Media." *Nuclear Science and Engineering*, vol. 64, pp. 317–331, 1977.

[12] M. L. Hall. "Spartan/Augustus Overview: Simplified Spherical Harmonics and Diffusion for Unstructured Hexahedral Lagrangian Meshes." Tech. Rep. LA-UR-98-3766, Los Alamos National Laboratory, 1998.

[13] H. L. Hanshaw. *The Multidimensional Multiple Balance Method for S_n Radiation Transport*. Ph.D. thesis, University of Michigan, Ann Arbor, 2005.

[14] M. Heroux, R. Bartlett, V. H. R. Hoekstra, J. Hu, T. Kolda, R. Lehoucq, K. Long, R. Pawlowski, E. Phipps, A. Salinger, H. Thornquist, R. Tuminaro, J. Willenbring, and A. Williams. "An Overview of Trilinos." Tech. Rep. SAND2003-2927, Sandia National Laboratories, 2003.

[15] Kambiz Salari and Patrick Knupp. "Code verification by the method of manufactured solutions." Tech. Rep. SAND2000-1444, Sandia National Laboratories, Jun 2000.

[16] C. Kelley. *Iterative Methods for Linear and Nonlinear Equations*. Frontiers in Applied Mathematics. Society for Industrial and Applied Mathematics, Philadelphia, USA, first edn., 1995.

[17] E. W. Larsen. "Infinite-medium solutions of the transport equation, S_N discretization schemes, and the diffusion approximation." *Transport Theory and Statistical Physics*, vol. 32(5-7), pp. 623 – 643, 2003.

[18] R. J. LeVeque. *Numerical Methods for Conservation Laws*. Birkhäuser Verlag, 1992. ISBN 3-7643-2723-5 0-8176-2723-5.

[19] E. E. Lewis and W. F. Miller, Jr. *Computational Methods of Neutron Transport*. American Nuclear Society, 1993. ISBN 0-89448-452-4.

[20] C. Lingus. "Analytical Test Case's[sic] for Neutron and Radiation Transport Codes." In "Second Conference on Transport Theory," pp. 655–659. United States Atomic Energy Commission - Division of Technical Information, Los Alamos, New Mexico, January 1971.

[21] D. Mihalas and B. Weibel-Mihalas. *Foundations of Radiation Hydrodynamics*. Dover, 1999. ISBN 0-486-40925-2.

[22] J. E. Morel. "The Linear Multifrequency-Grey Acceleration Method Recast as a Preconditioned Krylov Method." Research Memo, AUG 2005.

[23] G. L. Olson, L. H. Auer, and M. L. Hall. "Diffusion, P1, and Other Approximate Forms of Radiation Transport." *Journal of Quantitative Spectroscopy and Radiative Transfer*, vol. 64(6), pp. 619–634, March 2000.

[24] K. O. Ott and W. A. Bezella. *Introductory Nuclear Reactor Statics*. American Nuclear Society, revised edn., 1989. ISBN 0-89448-033-2.

[25] S. D. Pautz. "Verification of transport codes by the moethod of manufactured solutions: the ATTILA experience." Tech. Rep. LA-UR-01-1487, Los Alamos National Laboratory, 2001. Also in proceedings of ANS M&C 2001 Salt Lake City conference.

[26] G. C. Pomraning. *The Equations of Radiation Hydrodynamics*. Pergamon Press, 1973. ISBN 0-08-016893-0.

[27] W. Reed. "New difference schemes for the neutron transport equation." *Nuclear Science and Engineering*, vol. 46, pp. 31–39, 1971.

[28] W. H. Reed. "Spherical Harmonic Solutions of the Neutron Transport Equation from Discrete Ordinate Codes." *Nuclear Science and Engineering*, vol. 49, p. 10, 1972.

[29] B. Su. "Variable Eddington Factors and Flux Limiters in Radiative Transfer." *Nuclear Science and Engineering*, vol. 137, pp. 281–297, March 2001.

[30] B. Su and G. L. Olson. "Benchmark results for the non-equilibrium Marshak diffusion problem." *Journal of Quantitative Spectroscopy and Radiative Transfer*, vol. 56(3), pp. 337–351, 1996.

[31] B. Su and G. L. Olson. "An analytical benchmark for non-equilibrium radiative transfer in an isotropically scattering medium." *Annals of Nuclear Energy*, vol. 24(13), pp. 1035–1055, 1997.

[32] B. Su and G. L. Olson. "Non-grey benchmark results for two temperature non-equilibrium radiative transfer." *Journal of Quantitative Spectroscopy and Radiative Transfer*, vol. 62, pp. 279–302, 1999.

[33] B. van Leer. "Towards the ultimate conservative difference scheme. II. Monotonicity and conservation combined in a second-order scheme." *Journal of Computational Physics*, vol. 14, pp. 361–370, 1974.

[34] C. Yin and B. Su. "A nonlinear diffusion theory for particle transport in strong absorbers." *Annals of Nuclear Energy*, vol. 29(12), pp. 1403–1419, 2002.

DISTRIBUTION:

2 James Paul Holloway
Department of Nuclear Engineering and Radiological Sciences
University of Michigan
Ann Arbor, MI 48109-2014

1 Christopher J. Kurecka
1883 Pointe Crossing #203
Ann Arbor, MI 48105

1 MS 1186
Thomas A. Brunner, 1674

1 MS 1186
Thomas A. Mehlhorn, 1674

1 MS 1110
Michael A. Heroux, 1414

3 MS 9018
Central Technical Files, 8945-1

2 MS 0899
Technical Library, 9616

1 MS 0123
D. Chavez, LDRD Office, 1011